Amanda Faria Assoni

A função de proteínas associadas à Esclerose Lateral Amiotrófica em diferentes contextos celulares

The role of ALS-related proteins in different cellular contexts

São Paulo

2021

Amanda Faria Assoni

A função de proteínas associadas à Esclerose Lateral Amiotrófica em diferentes contextos celulares

The role of ALS-related proteins in different cellular contexts

Tese apresentada ao Instituto de Biociências da Universidade de São Paulo, para a obtenção de Título de Doutora em Ciências, na Área de Biologia (Genética).

Orientador: Oswaldo Keith Okamoto

São Paulo

2021

Ficha Catalográfica

FARIA ASSONI, AMANDA

A função de proteínas associadas à Esclerose Lateral Amiotrófica em diferentes contextos celulares / AMANDA FARIA ASSONI ; orientador Oswaldo Keith Okamoto ; orientador dupla titulação Floris Foijer -- São Paulo, 2021. p.

Tese (Doutorado) -- Instituto de Biociências da Universidade de São Paulo. Programa de Pós-Graduação em Genética e Biologia Evolutiva.

1. Esclerose Lateral Amiotrófica. 2. Meduloblastoma. 3. Síntese protéica. I. Keith Okamoto, Oswaldo, orient. II. Foijer, Floris , orient. Dupla titulação III. Título.

Comissão Julgadora:

_____ _____

Prof(a). Dr(a). Prof(a). Dr(a).

_____ _____

Prof(a). Dr(a). Prof. Dr. Oswaldo Keith Okamoto

Orientador

TABLE OF CONTENTS

RESUMO

A Esclerose Lateral Amiotrófica (ELA) é uma doença neurodegenerativa para a qual não existe atualmente um tratamento eficaz. Portanto, é de grande importância investigar mais profundamente os mecanismos que levam à morte do neurônio motor para encontrar novos alvos terapêuticos. Nesta tese, aprofundamos nossa compreensão sobre três proteínas envolvidas na patogênese da ELA (Fused in Sarcoma -FUS, Vesicle-associated Membrane Protein B -VAPB e o receptor de efrina A4-EPHA4), analisando seus efeitos quando mutadas, ausentes, ou quando sua atividade é inibida. Além disso, há evidências de mecanismos em comum na neurodegeneração e transformação celular. Portanto, investigamos essas proteínas relacionadas com ELA em diferentes contextos celulares (neurodegeneração e câncer). Para este fim, usamos os modelos celulares de iPSCs de pacientes com ELA tipo 6, bem como um tumor do sistema nervoso central, meduloblastoma.

Aqui, nós descrevemos que a tradução de proteínas é uma das primeiras e mais importantes vias afetadas por mutações relacionadas com ELA. Todos os mecanismos que são interrompidos nas células com ELA, levam à regulação negativa da síntese de proteínas. Consistente com a literatura, nossos resultados mostram que a síntese de proteínas está diminuída em neurônios motores (NMs) derivados de iPSC de pacientes com ELA6, e isso se correlaciona com a presença da proteína FUS (normalmente nuclear) no citoplasma. Também mostramos que interferon-gama (IFN-y) - uma citocina multifuncional que, entre outras atividades, auxilia na resposta antiviral - regula positivamente genes associados à tradução especificamente em NMs com ELA6 quando esses neurônios motores são tratados na presença de estresse oxidativo, e que a localização citoplasmática de FUS é reduzida em ELA6-NMs após o tratamento com IFN-y. Este tratamento evita a apoptose de ELA6-NMs. Portanto, a diminuição da síntese de proteínas pode ser característica da patogênese de ELA, e o aumento da tradução pela administração de IFN-y deveria ser estudado como um possível tratamento para esses pacientes.

Em relação à função das proteínas associadas a ELA no meduloblastoma, revelamos novas funções para VAPB e EPHA4 na progressão tumoral. Descobrimos que a VAPB - que tem níveis mais baixos de mRNA no líquido cefalorraquidiano de casos esporádicos de ELA - se correlaciona com menor sobrevida geral de pacientes quando expresso em níveis mais altos no meduloblastoma. Além disso, o nocaute de *VAPB* causa parada do ciclo celular em G1 / 0 e altera os níveis de transcrição de genes relacionados à via do WNT, incluindo *CTNNB1*. Também mostramos que a regulação negativa de EPHA4 parece ser benéfica para a proliferação celular em meduloblastoma. Além disso, demonstramos que a VAPB se liga a EPHA4 em tecidos neuronais não transformados, mas não em células de meduloblastoma. No entanto, a remoção de VAPB no meduloblastoma aumentou a fosforilação de EPHA4, enquanto a inibição da fosforilação da EPHA4 aumentou a proliferação das células VAPB-KO, destacando a interação entre estas diferentes vias de sinalização.

Em resumo, aqui fornecemos evidências para apoiar a hipótese de que a neurodegeneração e a tumorigênese são o resultado da desregulação das mesmas vias de sinalização, embora em direções diferentes. Portanto, é de extrema importância conectar o conhecimento das pesquisas em câncer e em doenças neurodegenerativas. O que pode levar a uma melhor compreensão dessas doenças devastadoras e gerar novas estratégias de intervenção para melhorar a vida dos pacientes no futuro.

ABSTRACT

Amyotrophic Lateral Sclerosis (ALS) is a neurodegenerative disease for which there is currently no effective treatment. Therefore, it is of great importance to further investigate the mechanisms leading to motor neuron death to find new potential therapeutic targets. In this thesis, we deepen our understanding of 3 proteins involved in the pathogenesis of ALS (Fused in Sarcoma -FUS, Vesicle-associated Membrane Protein B -VAPB, and the ephrin receptor A4-EPHA4) by analyzing their effects when mutated, absent, or when their activity is inhibited. In addition, there is evidence for overlapping mechanisms in neurodegeneration and cell transformation. Therefore, we further investigated these ALS -related proteins in different cellular contexts (neurodegeneration and cancer). To this end, we used the cellular models of iPSCs from ALS type 6 patients as well as a central nervous system tumor, medulloblastoma. Herein, we describe that protein translation is one of the first and most important pathways affected by ALS -related mutations. Indeed, all mechanisms that are disrupted in ALS -cells ultimately lead to downregulation of protein synthesis rates. Consistent with the literature, our results show that protein synthesis rates are decreased in iPSC-derived motor neurons from ALS6 patients, and this correlates with the presence of the generally nuclear localized FUS protein in the cytoplasm. We also show that interferon-gamma (IFN-y) - a multifunctional cytokine that, among other things, aids in antiviral response - upregulates translation-associated genes specifically in ALS MNs when these iPSC-derived motor neurons from ALS patients are treated in the presence of oxidative stress, and that the cytoplasmic localization of FUS is reduced in ALS6 MNs after IFN-y treatment. This treatment prevents apoptosis of ALS6 MNs. Therefore, decreased protein synthesis may be a hallmark of ALS pathogenesis, and increasing translation with IFN-y is a potential treatment for these patients.
Regarding the function of ALS associated proteins in medulloblastoma, we reveal novel roles for VAPB and EPHA4 in tumor progression. We find that VAPB - which has lower mRNA levels in the cerebrospinal fluid of sporadic ALS cases - correlates with lower overall patient survival when expressed at higher levels in medulloblastoma. Moreover, VAPB knockout arrests cells in G1/0 and alters transcript levels of many WNT-related proteins, including CTNNB1. We also show that downregulation of EPHA4 appears to be beneficial for cell proliferation in medulloblastoma. Furthermore, we found that VAPB binds to EPHA4 in nontransformed neuronal tissues but not in medulloblastoma cells. However, removal of VAPB in medulloblastoma increased EPHA4 phosphorylation, whereas inhibition of EPHA4 phosphorylation increased the cycling of VAPB-KO cells, highlighting the interplay between different signaling pathways.
In summary, here we provide evidence to support the hypothesis that neurodegeneration and tumorigenesis are the result of the same deregulated signaling pathways, albeit in different directions. Therefore, it is of utmost importance to connect knowledge of cancer research and neurodegenerative diseases. This will not only lead to a better understanding of these devastating diseases, but could generate new intervention strategies to improve the lives of patients in the future.

GENERAL INTRODUCTION AND THESIS OUTLINE

Amyothopic lateral sclerosis (ALS) is a late-onset neurodegenerative disease that kills 30,000 patients annually(Logroscino et al., 2010). The first cells affected are the motor neurons, and symptoms include muscle twitching, spasms, stiffness, and weakness(Tiryaki and Horak, 2014). As the disease progresses, patients' muscles weaken, muscle tissue atrophies, and patients usually die of respiratory failure. However, non-motor signs may also appear (including cognitive dysfunction, frontotemporal dementia, extrapyramidal features). For this reason, ALS is now widely considered a multisystem degeneration(Grossman, 2018).

ALS is the most common motor neuron disease in which the mechanism leading to motor neuron death is still not fully understood(Ferraiuolo et al., 2011), thus any effort made to elucidate the pathogenesis of the disease is very valuable.

ALS patients are classified into two categories depending on the etiology of the disease: sporadic (SALS - 90% of cases), meaning the cause or causes of the disease are unknown, or familial (FALS – 10% of cases), where more than one family member is affected by the disease and it has been linked to inherited mutations(Hardiman et al., 2017a). Familial cases of ALS can be numbered according to the gene that is mutated in each patient. Currently, mutations in more than 40 genes have been identified in familial forms of ALS, including superoxide dismutase 1 (SOD1) in ALS1, TAR DNA binding protein 43 (TARDBP) in ALS10, vesicle-associated membrane protein B (VAPB) in ALS8, and fused in sarcoma (FUS) in ALS6(Mathis et al., 2019).

As ALS is a disease of motor neurons, the strategies to study its phenotype are challenging since biopsies are not recommended, many nerve biopsies do not provide a definitive pathological diagnosis and the procedure is associated with significant cost and morbidity(Nathani et al., 2021). Therefore, the model used to elucidate disease mechanisms is of great importance. Here, we used human induced pluripotent stem cells (hIPSCs) to study FUS functions on ALS.

Since neurodegenerative diseases are challenging to study because of the unavailability of the ideal model to be used, possibly transposing knowledge acquired researching other diseases could save years of investigation to find new therapy targets. Recently, there has been increasing evidence of a link between neurodegenerative diseases and cancer, as results have shown an inverse correlation between the occurrence of cancer in patients with neurodegenerative diseases and vice versa, suggesting a possible common mechanism for the development of both disorders that could be deregulated in opposite directions(Houck et al.,

2018). Medulloblastoma is a neoplasm of the central nervous system (CNS) that arises from undifferentiated cells during neurodevelopment(Dolecek et al., 2012), making it an interesting model to understand ALS relationship with cancer.

Below, we will elaborate on the details of the IPSCs and medulloblastoma models, as well as on the functions of the proteins we focus on in this work: FUS, VAPB and EPHA4:

IPSCs

Induced pluripotent stem cells (IPSCs) are generated from somatic cells that are reprogrammed into the pluripotent embryonic state by the expression of specific ectopic transcription factors.

In 2006, Takahashi and Yamanaka, and later several other groups, reported a significant advance in understanding the acquisition of the pluripotent state *in vitro* when they reprogrammed mouse (and later human) fibroblasts into pluripotent cells resembling embryonic stem cells (ESCs) by exogenously expressing a combination of specific transcription factors-originally the OCT4, SOX2, KLF4, and c- MYC (OKSM) genes(Takahashi and Yamanaka, 2006). The resulting cells were termed induced pluripotent stem cells (iPSCs) and characterized as pluripotent based on properties similar to those of embryonic stem cells (ESCs). These include the formation of embryoid bodies, *in vitro* differentiation into different cell types, *in vivo* teratoma formation and the ability to generate chimaera embryos(Takahashi et al., 2007; Tsubouchi et al., 2013) .

As it is possible to differentiate IPSCs into most cell lineages, hIPSCs have opened new possibilities for understanding human development, modelling disease processes, and developing new therapeutics, including for CNS diseases. Here, we applied a previously published method using a combination of small molecules regulating multiple signaling pathways to differentiate human pluripotent stem cells into a nearly pure population (> 95%) of motor neuron progenitor cells (MNPs) in 12 days and an enriched population (> 90%) of functionally mature MNs in another 16 days(Du et al., 2015).

Since we were able to collect somatic cells from ALS patients, we believe that such IPSC models represent one of the best models to understand the phenotype of the disease, since it allows to generate the cells that are first affected by the disease within the genetic background of the patients. We are aware of the limitations of IPSC models in terms of its ability to simulate aged cells, as the expression of the OKSM transcription factors act like a developmental reset and erase many of the desired traits of age-associated diseases(E et al., 2016). However, we believe that in this situation it is possible to understand the earliest phenotypes of cells when patients are still asymptomatic, and potentially avoid switching to the symptomatic stage when patients' MNs begin to die.

Medulloblastoma

There is growing evidence of a link between neurodegenerative diseases and cancer in literature, particularly showing an inverse correlation between the incidence of cancer in patients with neurodegenerative diseases (Harris et al., 2014; Klus et al., 2015; Houck et al., 2018; Jaberi et al., 2020) . ALS is a disease that primarily affects motor neurons, so CNS tumors would be the best model to study the functions of ALS -related proteins in cancer.

Additionally, there is the clinical relevance of this type of study, CNS tumors are the second most common neoplasm in children(Sadighi et al., 2012; MacDonald et al., 2014; FMG et al., 2017). Medulloblastoma is a malignant embryonal tumor that arises from primitive cells that are poorly differentiated during neuronal development. It is the most common brain tumor in children aged zero to four years and accounts for approximately 18% of pediatric brain tumors(Dolecek et al., 2012). It is classified by the World Health Organization (WHO) as a grade IV tumor, consists of highly proliferative and invasive cells that can spread throughout the CNS and form local metastases (ABTA, 2012). Medulloblastoma is a major cause of morbidity and mortality in children, as a significant proportion of patients do not respond to available treatments and/or develop motor and cognitive disorders(Rodini et al., 2010).

In general, medulloblastoma cells exhibit features of primitive cells and often show abnormalities in the activity of proteins involved in signaling pathways relevant to nervous system development. Medulloblastoma is divided in four subgroups of tumors that differ according to the molecular pathway altered in each subgroup: Wingless (WNT), Sonic Hedgehog (SHH), Group 3 and Group 4. In the first two groups, genetic alterations with mutations on the WNT or SHH pathways predominate, whereas the other groups are more heterogeneous and do not show a uniform dominance of altered pathways. However, group 3 is often correlated with alterations in the MYC pathway and group 4 with alterations in neuronal differentiation pathways(Rodini et al., 2010; Northcott et al., 2012a). The WNT subgroup is the least aggressive, followed by SHH, group 4 and finally group 3 has the worst prognosis (Kool et al., 2008; Manoranjan et al., 2013; Staal et al., 2015).

From a molecular perspective, medulloblastoma is considered a highly heterogeneous tumor type. Recent research in cancer biology has provided irrefutable evidence of the clinical implications of this inter- and intratumoral heterogeneity(Bedard et al., 2013; Almendro et al., 2014; Navin, 2014). Theoretically, tumors arise from a single transformed cell. However, at the time of diagnosis, multiple genetically distinct cell populations are often detected (Paguirigan et al., 2015). From a cellular perspective, the existence of highly tumorigenic cancer cells with stem cell-like properties that give rise to heterogeneity within the tumor makes the understanding of mechanisms more complex.

Such cancer stem cells (CSCs) have been identified in medulloblastoma as well as several other types of malignant tumors (Singh et al., 2003). Because of their ability to self-renew through asymmetric cell divisions, it is postulated that these cells give rise to diverse cellular progeny during tumor development. The increasing heterogeneity within the tumor would

therefore be the result of a continuous process of expansion and differentiation of cell subclones (Magee et al., 2012), which affects treatment resistance and clinical outcome of patients.

However, little is yet known about the development and maintenance of stem cell-like cancer cells. Given its pathophysiology, medulloblastoma is an interesting model to study this question. Considering that we want to better understand ALS-related proteins in cancer, medulloblastoma provides interesting model because it arises from poorly differentiated primitive cells during neural development and medulloblastoma tumorigenesis is associated with deregulation of signalling pathways relevant to nervous system homeostasis.

Moreover, pathways that have been described as regulators of the ALS phenotype are often involved in medulloblastoma development. For example, the ephrin pathway is altered in medulloblastoma, and the Ephrin receptor type A4 (EPHA4) has also been associated with ALS progression(Picco et al., 2007; A et al., 2012; Ferluga et al., 2015; N et al., 2015). Indeed, the EPHA4 was found to interact with VAPB(Tsuda et al., 2008), which, when mutated, causes ALS8(Nishimura et al., 2004) and for which RNA expression is downregulated in sporadic cases of ALS(Deidda et al., 2014). Therefore, we investigated the effects of EPHA4 and VAPB expression on medulloblastoma development.

In summary, here we focused our analysis on 3 proteins in ALS or in medulloblastoma to understand their role in different diseases, but in the same tissue origin. These proteins are FUS, VAPB and EPHA4, which were chosen because there is evidence for their involvement in the overall pathogenesis of ALS in different ALS types. Hereunder, we will detail their structure and functions:

FUS

FUS is a 526 amino acid protein with the following domains: Gln-Gly-Ser-Tyr-rich (or prion-like) domain; Gly-rich domain; Arg-Gly-Gly-rich domain; RNA recognition motif; zinc finger domain; and a C-terminal nuclear localization signal (NLS)(Mastrocola et al., 2013) (Figure1). It is ubiquitously expressed and is mainly localized in the nucleus, but can switch between the nucleus and cytoplasm(Lo Bello et al., 2017a).

FUS is a DNA-RNA binding protein with functions that regulate many aspects of cellular metabolism, including the DNA repair pathway, microRNA biogenesis, RNA splicing, stress granule dynamics, and axon transport. It was first discovered as a fused gene with CHOP in an adipose tissue tumor(Mastrocola et al., 2013).

When mutated, FUS can cause frontotemporal dementia (FTD) or ALS6(Vance et al., 2009). In addition, FUS has been found to mislocalize to the cytoplasm in motor neurons from sporadic ALS patients and from familial ALS cases with mutations in genes other than

FUS(Tyzack et al., 2019). Since FUS is a multifunctional protein with deregulated localization in ALS, we were interested in better understanding the mechanism of action of the FUS mutation and the type of cellular phenotypes it deregulates most strongly and earliest in ALS6 cells.

VAPB

VAPB is a 243 amino acid protein with an N-terminal globular domain called the MSP domain that has a 22% sequence homology with a protein called Major Sperm Protein expressed in C. elegans; a coiled-coil domain; and a C-terminal transmembrane domain (TMD) that allows homo- or heterodimerization of VAP proteins(Kim et al., 2010) (Figure 1). VAPB is ubiquitously expressed and is located in the endoplasmic reticulum and cis-Golgi (Teuling et al., 2007). Its functions include lipid metabolism, vesicle transport, organelle binding, activation of the unfolded protein response, and calcium homeostasis(De vos et al., 2012; Lindhout et al., 2019; Mao et al., 2019).

When mutated, VAPB causes ALS type 8 and its RNA expression has been found to be downregulated in sporadic ALS cases and upregulated and pro-oncogenic in some cancers(Rao et al., 2012).

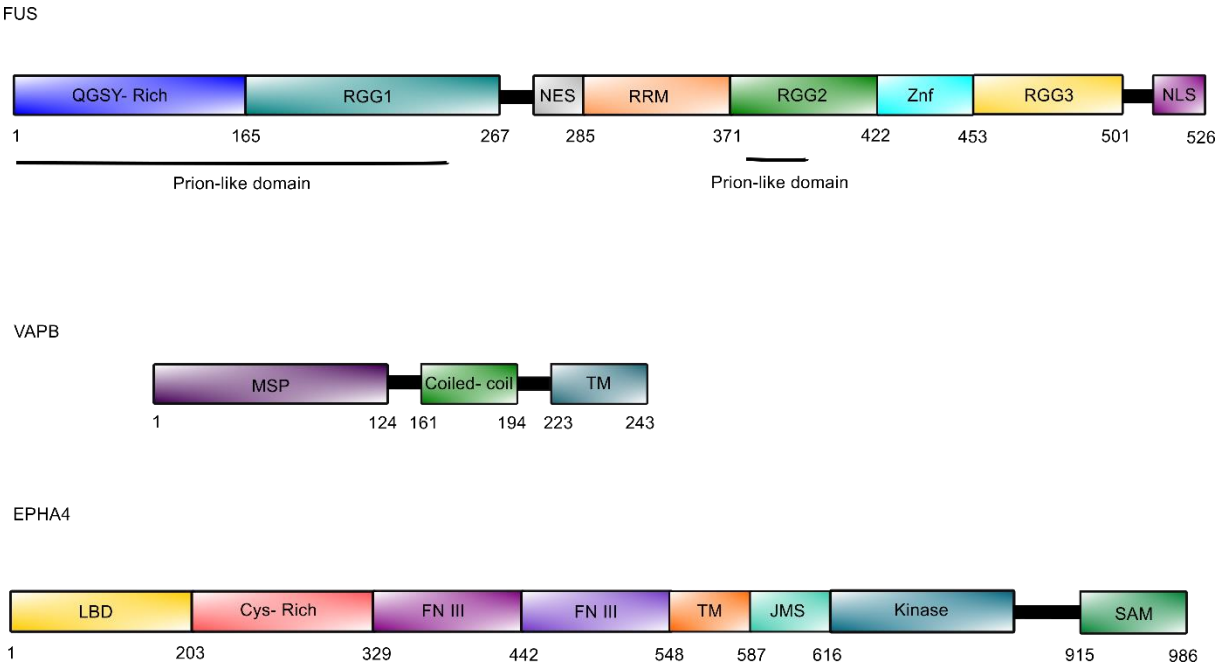

Figure 1: Schematic representation of the protein structures of FUS, VAPB and EPHA4.

EPHA4

Ephrin receptor type A4 is a protein of 986 amino acids. EPHA4 contains an N-terminal ligand binding domain (LBD), two fibronectin-type III domains, a juxtamembrane region, a tyrosine kinase domain, a sterile-α-motif domain (SAM) (Lisabeth et al., 2013) (Figure 1).

EPHA4 is ubiquitously expressed and localizes to the cell membrane. Functions of EPHA4 include regulation of the spatial organization of cell populations, tissue remodeling, axon orientation, and synaptic formation (Barquilla and Pasquale, 2015).

Epha4 has been described as one of the few proteins that can modulate the phenotype of ALS: when downregulated, EPHA4 can increase the life expectancy of ALS patients(A et al., 2012). The potential roles of Epha4 in cancer are still under debate and not clearly elucidated, as EPHA4 has been reported to be overexpressed in some cancers and downregulated in others(Fukai et al., 2008; Bhatia et al., 2015; Zhou et al., 2017; KT et al., 2018).

THESIS OUTLINE

Since the discovery of ALS, great efforts have been made to understand the major pathomechanisms and to identify which molecular signaling pathways are disrupted in all ALS types. In **Chapter 1**, we provide an overview of what is known about ALS, including the major cellular phenotypes that are deregulated in this devastating disease, and discuss how despite the many functions affected, all defects converge to attenuated protein synthesis. Protein synthesis is the ultimate process that controls cell fate and behavior(Kim, 2019), and we therefore argue that it may be an interesting target for new therapies. Moreover, the FUS protein appears to regulate most functions that are deregulated in ALS cells, and FUS has been found to mislocalize into the cytoplasm in MNs from sporadic ALS patients(Tyzack et al., 2019). Therefore, it is of crucial importance to understand the molecular role of FUS and how FUS activity can be modulated. To investigate this, we studied cells with mutant FUS, which will be discussed in the next chapter.

ALS type 6 - with mutations on the FUS gene - is the type of ALS with the earliest average disease onset(Vance et al., 2009). Therefore, understanding why motor neurons with mutations on this specific gene die off may be a way to elucidate the initial cellular symptoms and address potential treatments. In **Chapter 2**, we used patient-derived IPSC models to better understand the cellular phenotypes of ALS6 cells in a cell type most relevant for ALS, i.e. motor neurons. We began by identifying the binding partners of FUS in cells with or without the dominant FUS mutation R521H, and find that this mutant acquires a gain of function mechanisms as mutant FUS interacts with many more proteins than wild type FUS. The binding partners unique to mutant FUS are mostly proteins with functions associated with the translation initiation process, which fits well with the hallmark phenotype of ALS cells: decreased protein translation.

Inflammation is one of the few common characteristics between the different types of ALS(Hu et al.; Vérièpe et al., 2015; Lu et al., 2016; McDonald et al., 2020). As currently there is no cure for this disease, for most patients the main treatment is to relieve symptoms. Since inflammation and the downstream immune system can be modulated, it provides an interesting target for the development of new therapies. Viral infections form a major risk factor for the development of ALS (Xue et al., 2018), and interferon-gamma (IFNy) is a pleiotropic cytokine that acts as an antiviral mediator and plays a fundamental role in the elimination of viruses from the CNS and is also differentially expressed in ALS patients(DA and CS, 2002; AJ and AA, 2018; S et al., 2019). Therefore, in **Chapter 3**, we investigated the response of IPSC-derived motor neurons generated from ALS6 patients to treatment with IFNy in the presence of cellular stressors. Surprisingly, INFy - a pro-inflammatory molecule - did not lead to a decrease in cell viability in either controls or patient MNs. Instead, IFNy treatment of ALS6 MNs prevented these cells from going into apoptosis upon oxidative stress. Overall, our results show that IFNy treatment rescues the sensitivity of ALS MNs to oxidative stress. This rescue coincides with reduced cytoplasmic localization of FUS and alleviation of the protein translation defect . Therefore, IFNy treatment should be further investigated as a potential treatment for all types of ALS.

Currently there is a lot of interest in pathways that are deregulated both in neurodegenerative diseases and cancer(Driver, 2014), a better understanding of such pathways could enable the repurposing of drugs used to treat cancer for ALS patients. In **Chapter 4**, we explore the effects of inactivation of the ALS-associated gene *VAPB* in medulloblastoma cell lines. We find that VAPB plays an important role in cellular proliferation and cancer stem cell maintenance in medulloblastoma by regulating cell cycle progression. We demonstrate that high *VAPB* expression in medulloblastomas correlates with lower overall patient survival and, using RNA sequencing data, that transcript levels of many WNT pathway proteins, including CTNNB1, are decreased in VAPB knockout cells. In conclusion, our results reveal a novel pro-oncogenic function of VAPB in medulloblastoma cells that involves modulation of the WNT pathway, a known regulator of neurodevelopment(Mulligan and Cheyette, 2012).

To further explore this oncogenic function of VAPB, in **Chapter 5** we investigate its interaction with the ephrin recptor A4 in medulloblastoma. EPHA4 is highly expressed in the CNS and is emerging as a key factor in various nervous system diseases, including ALS and cancer(Fukai et al., 2008; Tsuda et al., 2008; A et al., 2012). VAPB is one of the proteins that binds EPHA4. Therefore, we investigated the regulatory mechanism of cancer stem cells (CSCs) proliferation through the VAPB/Eph interaction, and the implications for medulloblastoma development. We show that the presence of the EPHA4 receptor alone is not responsible for the maintenance of CSCs, but that it may act as a cell-cell contact molecule that, when downregulated, enhances CSC formation. We also find that VAPB binds to EPHA4 in non-transformed neuronal tissues, but not in medulloblastoma cells. However, removing VAPB in medulloblastoma cells increases EPHA4 phosphorylation, and conversely, inhibition of EPHA4 phosphorylation rescues the cell cycle defect of *VAPB*-KO cells. Collectively, these observations suggest that downregulation of VAPB may be an

interesting strategy to increase EPHA4 phosphorylation and impair proliferation of medulloblastomas.

Finally, **Chapter 6** summarizes our findings, further discusses the implications of this thesis and suggests topics for further research.

REFERENCES:

1. Logroscino, G. *et al.* Incidence of amyotrophic lateral sclerosis in Europe. *J. Neurol. Neurosurg. Psychiatry* **81**, 385–390 (2010).
2. Tiryaki, E. & Horak, H. A. ALS and Other Motor Neuron Diseases. *Contin. Lifelong Learn. Neurol.* **20**, 1185–1207 (2014).
3. Grossman, M. Amyotrophic lateral sclerosis — a multisystem neurodegenerative disorder. *Nat. Rev. Neurol. 2018 151* **15**, 5–6 (2018).
4. Ferraiuolo, L., Kirby, J., Grierson, A. J., Sendtner, M. & Shaw, P. J. Molecular pathways of motor neuron injury in amyotrophic lateral sclerosis. *Nature Reviews Neurology* **7**, 616–630 (2011).
5. Hardiman, O. *et al.* Amyotrophic lateral sclerosis. *Nature Reviews Disease Primers* **3**, 17071 (2017).
6. Mathis, S., Goizet, C., Soulages, A., Vallat, J.-M. & Masson, G. Le. Genetics of amyotrophic lateral sclerosis: A review. *J. Neurol. Sci.* **399**, 217–226 (2019).
7. Nathani, D. *et al.* Nerve biopsy: Current indications and decision tools. *Muscle Nerve* **64**, 125–139 (2021).
8. Houck, A. L., Seddighi, S. & Driver, J. A. At the Crossroads Between Neurodegeneration and Cancer: A Review of Overlapping Biology and Its Implications. *Curr. Aging Sci.* **11**, 77–89 (2018).
9. Dolecek, T. A., Propp, J. M., Stroup, N. E. & Kruchko, C. CBTRUS statistical report: primary brain and central nervous system tumors diagnosed in the United States in 2005-2009. *Neuro. Oncol.* **14 Suppl 5**, v1-49 (2012).
10. Takahashi, K. & Yamanaka, S. Induction of pluripotent stem cells from mouse embryonic and adult fibroblast cultures by defined factors. *Cell* **126**, 663–76 (2006).
11. Takahashi, K. *et al.* Induction of pluripotent stem cells from adult human fibroblasts by defined factors. *Cell* **131**, 861–872 (2007).
12. Tsubouchi, T. *et al.* DNA Synthesis Is Required for Reprogramming Mediated by Stem Cell Fusion. *Cell* **152**, 873–883 (2013).
13. Du, Z.-W. *et al.* Generation and expansion of highly pure motor neuron progenitors from human pluripotent stem cells. *Nat. Commun.* **6**, 6626 (2015).
14. E, V., N, B. & L, S. Generating Late-Onset Human iPSC-Based Disease Models by Inducing Neuronal Age-Related Phenotypes through Telomerase Manipulation. *Cell Rep.* **17**, 1184–1192 (2016).

15. Klus, P., Cirillo, D., Botta Orfila, T. & Tartaglia, G. G. Neurodegeneration and Cancer: Where the Disorder Prevails. *Sci. Reports 2015 51* **5**, 1–7 (2015).

16. Jaberi, E., Tresse, E., Grønbæk, K., Weischenfeldt, J. & Issazadeh-Navikas, S. Identification of unique and shared mitochondrial DNA mutations in neurodegeneration and cancer by single-cell mitochondrial DNA structural variation sequencing (MitoSV-seq). *EBioMedicine* **57**, (2020).

17. Harris, R. A., Tindale, L. & Cumming, R. C. Age-dependent metabolic dysregulation in cancer and Alzheimer's disease. *Biogerontology* **15**, 559–577 (2014).

18. MacDonald, T. J., Aguilera, D. & Castellino, R. C. The rationale for targeted therapies in medulloblastoma. *Neuro. Oncol.* **16**, 9–20 (2014).

19. Sadighi, Z., Vats, T. & Khatua, S. Childhood medulloblastoma: the paradigm shift in molecular stratification and treatment profile. *J. Child Neurol.* **27**, 1302–7 (2012).

20. FMG, C. *et al.* Intertumoral Heterogeneity within Medulloblastoma Subgroups. *Cancer Cell* **31**, 737-754.e6 (2017).

21. Rodini, C. O. *et al.* Aberrant signaling pathways in medulloblastomas: a stem cell connection. *Arq. Neuropsiquiatr.* **68**, 947–52 (2010).

22. Northcott, P. A. *et al.* Medulloblastomics: the end of the beginning. *Nat. Rev. Cancer* **12**, 818–34 (2012).

23. Kool, M. *et al.* Integrated genomics identifies five medulloblastoma subtypes with distinct genetic profiles, pathway signatures and clinicopathological features. *PLoS One* **3**, e3088 (2008).

24. Manoranjan, B. *et al.* Medulloblastoma stem cells: modeling tumor heterogeneity. *Cancer Lett.* **338**, 23–31 (2013).

25. Staal, J. A. *et al.* Proteomic profiling of high risk medulloblastoma reveals functional biology. *Oncotarget* **6**, 14584–95 (2015).

26. Almendro, V. *et al.* Inference of tumor evolution during chemotherapy by computational modeling and in situ analysis of genetic and phenotypic cellular diversity. *Cell Rep.* **6**, 514–27 (2014).

27. Navin, N. E. Tumor evolution in response to chemotherapy: phenotype versus genotype. *Cell Rep.* **6**, 417–9 (2014).

28. Bedard, P. L., Hansen, A. R., Ratain, M. J. & Siu, L. L. Tumour heterogeneity in the clinic. *Nature* **501**, 355–64 (2013).

29. Paguirigan, A. L. *et al.* Single-cell genotyping demonstrates complex clonal diversity in acute myeloid leukemia. *Sci. Transl. Med.* **7**, 281re2 (2015).

30. Singh, S. K. *et al.* Identification of a cancer stem cell in human brain tumors. *Cancer Res.* **63**, 5821–8 (2003).

31. Magee, J. A., Piskounova, E. & Morrison, S. J. Cancer stem cells: impact, heterogeneity, and uncertainty. *Cancer Cell* **21**, 283–96 (2012).

32. N, M. *et al.* EphrinB1 expression is dysregulated and promotes oncogenic signaling in medulloblastoma. *J. Neurooncol.* **121**, 109–118 (2015).

33. Ferluga, S., Debinski, W., Ferluga, S. & Debinski, W. Ephs and Ephrins in malignant gliomas Ephs and Ephrins in malignant gliomas. **7194**, (2015).

34. Picco, V., Hudson, C. & Yasuo, H. Ephrin-Eph signalling drives the asymmetric division of notochord / neural precursors in Ciona embryos. **1497**, 1491–1497 (2007).

35. A, V. H. *et al.* EPHA4 is a disease modifier of amyotrophic lateral sclerosis in animal models and in humans. *Nat. Med.* **18**, 1418–1422 (2012).

36. Tsuda, H. *et al.* The Amyotrophic Lateral Sclerosis 8 Protein VAPB Is Cleaved, Secreted, and Acts as a Ligand for Eph Receptors. *Cell* **133**, 963–977 (2008).

37. Nishimura, A. L. *et al.* A mutation in the vesicle-trafficking protein VAPB causes late-onset spinal muscular atrophy and amyotrophic lateral sclerosis. *Am. J. Hum. Genet.* **75**, 822–831 (2004).

38. Deidda, I. *et al.* Expression of vesicle-associated membrane-protein-associated protein B cleavage products in peripheral blood leukocytes and cerebrospinal fluid of patients with sporadic amyotrophic lateral sclerosis. *Eur. J. Neurol.* **21**, 478–85 (2014).

39. Mastrocola, A. S., Kim, S. H., Trinh, A. T., Rodenkirch, L. A. & Tibbetts, R. S. The RNA-binding protein fused in sarcoma (FUS) functions downstream of poly(ADP-ribose) polymerase (PARP) in response to DNA damage. *J. Biol. Chem.* **288**, 24731–24741 (2013).

40. Lo Bello, M. *et al.* ALS-Related Mutant FUS Protein Is Mislocalized to Cytoplasm and Is Recruited into Stress Granules of Fibroblasts from Asymptomatic <i>FUS </i>P525L Mutation Carriers. *Neurodegener. Dis.* **17**, 292–303 (2017).

41. Vance, C. *et al.* Mutations in FUS, an RNA processing protein, cause familial amyotrophic lateral sclerosis type 6. *Science (80-.).* **323**, 1208–1211 (2009).

42. Tyzack, G. E. *et al.* Widespread FUS mislocalization is a molecular hallmark of amyotrophic lateral sclerosis. *Brain* (2019). doi:10.1093/brain/awz217

43. Kim, S. H., Leal, S. S., Halevy, D. Ben, Gomes, C. M. & Lev, S. Structural requirements for VAP-B oligomerization and their implication in amyotrophic lateral sclerosis-associated VAP-B(P56S) neurotoxicity. *J. Biol. Chem.* **285**, 13839–13849 (2010).

44. Teuling, E. *et al.* Motor neuron disease-associated mutant vesicle-associated membrane protein-associated protein (VAP) B recruits wild-type VAPs into endoplasmic reticulum-derived tubular aggregates. *J. Neurosci.* **27**, 9801–15 (2007).

45. De vos, K. J. *et al.* VAPB interacts with the mitochondrial protein PTPIP51 to regulate calcium homeostasis. *Hum. Mol. Genet.* **21**, 1299–311 (2012).

46. Mao, D. *et al.* VAMP associated proteins are required for autophagic and lysosomal degradation by promoting a PtdIns4P-mediated endosomal pathway. *Autophagy* 1–20 (2019). doi:10.1080/15548627.2019.1580103

47. Lindhout, F. W. *et al.* VAP-SCRN1 interaction regulates dynamic endoplasmic reticulum remodeling and presynaptic function. *EMBO J.* **38**, (2019).

48. Rao, M. *et al.* VAMP-Associated Protein B (VAPB) Promotes Breast Tumor Growth by Modulation of Akt Activity. *PLoS One* **7**, e46281 (2012).

49. Lisabeth, E. M., Falivelli, G. & Pasquale, E. B. Eph receptor signaling and ephrins. *Cold*

Spring Harb. Perspect. Biol. **5**, 1–20 (2013).

50. Barquilla, A. & Pasquale, E. B. Eph Receptors and Ephrins : Therapeutic Opportunities. *Annu. Rev. Pharmacol. Toxicol.* **55**, 465–87 (2015).

51. Fukai, J. *et al.* EphA4 promotes cell proliferation and migration through a novel EphA4-FGFR1 signaling pathway in the human glioma U251 cell line. *Mol. Cancer Ther.* **7**, 2768–78 (2008).

52. Bhatia, S. *et al.* Effects of altered ephrin-A5 and EphA4/EphA7 expression on tumor growth in a medulloblastoma mouse model. *J. Hematol. Oncol.* **8**, 105 (2015).

53. KT, H. *et al.* miR-519d Promotes Melanoma Progression by Downregulating EphA4. *Cancer Res.* **78**, 216–229 (2018).

54. Zhou, S., Wang, L., Guo, S., Zhang, Z. & Wang, J. EphA4 protein promotes invasion in clear cell renal cell carcinomas. *Int. J. Clin. Exp. Pathol.* **10**, 11737–11742 (2017).

55. Kim, H. J. Cell fate control by translation: MRNA translation initiation as a therapeutic target for cancer development and stem cell fate control. *Biomolecules* **9**, (2019).

56. Lu, C.-H. *et al.* Systemic inflammatory response and neuromuscular involvement in amyotrophic lateral sclerosis. *Neurol. - Neuroimmunol. Neuroinflammation* **3**, e244 (2016).

57. Hu, Y. *et al.* Increased peripheral blood inflammatory cytokine levels in amyotrophic lateral sclerosis: a meta-analysis study OPEN. doi:10.1038/s41598-017-09097-1

58. McDonald, T. S., McCombe, P. A., Woodruff, T. M. & Lee, J. D. The potential interplay between energy metabolism and innate complement activation in amyotrophic lateral sclerosis. *FASEB J.* **34**, 7225–7233 (2020).

59. Vériène, J., Fossouo, L. & Parker, J. A. Neurodegeneration in C. elegans models of ALS requires TIR-1/Sarm1 immune pathway activation in neurons. *Nat. Commun.* **6**, 7319 (2015).

60. Xue, Y. C., Feuer, R., Cashman, N. & Luo, H. Enteroviral infection: The forgotten link to amyotrophic lateral sclerosis? *Frontiers in Molecular Neuroscience* (2018). doi:10.3389/fnmol.2018.00063

61. S, S. *et al.* Interferon-γ Receptor 1 and GluR1 upregulated in motor neurons of symptomatic hSOD1G93A mice. *Eur. J. Neurosci.* **49**, 62–78 (2019).

62. AJ, L. & AA, A. The Dual Nature of Type I and Type II Interferons. *Front. Immunol.* **9**, (2018).

63. DA, C. & CS, R. The role of IFN-gamma in immune responses to viral infections of the central nervous system. *Cytokine Growth Factor Rev.* **13**, 441–454 (2002).

64. Driver, J. A. Inverse association between cancer and neurodegenerative disease: review of the epidemiologic and biological evidence. *Biogerontology* **15**, 547–557 (2014).

65. Mulligan, K. A. & Cheyette, B. N. R. Wnt Signaling in Vertebrate Neural Development and Function. *J. Neuroimmune Pharmacol.* **7**, 774 (2012).

Chapter 1

Amyotrophic Lateral Sclerosis, FUS and protein synthesis defects

Amanda Faria Assoni [1,2], Floris Foijer[2], Mayana Zatz[1]

1 Human Genome and Stem Cell Research Center, Institute of Biosciences, University of São Paulo, Cidade Universitária, São Paulo 055080-090, Brazil;

2 European Research Institute for the Biology of Ageing, University of Groningen, Groningen, 9713 AV, the Netherlands.

ABSTRACT:

Amyotrophic lateral sclerosis (ALS) is a neurodegenerative disease that mainly affects the motor system. It is a very heterogeneous disorder, so far more than 40 genes have been linked as responsible for ALS. The cause of motor neuron degeneration is not yet fully understood, but there is consensus in the literature that it is the result of a complex interplay of several pathogenic processes, which include alterations in nucleocytoplasmic transport, defects in transcription and splicing, altered formation and/or disassembly of stress granules and impaired proteostasis. These defects result in protein aggregation, impaired DNA repair, mitochondrial dysfunction and oxidative stress, oligodendrocyte degeneration, neuroinflammation, impaired axonal transport, impaired vesicular transport, excitotoxicity, as well as impaired calcium influx. We argue here that all of the above functions ultimately lead to defects in protein synthesis. Fused in Sarcoma (FUS) is one of the genes associated with ALS. It causes ALS type 6 when mutated, and is found miss localized to the cytoplasm in the motor neurons of sporadic ALS (SALS) patients (without FUS mutations). In addition, FUS plays a role in all cellular functions that are impaired in degenerating motor neurons. Moreover, ALS patients with FUS mutations present the first symptoms significantly earlier than in other forms of the disease. Therefore, the aim of this review is to further discuss ALS6, detail the cellular functions of FUS, and suggest that the localization of FUS, as well as protein synthesis rates, could be hallmarks of the ALS phenotype and thus good therapeutic targets.

1 - INTRODUCTION

Amyotrophic lateral sclerosis (ALS) is a neurodegenerative devastating disease with currently no efficient treatment. It affects superior motor neurons from the motor cortex and inferior motor neurons from the brainstem and spinal cord. It was first discovered in 1869 by the neurologist Jean-Martin Charcot (Charcot, 1869) but was brought to attention in 1939 when Lou Gehrig, one of the most beloved baseball players of all time, ended his career because of symptoms of the disease (Cook and Petrucelli, 2019).

ALS patients can be separated into two categories depending on the etiology of the disease: sporadic (SALS) or familial (FALS). Ninety percent of the cases fall into the SALS group, where the cause or causes of the disease are unknown. The remaining ten percent, in which more than one family member may be affected by the disease, have been linked to hereditary mutations. Familial cases of ALS are mostly inherited in a dominant pattern and are numbered according to the gene which is found mutated in each patient and currently, mutations in more than 40 genes such as superoxide dismutase 1 (*SOD1*) in ALS1, Vesicle-associated membrane protein (*VAPB*) in ALS8, TAR DNA binding protein 43 (*TARDBP*) in ALS10, and fused in sarcoma (*FUS*) in ALS6 have been identified in familial forms of ALS (Mathis et al., 2019).

The estimated worldwide mortality is about 30,000 patients a year (Petrov et al., 2017) but the incidence rate varies across continents. It is estimated to be 2–3 per 100,000 individuals in Europe and 0.7–0.8 per 100,000 individuals in Asia (Hardiman et al., 2017b). The mean age of onset of ALS is 65, but younger patients may be affected (van Es et al., 2017), and is usually fatal within 2–5 years (van den Berg, 2014) after disease onset.

ALS symptoms occur due to the degeneration of the motor neurons (MNs). The usual clinical presentation in ALS patients involves the motor symptoms such as muscle twitching, cramping, stiffness, and weakness. Overall, the patient's muscles become weaker as the disease progresses and muscle tissue atrophies. However, non-motor signs can be associated as well (as cognitive dysfunction, frontotemporal dementia, extrapyramidal features, among others). Therefore, ALS is currently widely considered as a multisystem degeneration (Mathis et al., 2019).

The causes of motor neuron degeneration are not completely understood, but it is agreed across literature that is a consequence of a complex interplay between multiple pathogenic processes. Amongst these processes, there are some features considered as ALS hallmarks (Figure1). They include alterations in nucleocytoplasmic transport, defects in transcription and splicing, altered stress granule (SG) formation and/or disassembly, impaired proteostasis that results in aggregating proteins, impaired DNA repair, mitochondrial dysfunction and oxidative stress, oligodendrocyte degeneration, neuroinflammation, defective axonal transport, defective vesicular transport, excitotoxicity, and disturbed calcium influx (Van

Damme et al., 2017).The result is a multifactorial disorder caused by a combination of multiple genes effects as well as by interactions between genes activity and the environment.

One key feature found in 90% of ALS cases is ubiquitinated protein inclusions , in which TAR DNA-binding protein 43 (TDP-43) is a major constituent (Blair et al., 2010). TDP-43, besides being intrinsically predisposed to aggregation, is also normally involved in mRNA processing. In this way, ALS-linked mutations intensify aggregates formation and increase their toxicity, which emphasizes the relation between disease onset and severity and cell proteostasis defects.

Due to its heterogeneity in diverse aspects, such as age at onset, progression rate and local of first symptoms initiation, researchers have been failing to find new therapeutic approaches.

In 2009, the first mutations in the *FUS* gene, also known as translocated in liposarcoma (*TLS*), an RNA-processing protein, were identified in ALS families, which was classified as ALS type six (ALS6). *FUS* mutations have also been described in sporadic cases linked to chromosome 16q12. (Kwiatkowski et al., 2009; Vance et al., 2009) (Belzil et al., 2009).

Importantly, ALS patients harboring *FUS* mutations present the first symptoms significantly earlier than in other forms of the disease. Indeed, more than 60% of *FUS* mutant patients present the first signs of disease before 45 years of age. Moreover, many ALS6 juvenile cases have been described with disease onset in the early twenties (Bäumer et al., 2010; Huang et al., 2011).

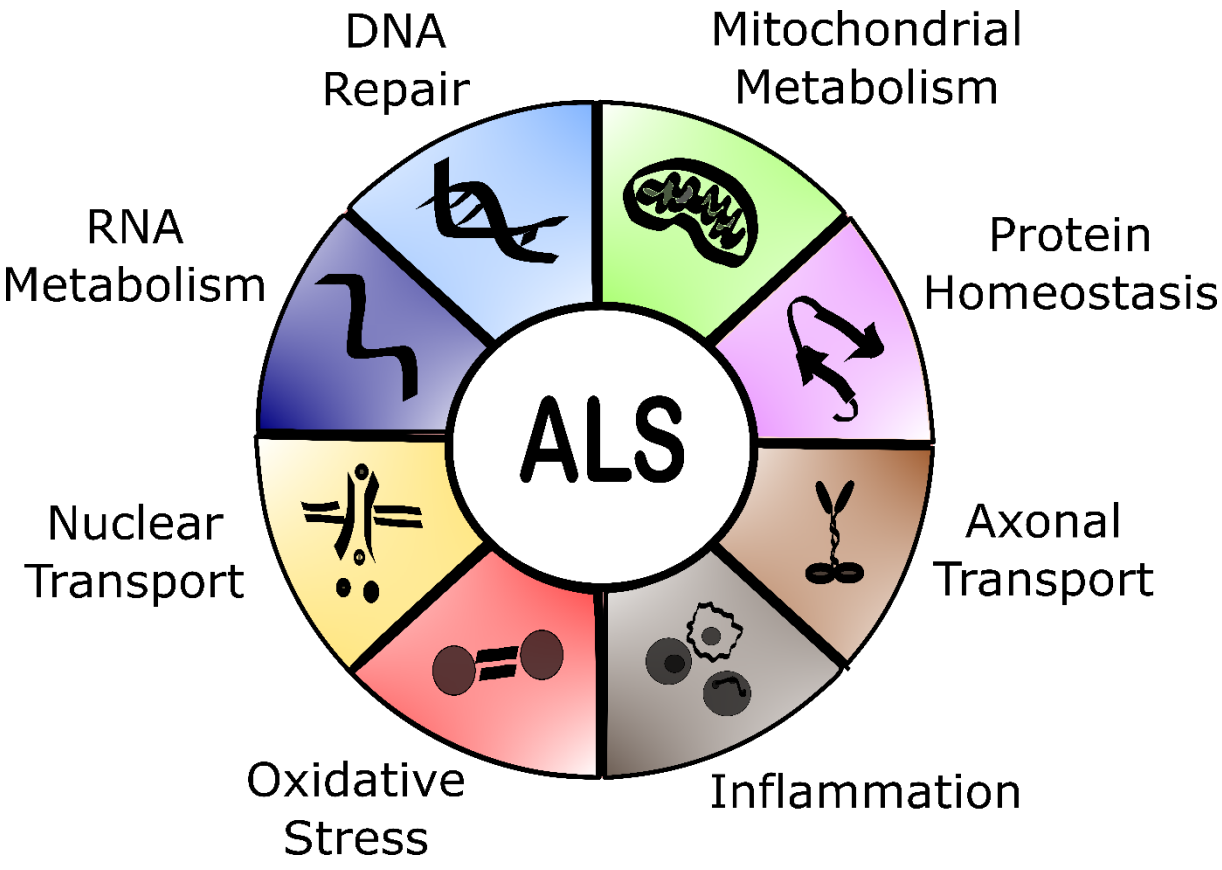

Figure 1: Functions altered in ALS.

FUS is also found mislocalized on MNs cytoplasm from SALS patients. Moreover, FUS is associated to all cellular functions found to be disturbed in the degenerating MNs. Therefore, the main objective of this review is to further discuss ALS6, detail FUS cellular functions, and suggest that FUS localization, as well as protein synthesis rates, might be hallmarks of the ALS phenotype and hence, potentially good therapy targets.

ALS 6

The clinical features of ALS6 are alike the classical ALS phenotype. Symptoms include progressive muscular atrophy, dysphagia, dysarthria, ultimately leading to respiratory failure. The neuropathological characteristics of these patients are upper and lower motor neurons degeneration, neuronal degeneration on the anterior horn of the spinal cord, mild pyramidal neuronal loss, dystrophic neurites, astrogliosis, and microglial activation. They generally present TDP43-negative and FUS-positive cytoplasmic inclusions in the motor neurons(Blair et al., 2010).

FUS was first identified in malignant human myxoid liposarcoma (a form of malignant tumor affecting adipose tissue), as a fused protein with CHOP (C/EBP homologous protein) a dominant transcription inhibitor. It was only in 2009 that the first cases of ALS with *FUS* mutations were described (Belzil et al., 2009).

Mutations in the *FUS* gene are responsible for both familial (4% of the cases) and sporadic forms of ALS (1% of the cases)(Kiernan et al., 2011). To date, more than 50 different mutations within the *FUS* gene were described to cause ALS. Most familial ALS mutations are found in the FUS C-terminal nuclear localization sequence (NLS), causing the mislocalization of the normally nuclear protein to the cytoplasm. Consequently, this leads to the accumulation of cytoplasmic protein inclusions (Gal et al., 2011). This suggests that either loss of FUS function in the nucleus or gain of toxic function in the cytoplasm are the disease-causing mechanisms(Reber et al., 2016), although both mechanisms are most likely acting together. However, to enhance our comprehension on the pathobiology underlying *FUS* mutations in ALS patients, understanding the role of wild-type (wt) *FUS* is crucial.

FUS protein

FUS is a 526 amino acid RNA binding protein (RBP) of the FET family that contains several functional domains including: Gln-Gly-Ser-Tyr-rich (or prion-like) domain; Gly-rich domain; Arg-Gly-Gly-rich domain; RNA recognition motif; zinc finger domain and a C-terminal nuclear localization signal (NLS)(Sama et al., 2014).

Under physiological conditions, FUS is mostly localized in the nucleus in neurons and is exclusively nuclear in glia(Andersson et al., 2008). Yet, FUS can be transported between the nucleus and cytoplasm (Brelstaff et al., 2011).

The exact function of FUS under normal physiological conditions is unclear. Some established roles include transcriptional control(Fujioka et al., 2013), RNA processing through splicing regulation of pre-mRNAs(Lagier-Tourenne et al., 2012), and DNA repair(Mastrocola et al., 2013), thus defining FUS as a pleiotropic protein. Concerning FUS structure, the N-terminus is most likely involved in transcriptional activation and C-terminus in protein and RNA binding.

There is evidence that FUS might have distinct roles during different stages throughout development. It was previously observed that FUS is ubiquitously expressed postnatally in mice and rats, but its expression decreases on most tissues by adult age, except in neuronal tissues(Huang et al., 2011). This suggests a role for FUS that is linked to neurodevelopment and neuronal homeostasis and highlights possible mechanisms of action of mutant FUS in ALS pathogenesis.

In addition, numerous studies report the role of FUS on diverse cellular processes, as summarized below.

FUS models

There are many available models to study FUS functions, which are reviewed in greater detail elsewhere(Guerrero et al., 2016). However, independently of the model itself, being drosophila, yeast, mice, or human cells, there is a particularly conserved characteristic of most FUS models that needs to be highlighted.

When overexpressed, wild-type human FUS induces cytoplasmic inclusions formation. The latter being a hallmark of ALS6 patients and, therefore, one of the putative causes of neuronal degeneration. Indeed, ALS phenotypes were recapitulated in a transgenic mouse model generated by using the pronuclear injection of wild type human *FUS* cloned into a modified mouse prion gene. The mice ended up overexpressing ubiquitously and constitutively wild type human FUS. These animals developed an aggressive ALS phenotype with early tremor outbreak followed by progressive posterior members paralysis and death after 12 weeks (Mitchell et al., 2013). The presence of neurological symptoms in a ubiquitously expressed system suggests that FUS plays an essential role in neural compartment ontogenesis which deserves further attention.

2- CELLULAR FUNCTIONS

FUS functions during embryonal development

When *FUS* is knocked down from frog embryos they fail to gastrulate and show mesodermal differentiation defects. In these embryos, it was demonstrated that intron retention in pre-

mRNA occurs in 3%–5% of all transcripts when FUS levels are decreased(Dichmann and Harland, 2012). Beyond that, it was shown that the C-terminal domain of FUS is not required for correct splicing, since embryos in which the FUS C-terminal part was missing developed normally and do not show miss splicing(Dichmann and Harland, 2012).

The consequences of disrupting *Fus* were also investigated in mice. Mice that are heterozygous for *Fus* mutation are indistinguishable from wild-type mice. On the other hand, homozygous *Fus* mutant mice fail to suckle and die within 16 hours of birth. Despite these *Fus*–/– mice develop normally (what the authors confirm with histology examination of major organs and tissues), *Fus* mutant mice do display genomic instability in their lymphocytes (Hicks et al., 2000).

Furthermore, *Fus* expression was previously analyzed in a longitudinal study in C57BL6 mice and Sprague-Dawley rats. High and ubiquitous levels of *FUS* mRNA were detected in neonate mice and rats but were significantly lower in most tissues in the adult rodents. Meanwhile, in adult individuals, FUS protein was undetectable in some peripheral organs such as skeletal muscles, liver, and kidney, but was constantly highly expressed in the central nervous system(Huang et al., 2011).

In summary, the studies discussed above suggest that during embryogenesis and in newborn developing tissues, FUS has an important role in mesoderm development due to its function in splicing. Of note, one copy of wild-type *FUS* is enough to sustain normal cellular functions during development as the heterozygotes show a wild type-like phenotype in neonatal rodents. However, homozygous mutations of *Fus* are lethal in mice.

Finally, *FUS* expression is maintained in the adult nervous tissue, and its functions are linked to neuronal homeostasis. FUS roles in adult cells are summarized below.

Genome maintenance

One of the reported roles for FUS is in the maintenance of genome integrity by having a role in DNA damage repair (DDR).

Previous reports provided evidence that FUS is recruited to sites of laser-induced DNA double-strand breaks (DSBs). This recruitment needs poly ADP-ribose polymerase (PARP) activity. The arginine/glycine-rich domains of FUS are responsible for the protein redistribution to the sites of DNA damage once these domains directly interact with PARP. In addition, depletion of FUS diminished DSB repair, decreasing both homologous recombination (HR) and non-homologous end-joining (NHEJ), implicating FUS as an upstream effector in both pathways(Mastrocola et al., 2013).

Furthermore, FUS localization after laser-induced DNA damage showed that recruitment of FUS to the damaged sites occurs earlier than for proteins with well-known roles in the DNA-repair process, including NBS1 (Nijmegen breakage syndrome-1), p-ATM (phosphorylated-ataxia telangiectasia mutated), γH2AX (phosphorylated histone 2 A.X), and Ku70(S.L. et al., 2014).

Specifically, in neurons, wild type FUS facilitates recruitment of XRCC1/DNA Ligase IIIα (LigIII) complex to oxidized genome sites and allow for base excision repair (BER). Consequently, insufficient nucleic FUS causes DNA nick ligation defects, which are toxic to MNs (Wang et al., 2018).

Many reports linked DNA repair defects to neurodegenerative diseases(Walker et al., 2017; Mitra et al., 2019; Kim et al., 2020). ALS patients display increased levels of the DNA damage marker γH2AX in cortical MNs (Wang et al., 2013). Similarly, MNs derived from induced pluripotent stem cells (iPSCs) with endogenous *FUS* mutations showed signs of DNA damage (Higelin et al., 2016).

When NHEJ and HR-mediated DNA repair capacity was measured in U2OS cells bearing different ALS-linked mutations, all the FUS mutants tested (R244C, R514S, H517Q, and R521C) had impaired HR-mediated DNA repair compared to wild- type FUS. However, localization of FUS variants either in the nucleus or in the cytoplasm did not correlate with HR activity. For example, the mutant FUS R244C was mostly identified in the nucleus, but exhibited a considerable decrease in HR, indicating that the loss of function of mutant FUS that caused defective HR is not simply a consequence of its absence from the nucleus. Overall, FUS mutants affected the HR DNA repair pathway more pronouncedly than NHEJ (Wang et al., 2013).

Familial cases of ALS that present mutations in the *FUS* gene show a reduced interaction within mutant FUS and HDAC1, causing defects in DDR and DNA repair (Wang et al., 2013). Indeed, in a transgenic mouse model expressing a frequent familial ALS-associated *FUS* mutation (FUS-R521C), mutant FUS proteins stably interact with wild type FUS, competing with HDAC1 and inhibiting HDAC1-FUS interactions. Consequently, FUS-R521C mice displayed increased DNA damage and a substantial decrease in dendritic growth and synaptic functions in the brain and spinal cord(Qiu et al., 2014).

FUS also participates in the cellular response to topoisomerase I (TOP1)-induced DNA breakage. When RNA polymerase II (Pol II) stops at sites of TOP1-induced DNA breaks, FUS relocalizes to the nucleolus. In this setting, *FUS*-mutant patient fibroblasts are more sensitive to TOP1-induced DNA breakage than wild type-*FUS* control fibroblasts(Martinez-Macias et al., 2019).

Overall, there is consistent evidence that FUS plays an important upstream role in the cellular response to diverse types of DNA damage induction (being TOP1, laser, or oxidative stress) and that it can recruit many DNA repair proteins. However, there is no consensus of whether FUS is more significant to the HR or NHEJ dependent DNA damage repair, but it seems to be enrolled in both pathways.

Regulation of gene expression

a. FUS and Post translation modifications on histone residues

Availability of DNA- therefore packing of nucleosomes- is expected to be important to transcription initiation. Post-translation modifications (PTMs) on histone residues can modulate nucleosome stability and dynamics and is one of the major mechanisms of gene expression control. Histone acetylation, methylation, and phosphorylation act in concert to modulate chromatin accessibility and FUS has been associated with deposition of all the mentioned modifications(Bennett et al., 2019). Recent evidence shows that alteration of the epigenetic landscape is one of the features that result in ALS pathology (Berson et al., 2018; Masala et al., 2018; Bennett et al., 2019).

Histone acetyl transferases (HATs) and histone deacetylases (HDACs) control histone acetylation in an antagonistic fashion. In a *FUS* overexpression model using HeLa cells, FUS was found binding to CBP/p300- a major HAT - and inhibiting its histone acetylation activity. This results in hypoacetylation of a region in proximity to the *CCND1* gene with reduction of cyclin D1expression, impairing progression through the cell cycle (Cui et al., 2018).

In a yeast model overexpressing human *FUS,* significantly reduced histone H3 lysine 14 and 56 (H3K14 and H3K56) acetylation levels were observed. These modifications are preserved in humans and acetylation of H3K14 is specifically found at actively transcribed genes promoters(Masala et al., 2018). Accordingly, FUS overexpression in this model presented reduced global RNA levels, another indication that histone hypoacetylation may reduce transcription (Chen et al., 2018).

Interestingly, HDAC inhibitors are arising as promising therapeutic strategies for ALS patients. Drugs inhibiting HDAC activity are used in the clinic as anticancer agents, showing that its administration is safe as a treatment for human diseases(McClure et al., 2018). Specifically for ALS, research is still ongoing and several steps are needed before clinical trials, but pre-clinical studies observed that treatment with different HDAC inhibitors decreased motor neuron degeneration in a *SOD1* mouse model (Ryu et al., 2005; Yoo and Ko, 2011).

Regarding ALS6, an *in-vitro* model using iPSC-derived MNs demonstrates that the genetic silencing and pharmacological inhibition of *HDAC6* were able to recover axonal transport problems caused by mutant *FUS*(Guo et al., 2017). Accordingly, transgenic mice overexpressing wild-type *FUS* ("Tg *FUS*+/+") had reduced histone acetylation. Continuous ACY-738 treatment (an HDAC inhibitor able to surpass the blood-brain barrier) in this mice reestablished global histone acetylation, ameliorated the motor degeneration, and significantly extended transgenic mice life span (Rossaert et al., 2019).

FUS overexpression also caused asymmetric dimethylation on arginine 3 of histone 4. Increased expression of FUS is associated with decreased levels of H4R3me2asym, which is known to promote histone acetylation and gene transcription(Litt et al., 2009). This feature is possibly related to the Protein arginine N-methyltransferase 1 (PRMT1),which is responsible for H4R3me2asym (Scaramuzzino et al., 2013). In a mouse model of ALS with FUS-R521C mutation, the interaction of mutant FUS with PRMT1 was responsible for PRMT1 activity inhibition. It was observed a reduction of H4R3me2asym in this model, ultimately leading to

transcriptional silencing. When PRMT1 was overexpressed the phenotype caused by the mutation was decreased (Tibshirani et al.).

FUS is also capable of modulating phosphorylation on histone residues. In NSC-34 and HEK-293T cells, *FUS* knockdown (KD) through RNA interference induced H3 phosphorylation. *FUS*-KD decreased cell proliferation and modulated expression levels of genes involved in cell cycle regulation, cytoskeletal organization, and oxidative stress(Ward et al., 2014).

Results relating FUS to the regulation of PTMs on histone residues seem to agree with the literature. Overall, mutations result in the downregulation in global gene transcription compared to controls.

b. FUS and miRNA regulation

Another mechanism by which FUS influences gene expression is through micro-RNA regulation. Micro RNAs (miRNAs) are small non-coding RNAs that can change the expression of many different mRNAs with high specificity (Rusk, 2008). The miRNA base pairing to mRNA untranslated region (UTR) sequences is responsible for target specificity. This binding results in mRNA destabilization or translation inhibition(Vasudevan et al., 2007).

One of the first pieces of evidence that FUS is capable of regulating miRNAs was demonstrated when FUS was identified as a protein that contributes to the biogenesis of a subset of miRNAs, including miRNAs with neuronal functions, differentiation, and synaptogenesis. FUS is recruited to the chromatin at miRNA transcription sites and binds their pre-miRNAs. Moreover, depletion of FUS leads to a decrease in Drosha (the main nuclease responsible for miRNA processing initiation step in the nucleus) levels at chromatin loci(Morlando et al., 2012).

ALS mutations were also recognized as responsible for general miRNA deregulation(De Santis et al., 2017; Zhang et al., 2018). Analysis of the whole transcriptome of isogenic iPSC-derived human motor neurons expressing either *FUS* wild-type or mutant identified several miRNAs deregulated on the mutant MNs, including miR-375, previously related to motor neuron survival(De Santis et al., 2017). Another ALS-related FUS mutation, FUS-R495X, also impairs miRNA-mediated gene silencing (Zhang et al., 2018). One mechanism by which FUS interferes with miRNA gene expression regulation is by directly binding the core miRNA-induced silencing complex (miRISC) component AGO2 and by directly interacting with miRNA and mRNA targets(Zhang et al., 2018).

Collectively, literature results strongly suggest a role of FUS in regulating the activity of miRNA-mediated gene silencing by directly binding miRISC components and consequently playing an important part in neuronal differentiation and maintenance in ALS patients.

c. FUS and splicing

Finally, one important feature of FUS regarding the regulation of gene expression is its role in splicing. FUS binds to several transcripts within the brain (Orozco and Edbauer, 2013). The exact mechanism by which it regulates splicing is unknown, although crosslinking and immunoprecipitation (iCLIP) in mouse brains showed that FUS binds along the full length of emerging RNAs and persist bound to the pre-mRNAs until splicing termination (Rogelj et al., 2012).

FUS also binds important spliceosome components. U1 snRNP is one of the most abundant FUS interactors. Components of U1 snRNP core particle (as Sm proteins and U1 snRNA) mislocalize with FUS to the cytoplasm in fibroblast of ALS6 patients with FUS NLS mutations. The mislocalization of snRNP core proteins seems to be dependent on the RRM domain of FUS. Moreover, FUS and U1 snRNP proteins KD caused motor axon truncations in zebrafish (Yu et al., 2015). FUS binding to U11 snRNP regulates the removal mainly of minor introns. In neuroblastoma cells, a *FUS* knockout (KO) disturbed the splicing of minor intron-containing mRNAs. Moreover, cytoplasmic aggregates formed by an ALS-associated FUS mutant traps U11 and U12 snRNAs in these aggregates, inhibiting the splicing of minor introns (Reber et al., 2016). Additionally, association of FUS to RNA polymerase II (RNAP II) is indispensable to U1 snRNP and RNAP II interaction: It was shown that proper splicing requires FUS presence during RNAP II transcription reaction, thus, coupling transcription to splicing (Yu and Reed, 2015).

Regarding alternative splicing, FUS-binding sites are present around the alternatively spliced exons and tend to form stable secondary structures. Moreover, FUS is commonly present in the antisense RNA strand at the promoter regions, which downregulates transcription of the coding strand (Ishigaki et al., 2012).

It is not clear whether mutations in the *FUS* gene causes gain or loss of functions on the FUS protein. To compare the mutation-induced changes to actual loss of function consequences (represented by the knockouts or knockdowns previously reported), knock-in models were created and high depth RNA-sequencing data on *FUS* mutants was performed in parallel to *FUS* KO. Still, a widespread loss of function on gene expression and splicing was caused by *FUS* ALS mutations, being RNA binding proteins preferential targets of this effect. Similarly, mutant FUS induces intron retention through RNA binding, even in FUS itself (Humphrey et al., 2019).

The brain proteomic diversity is a major consequence of alternative splicing spatial and temporal control (Grabowski, 2011), therefore highlighting the relevance of this mechanism to this specific tissue correct function. FUS is required for splicing events to occur but can also inhibit splicing and alternative splicing. Thus, it indicates that FUS might regulate splicing events and transcription in a position and interactor-dependent manner, which is of extreme importance for proper neuronal tissue homeostasis.

FUS and SG

ALS is considered to have multifactorial pathogenic mechanisms and SGs are one of the most well-studied hallmarks that can be influenced by epigenetic factors. Therefore, many modifiers of SG assembly are under research(Matus et al., 2014; Coyne et al., 2015; Casci et al., 2019; Rossi et al., 2020).

FUS is found within SGs and aggregation of FUS protein is believed to have a fundamental role in ALS pathogenesis, since FUS aggregates are found in the cytoplasm of motor neurons in post mortem sections of sporadic ALS patients(Tyzack et al., 2019).

The role of FUS in SGs was intensely studied and reviewed (Sama et al., 2014; Japtok et al., 2015; Marrone et al., 2018; Birsa et al., 2020). The main conclusions to these analyses are mentioned below.

Cytoplasmic granules

FUS is a member of ribonucleoprotein particles *(*RNPs), which are RNA and RNA-binding proteins (RBPs) complexes and can have different roles (Stefl et al., 2005). RBPs can form cytoplasmic granules, that are membraneless organelles and include different kinds of granules. Amongst them are processing bodies (p-bodies), transport and stress granules, (SGs), with the latter being RNA-containing cytoplasmic foci generated once the cell is exposed to stress. The SGs are assembled to allow the cell to handle cellular stresses by delaying mRNA translation and directing synthesis towards cytoprotective proteins. After the stress is relieved, these structures are disassembled(Nostramo et al., 2019). Most of the proteins that have been described in these structures are RNA binding proteins (RBPs) or are proteins involved in RNA metabolism and translation(Anderson and Kedersha, 2008).

FUS is one of these RBPs identified within both SGs and P-bodies and there is a consensus that the amount of FUS in granules depends on how much of the protein is mislocalized to the cytoplasm (Lenzi et al., 2015). Both wild type and mutated forms of FUS are found in SGs(Jain et al., 2016). However, FUS mutants are more present in these structures when compared to wild type (Bosco et al., 2010; Lenzi et al., 2015). It is worth pointing out that FUS is not required for the SG assembly once it is not impaired by endogenous wild-type *FUS* knockdown (Aulas et al., 2012). However, many results indicate that mutations in FUS make the protein become aggregation prone and alter many aspects of SGs, including granule size (Baron et al., 2013), abundance, assembly and disassembly speed (Marrone et al., 2018), and biophysical properties, such as viscosity and stiffness (Baron et al., 2013; Marrone et al., 2018). Although it is not a consensus whether mutations on FUS make SG more or less dynamic.

Most studies use oxidative stress to induce SG assembly and compare wild-type to mutated FUS functions. Regarding FUS^{wt} function in different cellular stress responses, FUS exhibits a vigorous response to hyper osmolar stress. Hyper osmolar stress causes an immediate nuclear FUS redistribution to the cytoplasm, with transient nuclear clearance and loss of

function. When in the cytoplasm, it integrates into stress granules. But, this redistribution is independent of SG formation, once FUS does not seem to migrate to the cytoplasm as a response to others stress granule assembly inducers, such as sodium arsenite, hydrogen peroxide, thapsigargin, or heat shock (Sama et al., 2013).

FUS translocation is also modulated by methyltransferase activity, Transportin 1, and is potentiated by transcriptional inhibition(Dormann et al., 2010). Interestingly, reduced *FUS* expression causes cell viability loss in response to hyperosmolar stress, indicating a protective role for FUS in this context (Sama et al., 2013).

The role of SG within the cells and how it can impact disease progression is not completely understood. How could a pro-survival trait maybe increase toxic protein aggregation? One accepted model is that SGs may aid the formation of cytoplasmic aggregates in ALS, while excessive SG assembly or defective SG clearance induced by mutations or cellular conditions increase SG persistence, consequently generating toxic aggregates (Sweeney et al., 2017). It was previously shown that repetitive assembly of SGs is toxic to motor neurons and is succeeded by SGs alteration into cytoplasmic inclusions similar to those found on the ALS pathology (Zhang et al., 2019). On the other hand, there is the possibility that SGs do not play a role in the formation of persistent aggregates or even that SGs present a protective effect.

Pointing towards the latter hypothesis, when FUS domains responsible for RNA recognition and binding are disrupted, consequently decreasing SG assembly, it highly increases the formation of structures comparable to aggresomes (Shelkovnikova et al., 2013). Also, Protein ubiquilin 2 (UBQLN2) was shown to maintain the solubility of FUS in response to stress, increasing FUS–RNA complex formation and, therefore, acting as a negative regulator of SG formation (Alexander et al., 2018). FUS-mediated neurodegeneration is also modified by muscleblind (MBL) in an ALS6 drosophila model: MBL overexpression was able to decrease cytoplasmic mislocalization of mutant FUS and accumulation in stress granules (Casci et al., 2019). This evidence lead us to believe that the stress granules act as a protective feature when cells are stressed by aggregating FUS because when FUS is soluble in the cytoplasm it is toxic for cells. However, when SGs become permanent aggregates, they become toxic for cells.

Besides these specific proteins that can modulate mutated FUS localization and solubility, studies report that enhancing autophagy reduces cytoplasmic FUS, decreases the number of stress granules, and rescues motor function (Ryu et al., 2014).

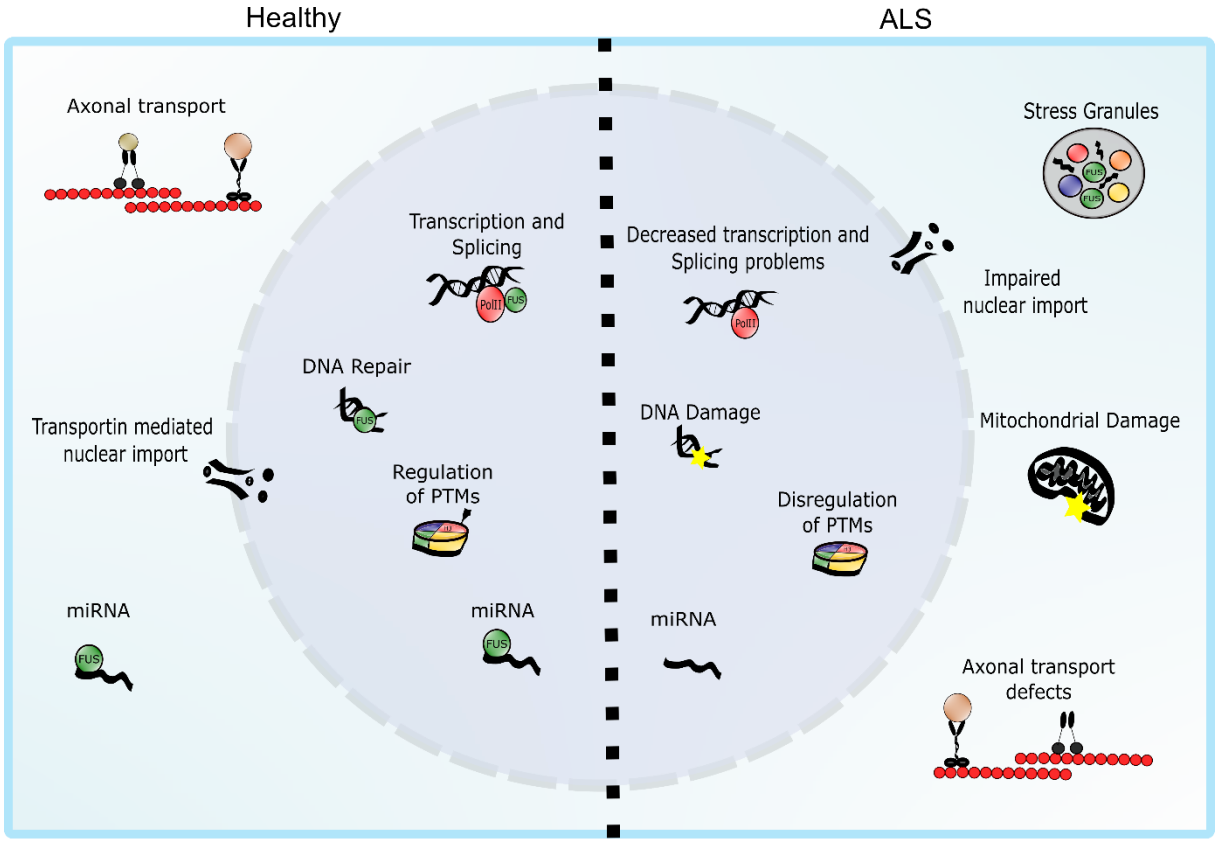

Figure 2: FUS functions in healthy versus diseased cells.

Lastly, multiple viruses can induce SG assembly (McCormick and Khaperskyy, 2017). Several studies have reported epidemiological and clinical evidence connecting viral infection and ALS (Limongi and Baldelli, 2016; Celeste and Miller, 2018a; Xue et al., 2018). For example, it is known that individuals infected with HIV or human T cell leukemia virus 1 develop neurological disorders with clinical features of ALS (Verma and Berger, 2006). Accordingly, synthetic dsRNA poly (I:C) (a viral mimic) or an SG-inducing virus causes the persistent presence of mutant FUS granules. These inclusions sequester the autophagy receptor optineurin and nucleocytoplasmic transport factors. Moreover, mutant *FUS*-expressing cells are more susceptible to dsRNA toxicity, suggesting that the antiviral immune response is likely a second hit for FUS pathological phenotype (Shelkovnikova et al., 2019).

PTMs on FUS protein itself can also influence ALS pathology. Post-translational modifications of FUS can occur at different positions, affecting its localization and aggregation propensity. Although the roles of PTMs in FUS aggregation pathology remain unresolved and depends on the type of PTM and interactors, several putative PTM share overlapping sites with disease-associated mutations, which could indicate their relevance to the development of ALS phenotype(Rhoads et al., 2018).
In summary, wild-type FUS seems to have protective effects when cells suffer from stress exposure. While mutant-FUS seems to have a gain-of-toxic mechanism, modifying the

dynamic properties of stress granules (Figure 2) (Baron et al., 2013). Overall, disease pathogenesis could be a result of the presence of FUS in the cytoplasm and the assembly of FUS protein into stress granules, acting as an interface between genetic susceptibility and environmental factors (Aulas and Velde, 2015).

Protein synthesis

Subcellular localization of proteins is essential to the establishment of the body axis, cell migration, synaptic plasticity, and other biological processes in neurons, the first affected cells in ALS. Three processes control protein localization: transport, localization of mRNAs, and local translation. A comparison between isolated cell bodies and neurites of neurons differentiated from mouse embryonic stem cells, identified with a global analysis of protein presence, RNA expression, and translation rates that mRNA position is the primary mechanism defining protein localization in neurites. (Zappulo et al., 2017).

Localization of mRNAs is highly conserved in eukaryotes (Eliscovich and Singer, 2017) and mechanisms of axonal mRNA translation might be the link to axon guidance, survival, regeneration, and neurological disorders (Jung et al., 2012).

Protein synthesis, proteasome, or autophagy activation are energetically expensive processes and ribosome quality control can prevent unnecessary translation. Another way of avoiding this energetic waste is by nonsense-mediated decay (NMD), which distinguishes and erases mRNAs with premature termination codons (PTCs)(Karamyshev and Karamysheva, 2018). In this way, the NMD pathway regulates protein translation. It was found that in N2a cells expressing mutant FUS, NMD was altered, meaning that NMD-promoting factors UPF1 and UPF3b were increased, while a negative NMD regulator, UPF3a, was decreased, resulting in hyperactivation of NMD (Kamelgarn et al., 2018), consequently decreasing protein synthesis due to lack of mRNA.

In mice, either expressing both mouse and human FUS or only full-length human FUS, ALS-related mutant FUS and not wild type accumulated in the axons in hippocampal neurons and sciatic nerves and caused decreased intra-axonal protein synthesis. Unlike in other models, this specific study showed that mutations did not cause FUS cytoplasmic aggregation, as well as did not alter FUS-bound pre-mRNAs splicing, but rather, induced a gain of toxic function that resulted in suppression of intra-axonal translation, synaptic dysfunction, and progressive motor degeneration (López-Erauskin et al., 2018).

In cultured neurons differentiated from mouse embryonic stem cells bearing an R495X FUS mutation, analysis by CLIP-Seq and Ribo-seq showed that wild type FUS binds on precursor mRNAs (pre-mRNAs), while mutated FUS binds mature mRNAs. Surprisingly, this binding did not change the translation levels of the attached mRNAs. However, it was found that R495X decreases mitochondria function-associated genes translation, resulting in an important decrease in mitochondrial size (Nakaya and Maragkakis, 2018).

Beyond that, translation inhibition in both mouse and human MNs could be achieved by mutant FUS expression at physiological levels. Mutant FUS did not act directly on the translation machinery but was found to form cytoplasmic inclusions containing FMRP (a neurodegeneration-associated RBP involved in translation regulation). This causes the repression of translation *in vitro* and *in vivo*(de la Fuente and Emc, 2020).

The role of wild-type FUS in protein synthesis is yet to be completely understood and it may be an exclusive function of the mutant forms due to their mislocalization in the cytoplasm. Nonetheless, protein synthesis suppression seems to be a common consequence of *FUS* mutations.

It is not clear whether the decreased translation is protective or harmful in the neurodegeneration context. However, the phosphorylation of eukaryotic initiation factor 2α (eIF2α) is one of the most consistent observations related to neurodegenerative diseases. eIF2α is a translation initiation factor, involved in cap-dependent protein translation and its phosphorylated form causes global translation suppression (Bond et al., 2020).

In summary, there is accumulating evidence about the importance of protein synthesis to the ALS disease onset and progression. Therefore, further investigation on the role of translation rates on ALS phenotypes can help increase understanding of the disease pathways and the development of further and more efficient therapeutics.

3 - DISCUSSION AND CONCLUSION

There is a variety of molecular mechanisms underlying neurodegenerative pathogenesis, hampering the development of effective therapies for these disorders. Protein synthesis is a major process that controls cell behavior since proteins are the functional molecules that determine cell types and functions(Kim, 2019). Accordingly, understanding and targeting protein synthesis defects might help stop disease progression.

All processes in which mutant *FUS* leads to aberrations ultimately change protein translation rates (Figure 3):

-Wild type *FUS* is relevant for the DNA damage repair mechanism and ALS patients have higher amount of damage in the DNA, as previously discussed. It is known that DNA damage inhibits protein translation. For example, damage in the DNA caused by UVB inhibits overall protein synthesis, and causes translational reprogramming, allowing the selective synthesis of DDR proteins, such as ERCC1, ERCC5, DDB1, XPA, XPD, and OGG1 mRNAs (Powley et al., 2009). Also, ionizing radiation (IR) that causes DNA double-strand breaks (DSBs), results in changes in levels of proteins involved in autophagy, proteasome degradation, mitochondrial proteins, and a striking downregulation of ribosomal and translation factors that rapidly changes the translation pattern after IR (Bennetzen et al., 2018).

-FUS roles in transcription involving PTMs on histones decrease global RNA levels, which could also result in the decrease of global translation because of the lack of mRNA availability.

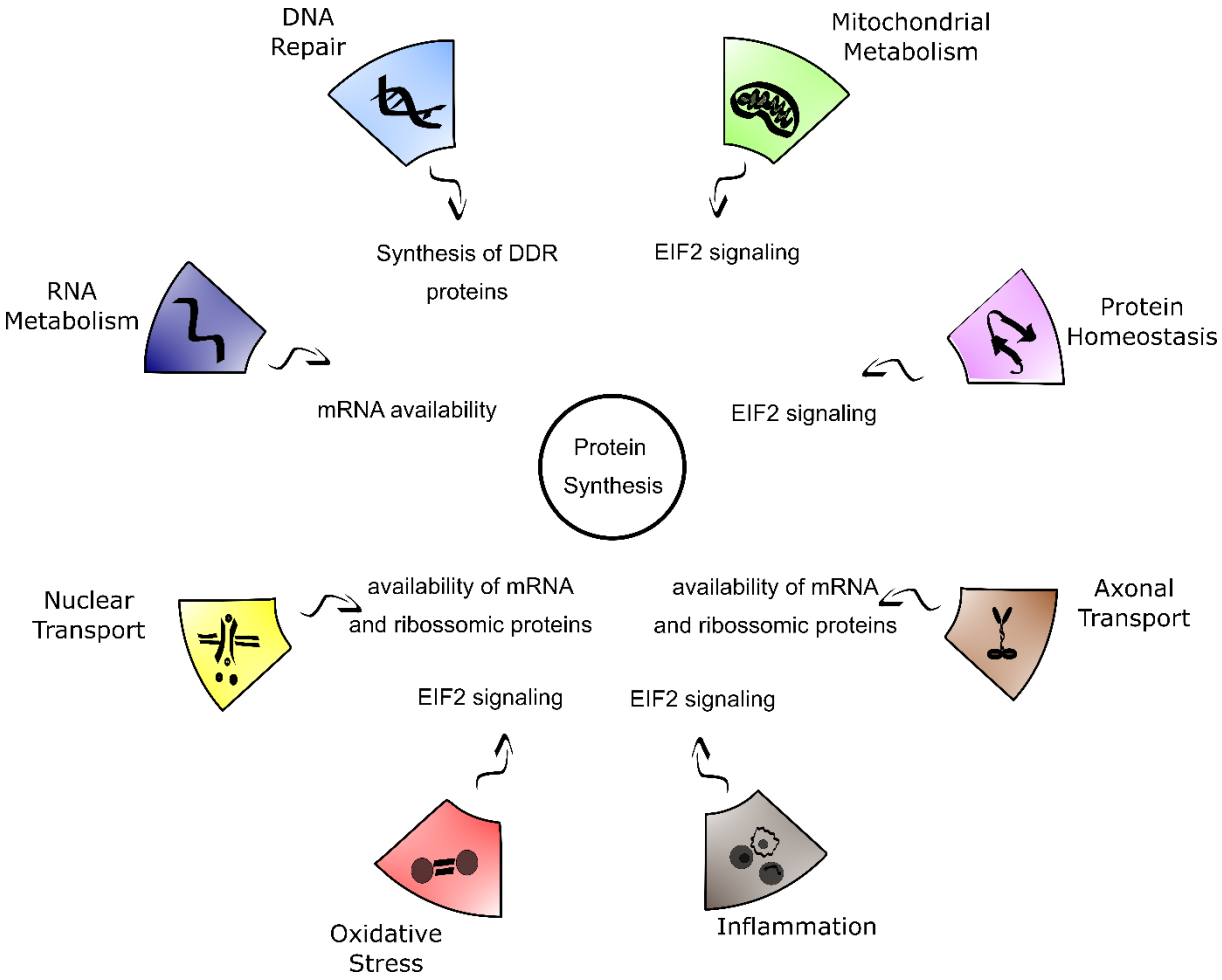

Figure 3: All altered functions in ALS converging into protein synthesis defects.

-Disturbing splicing events can affect mRNA availability and localization, and rates of protein translation, consequently. It was previously shown that in mammalian cells, spliced mRNAs generate greater protein amounts per mRNA molecule than identical mRNAs not made by splicing. This correlates with augmented polysome association with spliced mRNAs, possibly due to exon junction complexes (EJCs) deposition(Nott et al., 2004).

- Stress granules' central role is changing synthesis towards cytoprotective proteins by delaying mRNA translation. Their permanent presence and translation suppression might be the trigger to cytotoxicity in a late-onset disease like ALS.

Many efforts were made to understand the main and common processes underlying the pathobiology of all ALS types. Synaptic loss is a crucial event in neurodegenerative disorders and should be considered as one of these overlapping processes. One of the several

mechanisms involved in sustaining synapses integrity is local protein translation, as it can directly affect the synaptic formation, communication, and maintenance. Local protein synthesis is regulated by RNA-binding proteins and their association with RNA granules. Consequently, the loss of synapses in neurodegenerative diseases could be a result of RNA metabolism malfunction and further investigation into RBPs like FUS could lead to important insights into how their disruption can cause disease onset(Sephton and Yu, 2015).

In conclusion, FUS is a protein related to many cellular processes, and there is growing evidence that its dysfunction might be involved in the mechanism of the pathogenesis of not only ALS6 but other types of familial and sporadic ALS (Tyzack et al., 2019). Here we argue that the mechanisms disrupted by FUS mutations ultimately result in the decrease of protein synthesis. Further studies should focus on translational rates to better understand if they are a cause or a consequence of the ALS phenotype and propose alternative therapies aiming to delay the disease onset and increase patients' survival.

4 - FUNDING AND ACKNOWLEDGEMENTS

This work was supported by the Fundação de Amparo à Pesquisa do Estado de São Paulo (FAPESP), Conselho Nacional de Desenvolvimento Científico e Tecnológico (CNPq) and an Able Tasman fellowship to AA awarded by the University of Groningen.

5 - CONFLICT OF INTEREST DISCLOSURE

The authors declare that the research was conducted in the absence of any commercial or financial relationships that could be construed as a potential conflict of interest.

6 - REFERENCES

1. Charcot, J.-M. *Deux cas d'atrophie musculaire progressive : avec leÌ• sions de la substance grise et des faisceaux anteÌ• rolateÌ• raux de la moelle eÌ• pinieÌ€ re*. (Masson, 1869).

2. Cook, C. & Petrucelli, L. Genetic Convergence Brings Clarity to the Enigmatic Red Line in ALS. *Neuron* **101**, 1057–1069 (2019).

3. Mathis, S., Goizet, C., Soulages, A., Vallat, J.-M. & Masson, G. Le. Genetics of amyotrophic lateral sclerosis: A review. *J. Neurol. Sci.* **399**, 217–226 (2019).

4. Petrov, D., Mansfield, C., Moussy, A. & Hermine, O. ALS clinical trials review: 20 years of failure. Are we any closer to registering a new treatment? *Frontiers in Aging Neuroscience* **9**, 68 (2017).

5. Hardiman, O. *et al.* Amyotrophic lateral sclerosis. *Nature Reviews Disease Primers* **3**, (2017).

6. van Es, M. A. *et al.* Amyotrophic lateral sclerosis. *The Lancet* **390**, 2084–2098 (2017).

7. van den Berg, L. H. Therapy of amyotrophic lateral sclerosis remains a challenge. *The Lancet Neurology* **13**, 1062–1063 (2014).

8. Van Damme, P., Robberecht, W. & Van Den Bosch, L. Modelling amyotrophic lateral sclerosis: Progress and possibilities. *DMM Disease Models and Mechanisms* **10**, 537–549 (2017).

9. Blair, I. P. *et al.* FUS mutations in amyotrophic lateral sclerosis: Clinical, pathological, neurophysiological and genetic analysis. *J. Neurol. Neurosurg. Psychiatry* **81**, 639–645 (2010).

10. Vance, C. *et al.* Mutations in FUS, an RNA processing protein, cause familial amyotrophic lateral sclerosis type 6. *Science (80-.).* **323**, 1208–1211 (2009).

11. Kwiatkowski, T. J. *et al.* Mutations in the FUS/TLS Gene on Chromosome 16 Cause Familial Amyotrophic Lateral Sclerosis. *Science (80-.).* **323**, 1205–1208 (2009).

12. Belzil, V. V. *et al.* Mutations in FUS cause FALS and SALS in French and French Canadian populations. *Neurology* **73**, 1176–1179 (2009).

13. Bäumer, D. *et al.* Juvenile ALS with basophilic inclusions is a FUS proteinopathy with FUS mutations. *Neurology* **75**, 611–618 (2010).

14. Huang, C. *et al.* FUS Transgenic Rats Develop the Phenotypes of Amyotrophic Lateral Sclerosis and Frontotemporal Lobar Degeneration. *PLoS Genet.* **7**, e1002011 (2011).

15. Kiernan, M. C. *et al.* Amyotrophic lateral sclerosis. in *The Lancet* **377**, 942–955 (2011).

16. Gal, J. *et al.* Nuclear localization sequence of FUS and induction of stress granules by ALS mutants. *Neurobiol. Aging* **32**, 2323.e27-2323.e40 (2011).

17. Reber, S. *et al.* Minor intron splicing is regulated by FUS and affected by ALS-associated FUS mutants. *EMBO J.* **35**, 1504–1521 (2016).

18. Sama, R. R. anjit. K., Ward, C. L. & Bosco, D. A. Functions of FUS/TLS from DNA repair to stress response: implications for ALS. *ASN neuro* **6**, (2014).

19. Andersson, M. K. *et al.* The multifunctional FUS, EWS and TAF15 proto-oncoproteins show cell type-specific expression patterns and involvement in cell spreading and stress response. *BMC Cell Biol.* **9**, 37 (2008).

20. Brelstaff, J. *et al.* Transportin1: A marker of FTLD-FUS. *Acta Neuropathol.* **122**, 591–600 (2011).

21. Fujioka, Y. *et al.* FUS-regulated region- and cell-type-specific transcriptome is associated with cell selectivity in ALS/FTLD. *Sci. Rep.* **3**, 2388 (2013).

22. Lagier-Tourenne, C. *et al.* Divergent roles of ALS-linked proteins FUS/TLS and TDP-43 intersect in processing long pre-mRNAs. *Nat. Neurosci.* **15**, 1488–1497 (2012).

23. Mastrocola, A. S., Kim, S. H., Trinh, A. T., Rodenkirch, L. A. & Tibbetts, R. S. The RNA-binding protein fused in sarcoma (FUS) functions downstream of poly(ADP-ribose) polymerase (PARP) in response to DNA damage. *J. Biol. Chem.* **288**, 24731–24741 (2013).

24. Guerrero, E. N. *et al.* TDP-43/FUS in motor neuron disease: Complexity and challenges. *Progress in Neurobiology* (2016). doi:10.1016/j.pneurobio.2016.09.004

25. Mitchell, J. C. *et al.* Overexpression of human wild-type FUS causes progressive motor neuron degeneration in an age- and dose-dependent fashion. *Acta Neuropathol.* **125**, 273–288 (2013).

26. Dichmann, D. S. & Harland, R. M. fus/TLS orchestrates splicing of developmental regulators during gastrulation. *Genes Dev.* **26**, 1351–63 (2012).

27. Hicks, G. G. *et al.* Fus deficiency in mice results in defective B-lymphocyte development and activation, high levels of chromosomal instability and perinatal death. *Nat. Genet.* **24**, 175–179 (2000).

28. S.L., R. *et al.* PARP-1 dependent recruitment of the amyotrophic lateral sclerosis-associated protein FUS/TLS to sites of oxidative DNA damage. *Nucleic Acids Res.* **42**, 307–314 (2014).

29. Wang, H. *et al.* Mutant FUS causes DNA ligation defects to inhibit oxidative damage repair in Amyotrophic Lateral Sclerosis. *Nat. Commun.* **9**, 3683 (2018).

30. Kim, B. W., Jeong, Y. E., Wong, M. & Martin, L. J. DNA damage accumulates and responses are engaged in human ALS brain and spinal motor neurons and DNA repair is activatable in iPSC-derived motor neurons with SOD1 mutations. *Acta Neuropathol. Commun.* (2020). doi:10.1186/s40478-019-0874-4

31. Mitra, J. *et al.* Motor neuron disease-associated loss of nuclear TDP-43 is linked to DNA double-strand break repair defects. *Proc. Natl. Acad. Sci. U. S. A.* (2019). doi:10.1073/pnas.1818415116

32. Walker, C. *et al.* C9orf72 expansion disrupts ATM-mediated chromosomal break repair. *Nat. Neurosci.* (2017). doi:10.1038/nn.4604

33. Wang, W. Y. *et al.* Interaction of FUS and HDAC1 regulates DNA damage response and repair in neurons. *Nat. Neurosci.* **16**, 1383–1391 (2013).

34. Higelin, J. *et al.* FUS Mislocalization and Vulnerability to DNA Damage in ALS Patients Derived hiPSCs and Aging Motoneurons. *Front. Cell. Neurosci.* **10**, (2016).

35. Qiu, H. *et al.* ALS-associated mutation FUS-R521C causes DNA damage and RNA splicing defects. *J. Clin. Invest.* **124**, 981–999 (2014).

36. Martinez-Macias, M. I. *et al.* FUS (fused in sarcoma) is a component of the cellular response to topoisomerase I-induced DNA breakage and transcriptional stress. *Life Sci. alliance* **2**, (2019).

37. Bennett, S. A., Tanaz, R., Cobos, S. N., Torrente, M. P. & Torrente Brooklyn, M. P. *Epigenetics in amyotrophic lateral sclerosis: a role for histone post-translational modifications in neurodegenerative disease*. *Translational Research* **204**, 19–30 (2019).

38. Masala, A. *et al.* Epigenetic Changes Associated with the Expression of Amyotrophic Lateral Sclerosis (ALS) Causing Genes. *Neuroscience* **390**, 1–11 (2018).

39. Berson, A., Nativio, R., Berger, S. L. & Bonini, N. M. Epigenetic Regulation in Neurodegenerative Diseases. *Trends in Neurosciences* (2018). doi:10.1016/j.tins.2018.05.005

40. Cui, W., Yoneda, R., Ueda, N. & Kurokawa, R. Arginine methylation of translocated in liposarcoma (TLS) inhibits its binding to long noncoding RNA, abrogating TLS-mediated repression of CBP/p300 activity. *J. Biol. Chem.* **293**, 10937–10948 (2018).

41. Chen, K. *et al.* Neurodegenerative Disease Proteinopathies Are Connected to Distinct Histone Post-translational Modification Landscapes. *ACS Chem. Neurosci.* **9**, 938–948 (2018).

42. McClure, J. J., Li, X. & Chou, C. J. Advances and Challenges of HDAC Inhibitors in Cancer Therapeutics. in *Advances in Cancer Research* (2018). doi:10.1016/bs.acr.2018.02.006

43. Ryu, H. *et al.* Sodium phenylbutyrate prolongs survival and regulates expression of anti-apoptotic genes in transgenic amyotrophic lateral sclerosis mice. *J. Neurochem.* **93**, 1087–1098 (2005).

44. Yoo, Y. E. & Ko, C. P. Treatment with trichostatin A initiated after disease onset delays disease progression and increases survival in a mouse model of amyotrophic lateral sclerosis. *Exp. Neurol.* **231**, 147–159 (2011).

45. Guo, W. *et al.* HDAC6 inhibition reverses axonal transport defects in motor neurons derived from FUS-ALS patients. *Nat. Commun.* **8**, 861 (2017).

46. Rossaert, E. *et al.* Restoration of histone acetylation ameliorates disease and metabolic abnormalities in a FUS mouse model. *Acta Neuropathol. Commun.* **7**, 107 (2019).

47. Litt, M., Qiu, Y. & Huang, S. Histone arginine methylations: Their roles in chromatin dynamics and transcriptional regulation. *Bioscience Reports* **29**, 131–141 (2009).

48. Scaramuzzino, C. *et al.* Protein Arginine Methyltransferase 1 and 8 Interact with FUS to Modify Its Sub-Cellular Distribution and Toxicity *In vitro* and In Vivo. *PLoS One* **8**, (2013).

49. Tibshirani, M. *et al.* Cytoplasmic sequestration of FUS/TLS associated with ALS alters histone marks through loss of nuclear protein arginine methyltransferase 1. doi:10.1093/hmg/ddu494

50. Ward, C. L. *et al.* A loss of FUS/TLS function leads to impaired cellular proliferation. *Cell Death Dis.* **5**, (2014).

51. Rusk, N. When microRNAs activate translation. *Nat. Methods* **5**, 122–123 (2008).

52. Vasudevan, S., Tong, Y. & Steitz, J. A. Switching from Repression to Activation:

MicroRNAs Can Up-Regulate Translation. *Science (80-.).* **318**, 1931–1934 (2007).

53. Morlando, M. *et al.* FUS stimulates microRNA biogenesis by facilitating co-transcriptional Drosha recruitment. *EMBO J.* **31**, 4502–4510 (2012).

54. De Santis, R. *et al.* FUS Mutant Human Motoneurons Display Altered Transcriptome and microRNA Pathways with Implications for ALS Pathogenesis. *Stem Cell Reports* **9**, 1450–1462 (2017).

55. Zhang, T. *et al.* FUS Regulates Activity of MicroRNA-Mediated Gene Silencing. *Mol. Cell* **69**, 787-801.e8 (2018).

56. Orozco, D. & Edbauer, D. FUS-mediated alternative splicing in the nervous system: Consequences for ALS and FTLD. *Journal of Molecular Medicine* **91**, 1343–1354 (2013).

57. Rogelj, B. *et al.* Widespread binding of FUS along nascent RNA regulates alternative splicing in the brain. *Sci. Rep.* **2**, (2012).

58. Yu, Y. *et al.* U1 snRNP is mislocalized in ALS patient fibroblasts bearing NLS mutations in FUS and is required for motor neuron outgrowth in zebrafish. *Nucleic Acids Res.* **43**, 3208–3218 (2015).

59. Yu, Y. & Reed, R. FUS functions in coupling transcription to splicing by mediating an interaction between RNAP II and U1 snRNP. *Proc. Natl. Acad. Sci. U. S. A.* **112**, 8608–8613 (2015).

60. Ishigaki, S. *et al.* Position-dependent FUS-RNA interactions regulate alternative splicing events and transcriptions. *Sci. Rep.* **2**, (2012).

61. Humphrey, J. *et al.* FUS ALS-causative mutations impact FUS autoregulation and the processing of RNA-binding proteins through intron retention. *bioRxiv* 567735 (2019). doi:10.1101/567735

62. Grabowski, P. Alternative splicing takes shape during neuronal development. *Current Opinion in Genetics and Development* (2011). doi:10.1016/j.gde.2011.03.005

63. Rossi, S. *et al.* UsnRNP trafficking is regulated by stress granules and compromised by mutant ALS proteins. *Neurobiol. Dis.* **138**, 104792 (2020).

64. Coyne, A. N. *et al.* Fragile X protein mitigates TDP-43 toxicity by remodeling RNA granules and restoring translation. *Hum. Mol. Genet.* **24**, 6886–6898 (2015).

65. Matus, S., Bosco, D. A. & Hetz, C. Autophagy meets fused in sarcoma-positive stress granules. *Neurobiology of Aging* **35**, 2832–2835 (2014).

66. Casci, I. *et al.* Muscleblind acts as a modifier of FUS toxicity by modulating stress granule dynamics and SMN localization. *Nat. Commun.* **10**, (2019).

67. Tyzack, G. E. *et al.* Widespread FUS mislocalization is a molecular hallmark of amyotrophic lateral sclerosis. *Brain* (2019). doi:10.1093/brain/awz217

68. Japtok, J. *et al.* Stepwise acquirement of hallmark neuropathology in FUS-ALS iPSC

models depends on mutation type and neuronal aging. *Neurobiol. Dis.* **82**, 420–429 (2015).

69. Marrone, L. *et al.* Isogenic FUS-eGFP iPSC Reporter Lines Enable Quantification of FUS Stress Granule Pathology that Is Rescued by Drugs Inducing Autophagy. *Stem cell reports* **10**, 375–389 (2018).

70. Birsa, N., Bentham, M. P. & Fratta, P. Cytoplasmic functions of TDP-43 and FUS and their role in ALS. *Seminars in Cell and Developmental Biology* **99**, 193–201 (2020).

71. Stefl, R., Skrisovska, L. & Allain, F. H. T. RNA sequence- and shape-dependent recognition by proteins in the ribonucleoprotein particle. *EMBO Reports* (2005). doi:10.1038/sj.embor.7400325

72. Nostramo, R., Xing, S., Zhang, B. & Herman, P. K. Insights into the role of P-bodies and stress granules in protein quality control. *Genetics* (2019). doi:10.1534/genetics.119.302376

73. Anderson, P. & Kedersha, N. Stress granules: the Tao of RNA triage. *Trends in Biochemical Sciences* (2008). doi:10.1016/j.tibs.2007.12.003

74. Lenzi, J. *et al.* ALS mutant FUS proteins are recruited into stress granules in induced pluripotent stem cell-derived motoneurons. **8**, 755–766 (2015).

75. Jain, S. *et al.* ATPase-Modulated Stress Granules Contain a Diverse Proteome and Substructure. *Cell* (2016). doi:10.1016/j.cell.2015.12.038

76. Bosco, D. A. *et al.* Mutant FUS proteins that cause amyotrophic lateral sclerosis incorporate into stress granules. *Hum. Mol. Genet.* (2010). doi:10.1093/hmg/ddq335

77. Aulas, A., Stabile, S. & Vande Velde, C. Endogenous TDP-43, but not FUS, contributes to stress granule assembly via G3BP. *Mol. Neurodegener.* (2012). doi:10.1186/1750-1326-7-54

78. Baron, D. M. *et al.* Amyotrophic lateral sclerosis-linked FUS/TLS alters stress granule assembly and dynamics. *Mol. Neurodegener.* **8**, 30 (2013).

79. Sama, R. R. K. *et al.* FUS/TLS assembles into stress granules and is a prosurvival factor during hyperosmolar stress. *J. Cell. Physiol.* **228**, 2222–2231 (2013).

80. Dormann, D. *et al.* ALS-associated fused in sarcoma (FUS) mutations disrupt transportin-mediated nuclear import. *EMBO J.* (2010). doi:10.1038/emboj.2010.143

81. Sweeney, P. *et al.* Protein misfolding in neurodegenerative diseases: implications and strategies. *Transl. Neurodegener.* **6**, (2017).

82. Zhang, P. *et al.* Chronic optogenetic induction of stress granules is cytotoxic and reveals the evolution of ALS-FTD pathology. *Elife* **8**, (2019).

83. Shelkovnikova, T. A., Robinson, H. K., Connor-Robson, N. & Buchman, V. L. Recruitment into stress granules prevents irreversible aggregation of FUS protein mislocalized to the cytoplasm. *Cell Cycle* **12**, 3383–3391 (2013).

84. Alexander, E. J. *et al.* Ubiquilin 2 modulates ALS/FTD-linked FUS–RNA complex dynamics and stress granule formation. *Proc. Natl. Acad. Sci. U. S. A.* **115**, E11485–E11494

(2018).

85. Ryu, H. H. *et al.* Autophagy regulates amyotrophic lateral sclerosis-linked fused in sarcoma-positive stress granules in neurons. *Neurobiol. Aging* **35**, 2822–2831 (2014).

86. McCormick, C. & Khaperskyy, D. A. Translation inhibition and stress granules in the antiviral immune response. *Nature Reviews Immunology* (2017). doi:10.1038/nri.2017.63

87. Xue, Y. C., Feuer, R., Cashman, N. & Luo, H. Enteroviral infection: The forgotten link to amyotrophic lateral sclerosis? *Frontiers in Molecular Neuroscience* (2018). doi:10.3389/fnmol.2018.00063

88. Limongi, D. & Baldelli, S. Redox Imbalance and Viral Infections in Neurodegenerative Diseases. *Oxidative Medicine and Cellular Longevity* (2016). doi:10.1155/2016/6547248

89. Celeste, D. B. & Miller, M. S. Reviewing the evidence for viruses as environmental risk factors for ALS: A new perspective. *Cytokine* **108**, 173–178 (2018).

90. Verma, A. & Berger, J. R. ALS syndrome in patients with HIV-1 infection. *J. Neurol. Sci.* (2006). doi:10.1016/j.jns.2005.09.005

91. Shelkovnikova, T. A. *et al.* Antiviral Immune Response as a Trigger of FUS Proteinopathy in Amyotrophic Lateral Sclerosis. *Cell Rep.* **29**, 4496-4508.e4 (2019).

92. Rhoads, S. N., Monahan, Z. T., Yee, D. S. & Shewmaker, F. P. The Role of Post-Translational Modifications on Prion-Like Aggregation and Liquid-Phase Separation of FUS. *International journal of molecular sciences* **19**, 886 (2018).

93. Aulas, A. & Velde, C. Vande. Alterations in stress granule dynamics driven by TDP-43 and FUS: A link to pathological inclusions in ALS? *Front. Cell. Neurosci.* **9**, (2015).

94. Zappulo, A. *et al.* RNA localization is a key determinant of neurite-enriched proteome. *Nat. Commun.* **8**, 583 (2017).

95. Eliscovich, C. & Singer, R. H. RNP transport in cell biology: the long and winding road. *Current Opinion in Cell Biology* (2017). doi:10.1016/j.ceb.2017.02.008

96. Jung, H., Yoon, B. C. & Holt, C. E. Axonal mRNA localization and local protein synthesis in nervous system assembly, maintenance and repair. *Nature Reviews Neuroscience* (2012). doi:10.1038/nrn3210

97. Karamyshev, A. L. & Karamysheva, Z. N. Lost in translation: Ribosome-associated mRNA and protein quality controls. *Frontiers in Genetics* (2018). doi:10.3389/fgene.2018.00431

98. Kamelgarn, M. *et al.* ALS mutations of FUS suppress protein translation and disrupt the regulation of nonsense-mediated decay. *Proc. Natl. Acad. Sci. U. S. A.* **115**, E11904–E11913 (2018).

99. López-Erauskin, J. *et al.* ALS/FTD-Linked Mutation in FUS Suppresses Intra-axonal Protein Synthesis and Drives Disease Without Nuclear Loss-of-Function of FUS. *Neuron* **100**, 816-830.e7 (2018).

100. Nakaya, T. & Maragkakis, M. Amyotrophic Lateral Sclerosis associated FUS mutation shortens mitochondria and induces neurotoxicity. *Sci. Rep.* **8**, 1–15 (2018).

101. de la Fuente, F. R. & Emc, F. FUS-ALS mutants alter FMRP phase separation equilibrium and impair protein translation Birsa N. *bioRxiv* 2020.09.14.296038 (2020). doi:10.1101/2020.09.14.296038

102. Bond, S., Lopez-Lloreda, C., Gannon, P. J., Akay-Espinoza, C. & Jordan-Sciutto, K. L. The integrated stress response and phosphorylated eukaryotic initiation factor 2α in neurodegeneration. *Journal of Neuropathology and Experimental Neurology* (2020). doi:10.1093/jnen/nlz129

103. Kim, H. J. Cell fate control by translation: MRNA translation initiation as a therapeutic target for cancer development and stem cell fate control. *Biomolecules* **9**, (2019).

104. Powley, I. R. *et al.* Translational reprogramming following UVB irradiation is mediated by DNA-PKcs and allows selective recruitment to the polysomes of mRNAs encoding DNA repair enzymes. *Genes Dev.* **23**, 1207–1220 (2009).

105. Bennetzen, M. V. *et al.* DNA damage-induced dynamic changes in abundance and cytosol-nuclear translocation of proteins involved in translational processes, metabolism, and autophagy. *Cell Cycle* **17**, 2146–2163 (2018).

106. Nott, A., Le Hir, H. & Moore, M. J. Splicing enhances translation in mammalian cells: An additional function of the exon junction complex. *Genes Dev.* **18**, 210–222 (2004).

107. Sephton, C. F. & Yu, G. The function of RNA-binding proteins at the synapse: Implications for neurodegeneration. *Cellular and Molecular Life Sciences* (2015). doi:10.1007/s00018-015-1943-x

Chapter 2

Dissecting the role of R521H mutation in ALS6 motor neurons

Amanda Faria Assoni [1,2], René Wardenaar[2], Danyllo Oliveira[1], Petra Bakker [2], Valdemir Melechco Carvalho [3], Oswaldo Keith Okamoto[1] Mayana Zatz [1], Floris Foijer [2]

1 Instituto de Biociências, Universidade de São Paulo, São Paulo 05508-900, Brazil.

2 European Research Institute for the Biology of Ageing, University of Groningen, Groningen, 9713 AV, the Netherlands.

3 Division of Research and Development, Fleury Group, São Paulo 04344-070, Brazil.

ABSTRACT

Amyotrophic lateral sclerosis (ALS) is a neurological disorder characterized by the selective death of motor neurons. Fused in Sarcoma (FUS) is a gene located at 16p11.2 that when mutated causes ALS6, the type of ALS with the earlier average age of onset of symptoms. We have used IPSCs derived from ALS6 patients to understand the major and earliest phenotypes that mutant FUS causes in Motor Neurons (MNs), and investigated the cellular functions that FUS may interfere with. We find that RNA metabolism does not appear to be affected in ALS6 cells. However, FUS interacts with many more proteins in ALS cells than in cells expressing wild type FUS. These aberrant interacting proteins are largely associated with the protein translation machinery and are localized in the cytoplasm. Importantly, while FUS protein levels do not differ between control and ALS6 cells, we find that FUS protein is more localized to the cytoplasm in the neuroprogenitor and motor neuron stages of differentiation in ALS6 cells, which coincides with a decrease in global protein synthesis rates. In conclusion, we find that mutant FUS protein is mislocalized and alters protein synthesis rates in iPSC-derived motor neurons. As this phenotype may be the earliest phenotype caused by the mutation, this mechanism could provide an important therapeutic target to prevent or delay ALS symptoms.

1- INTRODUCTION

Amyotrophic lateral sclerosis (ALS) is a neurological disorder characterized by the selective death of motor neurons(Charcot, 1869). Patients carrying ALS typically present initially a progressive weakness followed by fasciculations leading to wheelchair confinement and death from respiratory failure within 3-5 years of symptom onset. Nevertheless, there is a great deal of clinical heterogeneity, with a variable rate of disease progression and age of onset of symptoms. To date, multiple pathogenic variants in more than 40 different genes have been associated with ALS, indicating the highly heterogeneous molecular basis of the disease(Mathis et al., 2019). Fused in Sarcoma (FUS) is a gene located at 16p11.2 that, when mutated, causes ALS6, a type of ALS with the earliest mean age-of-onset of symptoms(Vance et al., 2009).

The FUS gene encodes a DNA/RNA-binding multifunctional protein that regulates various aspects of the cellular metabolism such as DNA repair, splicing, and microRNA biogenesis(Dichmann and Harland, 2012; Morlando et al., 2012; Deng et al., 2014). However, the underlying mechanism by which FUS mutations lead to motor neuron death are largely unknown.

Protein synthesis is a crucial process that controls cell behavior, as proteins are the functional molecules that determine cell type and function (Kim, 2019). Mutant FUS has been associated with various aberrations that ultimately all alter the protein translation rate, as previously discussed in Chapter 2. FUS mutations have previously been reported to suppress protein translation, but the mechanisms causing this suppression have not been fully elucidated (Kamelgarn et al., 2018; López-Erauskin et al., 2018). Moreover, as mRNA localization is a major mechanism controlling protein translation(Zappulo et al., 2017) and FUS binds to pre-mRNAs during splicing (Rogelj et al., 2012), we wanted to investigate whether and how mutant FUS impair protein translation in the most relevant cell type for ALS: ALS patient-derived motor neurons (MNs).

Towards this aim, we collected skin samples from four individuals of a single family, two of whom were ALS carriers and had a single nucleotide variation in FUS responsible for the exchange of an arginine to histidine at position 521 of the protein (**c.1562G>A** e p.Arg521His) and two unaffected relatives which we used to derive ALS patient and matched control induced pluripotent stem cell (iPSC) lines. We find that RNA metabolism is unaltered in ALS6 cells. However, mutant FUS protein interacts with many more proteins than FUS in control MNs. Most of the proteins that only bind to mutant FUS play a role in the protein translational machinery and are localized in the cytoplasm. Even though total FUS levels do not differ between control and ALS6 cells, we find that mutant FUS localizes more to the cytoplasm, particularly in neuroprogenitor (NP) and motor neuron stages of differentiation, which

coincides with a decrease in global protein synthesis rates. Our observations therefore suggest that the cytoplasmic localization of mutant FUS promotes FUS binding to the translational machinery, thus functionally impairing it.

2- RESULTS

2.1 - FUS is mislocalized in ALS6 MNs and interacts with proteins of the translational machinery in the cytoplasm

To better understand how mutant FUS promotes a pathogenic phenotype, we compared the protein interaction partners between normal and mutant FUS. For this, we performed co-immunoprecipitation using an anti-FUS antibody in ALS6 MNs and control MNs followed by proteomic shotgun identification of the protein interactors (Fig 1A-C).

Interestingly, we found that samples from the ALS6 patients had many more protein interactors than the control samples (Fig. 1 A; Supplemental table 1). We then determined which proteins were unique binding partners of mutant FUS and found that these were enriched for having a function in translation initiation and were localized in the cytoplasm (Fig. 1B and C). To rule out that the additional binding partners of mutant FUS were an artefact of increased concentration of the mutant FUS protein, we compared FUS expression between MNs from ALS patients and unaffected controls and found no differences in protein concentration (Fig. 1 D and E). Furthermore, even though FUS can move between the nucleus and cytoplasm, FUS is mainly localized in the nucleus in healthy MNs (Deshpande et al., 2019), but is more often found in the cytoplasm in ALS MNs. To determine whether this is also true in our model system, we compared FUS localization in control and ALS patient-derived iPSC NPs and MNs (Fig. 1 F-H). Indeed, while FUS localization is unaltered in control vs. ALS-patient-derived iPSCs, we observed increased cytoplasmic localization of FUS in NPs as well as in MNs derived from ALS patients. We conclude that mutant FUS localizes to the cytoplasm more when differentiating towards NPs and MNs, which coincides with increased FUS binding to proteins involved in the translation machinery.

2.2 - Global translation rates are decreased in ALS6 NPs and MNs due to a gain of toxic function of the mutant FUS

Since we found that mutant FUS binds to cytoplasmic proteins of the translational machinery, we next tested whether this had functional consequences for the cells' protein translation capacity in iPSCs, NPs or MNs. To quantify translation rates, we used a puromycin (a tRNA mimic) incorporation assay, followed by quantification of incorporated puromycin using an anti-puro antibody, which is commonly used for this purpose (RM et al., 2016; Aviner, 2020).

To quantify puromycin incorporation, we used both Western blot (WB) and immunofluorescence (IF) (Fig. 2 A-C), which revealed that the protein synthesis rates are similar in all iPSC samples. However, both in NPs as well as in MNs derived from ALS6 patients, translation rates are significantly decreased (Fig. 2 A-C).

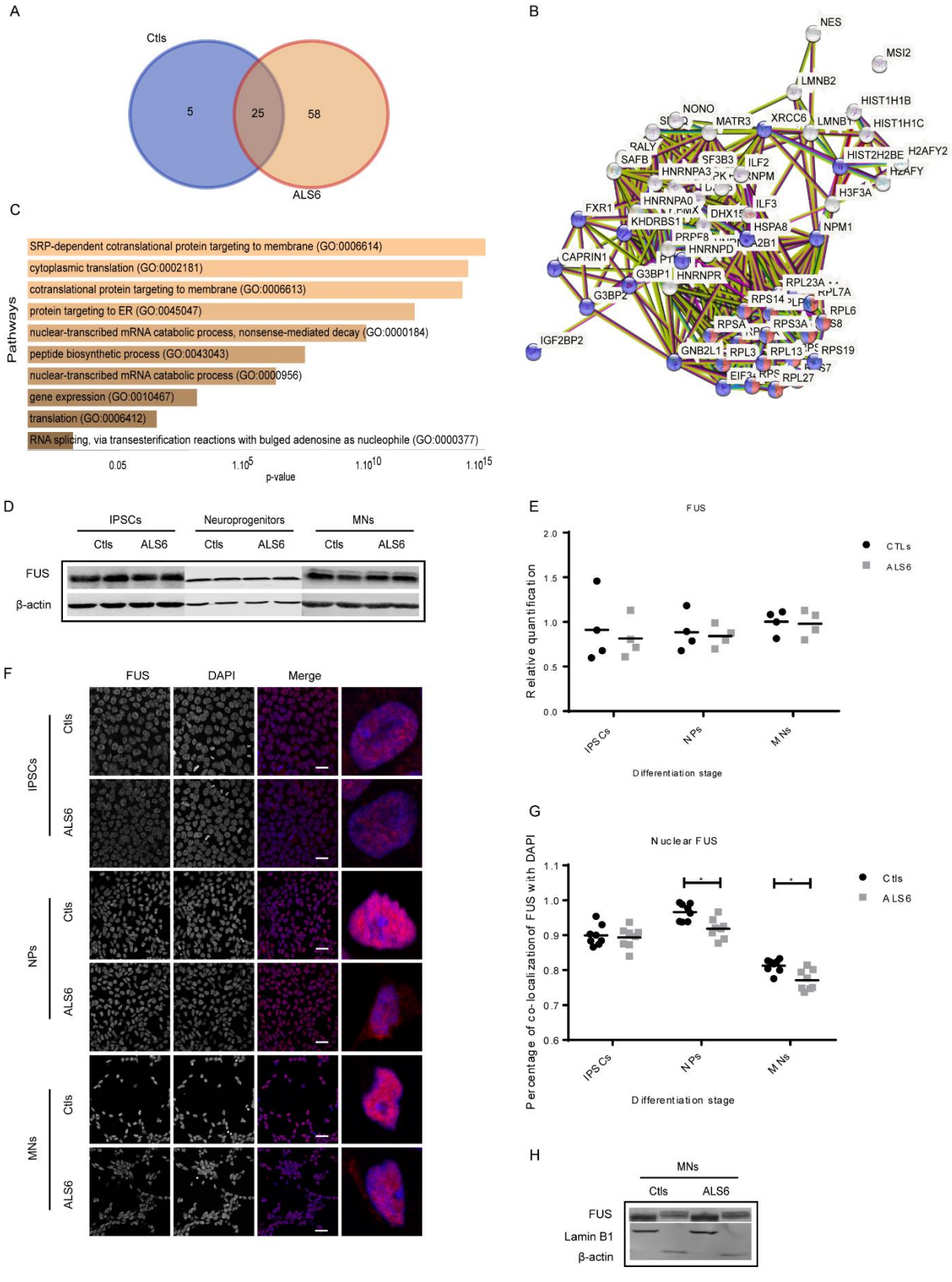

Fig 1: FUS localizes to the cytoplasm of ALS6 cells and interacts with cytoplasmic proteins of the translational machinery. a. Venn diagram of proteins interacting with FUS in each sample. **b**.String association of the proteins interacting with FUS only in the ALS6 samples. **c.** Panther bar graph of enriched pathways of the proteins FUS interacts with only in ALS6 cells. **d.** Western blot of total FUS in the IPSCs, NPs, and MNs. **e.** Densitometric quantification of the total amount of FUS in each sample relative to the amount of β-actin (n=4 each group). **f.** Representative immunofluorescence staining of FUS to observe its localization on Ctls and ALS6 IPSCs, NPs and MNs. IPSC scale bar 25 µm NPs and MNs scale bar 10 µm. **g.** Quantification of FUS localization by immunofluorescence staining with the anti-FUS antibody in Ctls and ALS6 IPSCs, NPs and MNs. (*, $P < 0.05$; two-way ANOVA with Sidak`s multiple comparison test; n = 8 per group). **h.** Western blot of FUS in the nuclear or cytoplasmic fraction of Ctls and ALS6 MNs.

To determine whether the decreased translation rate was caused by decreased levels of wild-type FUS protein (note that ALS6 patients carry a heterozygous mutation of FUS), or that the mutation in FUS is a gain-of-function mutation, we modulated mutant and wild-type FUS expression in control and ALS patient-derived MNs. First, we transiently overexpressed wild type FUS in ALS6 MNs (Fig. 2 D and E) and found that this did not increase protein translation rates. Conversely, we down-regulated FUS in control-derived MNs using siRNA targeting wild type FUS (Fig. 2 F and G). Even though this decreased FUS levels as expected, this did not lead to a decrease in protein synthesis rates . Finally, we transiently overexpressed mutant FUS protein (R521H ALS6 mutation) in control-derived MNs, which significantly decreased translation rates within the control-derived MNs (Fig. 2 H and I). These observations indicate that the R521H mutation in the FUS protein leads to a gain of function that impairs protein translation.

FUS is a DNA/RNA-binding protein and could therefore also affect RNA metabolism and RNA localization and, as a consequence of altered RNA availability, delay protein synthesis. To rule out this hypothesis, we examined transcription rates (Fig. 3 A and B) and RNA localization (Fig. 3 C-E) of control and ALS-derived iPSCs, NPs and MNs. Here we found no differences between the transcription rates at any of the differentiation stages, although the total quantification of RNA appears to be increased in ALS-derived NPs. However, especially since we do not observe any changes related to RNA availability in ALS-derived MNs, we conclude that this cannot explain the decreased protein synthesis observed in these MNs. Overall these observations show that protein synthesis rates are decreased in ALS6 NPs and MNs and suggest that this is caused by the increased cytoplasmic localization of FUS and increased binding to proteins of the translational machinery.

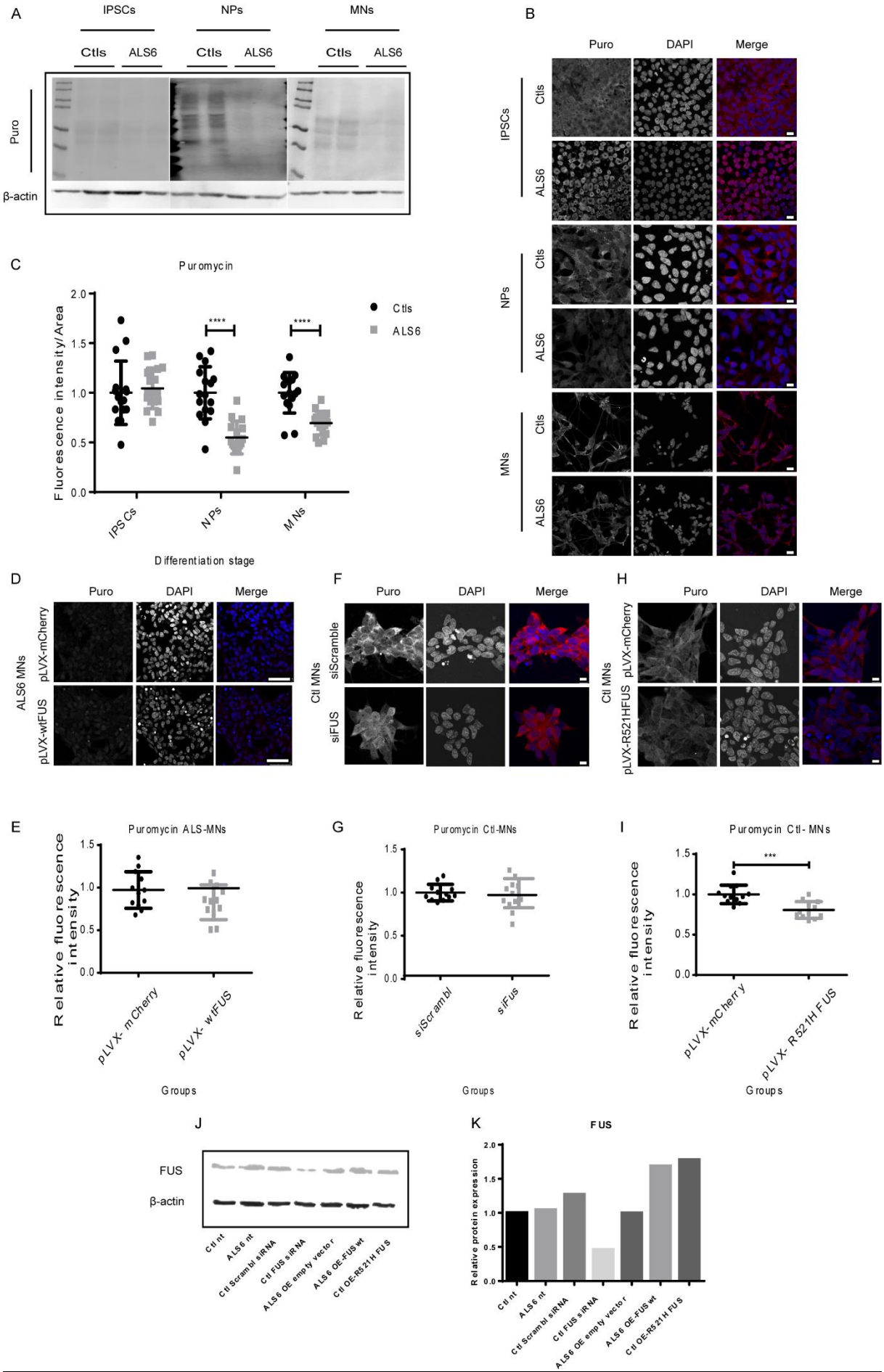
A
IPSCs
NPs
MNs
Ctls
ALS6
Puro
β-actin
B
Puro
DAPI
Merge
C
Puromycin
Fluorescence intensity/Area
Differentiation stage
D
ALS6 MNs
pLVX-mCherry
pLVX-wtFUS
E
Puromycin ALS-MNs
Relative fluorescence intensity
Groups
F
Ctl MNs
siScramble
siFUS
G
Puromycin Ctl-MNs
H
pLVX-R521HFUS
I
Puromycin Ctl- MNs
J
FUS
Ctl nt
ALS6 nt
Ctl Scrambl siRNA
Ctl FUS siRNA
ALS6 OE empty vector
ALS6 OE-FUS wt
Ctl OE-R521H FUS
K
Relative protein expression

Fig 2: - Global translation rate is decreased in ALS6 samples due to the presence of mutant FUS. **a.**Western blot with anti-puromycin antibody on total cell extract of IPSCs, NPs and MNs. **b.** Quantification of the relative intensity of puromycin incorporation in immunofluorescence staining of IPSCs, NPs and MNs.(****, P < 0.0001; two-way ANOVA with Sidak`s multiple comparison test; n = 16 per group). **c.** Representative images of immunofluorescence staining with anti-puromycin antibody in IPSCs, NPs and MN. IPSC scale bar 25 um NPs and MNs scale bar 10 um. **d.** Representative immunofluorescence staining with the anti-puromycin antibody in ALS6 MNs transiently transfected with the overexpression plasmids pLVX-mCherry or pLVX-mCherry-wtFUS. Scale bar 10 um. **e.** Quantification of the relative intensity of puromycin incorporation on immunofluorescence staining with the anti-puromycin antibody in ALS6 MNs transiently transfected with the pLVX-mCherry or pLVX-mCherry-wtFUS overexpression plasmids (n=12). **f.** Representative immunofluorescence staining of anti-puromycin antibody in Ctl-MNs transiently transfected with siRNA at 5 nM scramble or FUS. Scale bar 10 um. **g.** Quantification of relative intensity of puromycin incorporation in immunofluorescence staining of anti-puromycin antibody in Ctl-MNs transiently transfected with siRNA at 5 nM scramble or FUS (n=12). **h.** Representative immunofluorescence staining of anti-puromycin antibody in Ctl-MNs transiently transfected with pLVX-mCherry or pLVX-mCherry-R521H FUS overexpression plasmids. Scale bar 10 um. **i.** Quantification of the relative intensity of puromycin incorporation upon immunofluorescence staining of anti-puromycin antibody in Ctl-MNs transiently transfected with the overexpression plasmids pLVX-mCherry or pLVX-mCherry-R521H FUS (***, P < 0.001; Mann Whitney test; n = 12 per group). **j**. Western blot of total FUS in the transfected MNs with siRNA or overexpression (OE) plasmids. **k.** Densitometric quantification of the total amount of FUS in each sample relative to the amount of β-actin (n=1 each group).

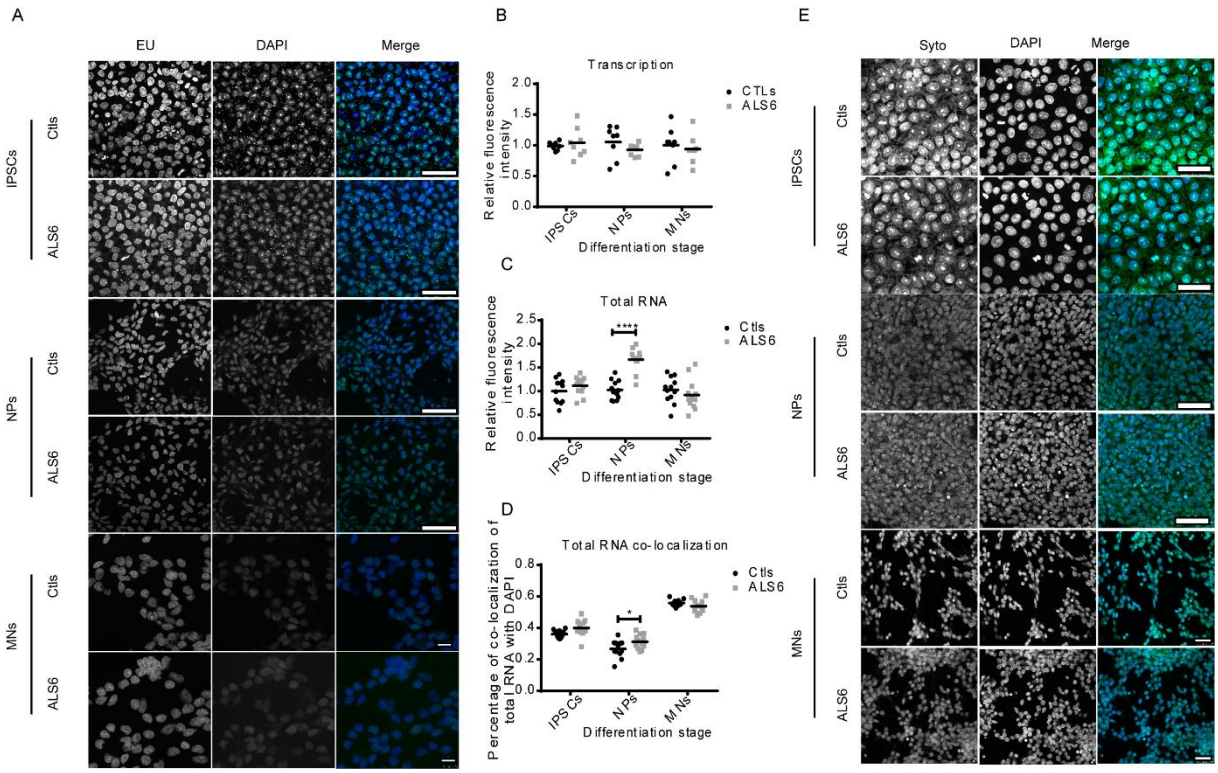

Figure 3: Transcription and RNA localization do not explain the decreased protein synthesis in ALS6. a. Representative images of 5-Ethynyl-uridine (5-EU) incorporation to measure RNA transcription in IPSCs, NPs and MNs. Scale bars: IPSC 50µm, NPs 50µm and MNs 10 µm. **b.** Quantification of the relative intensity of EU incorporation on immunofluorescence staining in IPSCs, NPs and MNs (n=8). **c.** Quantification of the relative intensity of the total RNA staining with Syto reagent in IPSCs, NPs and MNs.(***, $P < 0.001$; two-way ANOVA with Sidak`s multiple comparison test; n = 8 per group). **d.** Quantification of RNA localization by immunofluorescence staining with the Syto reagent in Ctls and ALS6 IPSCs, NPs and MNs. (*, $P < 0.05$; two-way ANOVA with Sidak`s multiple comparison test; n = 8 per group). **e.** Representative images of RNA localization in immunofluorescence staining with the Syto reagent in Ctls and ALS6 IPSCs, NPs and MNs. Scale bars: IPSC 50µm, NPs 100µm and MNs 50 µm.

To determine whether aberrant cytoplasmic FUS localization is a cause or consequence of the translation defects observed in ALS-derived NPs and MNs, we next interfered with RNA splicing and translation in control and ALS-derived MNs. (Suppl. 2 A and B). We found that treatment with a translation inducer (ISRIB)(Halliday et al., 2015) or inhibitor (Cycloheximide - CHX)(Schneider-Poetsch et al., 2010) did not significantly affect the localization of FUS in ALS-derived MNs. Treatment with the splicing inhibitor pladienolide B however, resulted in a significant increase of nuclear FUS in ALS-derived MNs. This was the opposite of what was found in the control MNs, in which FUS seems to be required in the cytoplasm when protein synthesis levels increase (Suppl. 2 A and B). These observations suggest that mutant FUS shifts to the cytoplasm more when splicing is active and ends up causing a translation defect in ALS-derived NPs and MNs due to its cytoplasmic localization.

2.3- FUS mislocalization as a hallmark of ALS

FUS has previously been reported to be mislocalized into the cytoplasm of postmortem neurons from sporadic ALS patients(Lo Bello et al., 2017b) suggesting that cytoplasmic FUS is a more general feature of ALS. We therefore assessed whether our findings also apply to other types of familial ALS (ALS with mutation in the *VAPB* and *VRK1* genes) and found FUS to be localized into the cytoplasm of IPSC-derived MNs of other familial forms of ALS compared to MNs derived from healthy controls (Fig. 4 A and B). Intriguingly, we also found that mislocalization of FUS is not exclusive to MNs derived from ALS patients that carried a mutation in the FUS gene.

To determine whether this mislocalization also would lead to decreased in protein synthesis, we quantified translation rates for these ALS-patient derived MNs as well and found that translation rates were also decreased in these samples (Fig. 4 C and D). Importantly, when we correlated puromycin incorporation for each sample with the percentage of nuclear FUS localization, we found a sigmoidal correlation (Fig. 4 E), *i.e.* the more FUS was localized in the nucleus, the higher the rate of protein synthesis until a saturation point is reached for which localization of FUS no longer limits translation.

Altogether, this study reveals that NP and MN cells derived from ALS6 patient samples display aberrant cytoplasmic localization of FUS, which coincides with decreased protein translation and increased binding of FUS to cytoplasmic protein translation machinery components. The decreased translation probably results from a toxic gain of function of the FUS protein because of its localization. Importantly, we also find that other types of familial ALS also display abnormal FUS localization and decreased protein translation, even when FUS is not mutated. These observations therefore suggest that compounds that can rescue cytoplasmic FUS localization have the potential to prevent or delay ALS initiation or progression.

3- DISCUSSION

In this study we show that basal rates of protein translation are decreased in motor neurons generated from ALS6 patient-derived iPS cells. We find that this coincides with aberrant cytoplasmic localization and binding to protein translation machinery components of mutant FUS protein, the driver of ALS6. As cytoplasmic localization of FUS has also been observed in MNs in postmortem tissues from sporadic ALS cases(Tyzack et al., 2019), we also assessed FUS localization in familial ALS-patient iPSC-derived NPs and MNs, including familiar ALS types that are not driven by FUS mutations. Here we found that mislocalized FUS is common in ALS-derived NPs and MNs and not specific to cells derived from patients with FUS mutation only.

Importantly, FUS mislocalization correlates with decreased translation rate in ALS6 samples (NPs and MNs) as well as in MNs of other familial forms of ALS (with mutations in the *VAPB* and *VRK1* gene), indicating that 1) protein translation defects can be generalized across multiple ALS subtypes and 2) that FUS mislocalization is a strong predictor of protein translation defects. While deregulation of translation was demonstrated in many other models of ALS, with mutations in the TDP43(S et al., 2020) , FUS(López-Erauskin et al., 2018) , VAPB(Oliveira et al., 2020) and SOD1(Cestra et al., 2017) genes, this has so far not been linked to mislocalized FUS. Further work is required to determine which other ALS drivers in addition to VAPB and VRK1 lead to this phenotype. The impaired neuronal viability observed for ALS-derived MNs (also see Chapter 3) is likely a consequence of this impaired protein translation (Lee et al., 2008; He et al., 2010; Song et al., 2021).

How does mislocalized FUS lead to decreased protein translation? Our experiments indicate that the reduced translation observed in ALS6 MNs is not due to an altered transcription rate, RNA quantity, or RNA localization in these cells. Furthermore, while ectopic expression of mutant FUS in control MNs is sufficient to induce decreased translation, overexpression or reduction of wild-type FUS does not alter protein translation rates, indicating that the mutation of FUS leads to a toxic gain of function phenotype. This is consistent with the identification of additional binding partners of mutant FUS in the ALS6 samples, which include mostly

cytoplasmic proteins involved in the translation initiation process. This could indicate that mutant FUS either actively inhibits translation, or that mutant FUS leads to altered splicing kinetics.

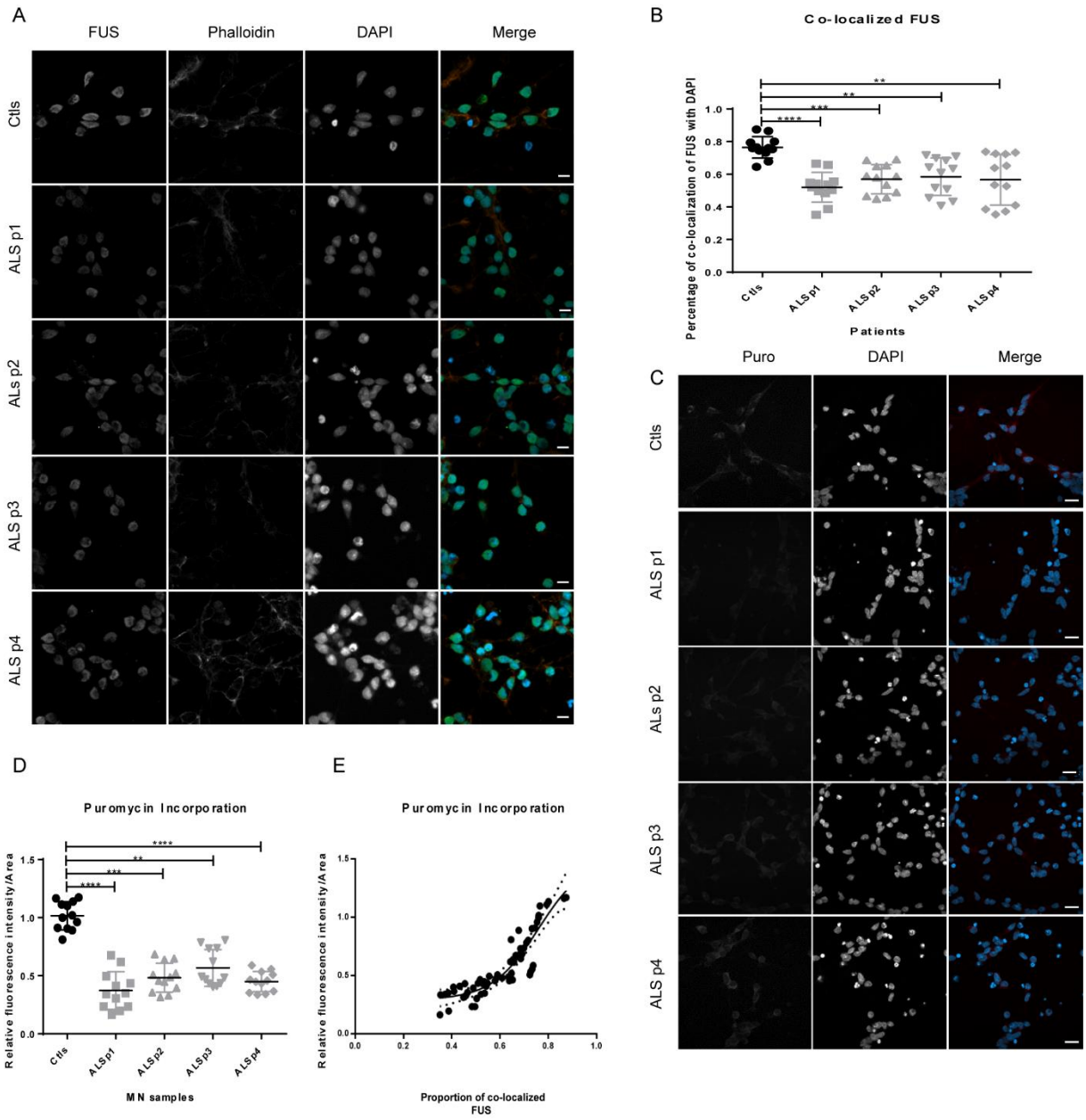

Figure 4: Other types of ALS MNs show the same chaacteristics as ALS6. **a.** Representative immunofluorescence staining of FUS to observe its localization on IPSCs- derived MNs from Ctls and ALS patients. Scale bar 10 µm. **b.** Quantification of FUS localization in immunofluorescence staining of Ctls and ALS patient IPSCs-derived MNs with anti-FUS antibody. (**, P < 0.01; ***, P < 0.001, and ****, P< 0.0001, Kruskal-Wallis test and Dunn`s multiple comparisons, n= 12 each). **c.** Representative images of immunofluorescence staining with anti-puromycin antibody in IPSCs-derived MNs from Ctls and ALS patients. Scale bar 20 µm. **d.** Quantification of relative intensity of puromycin incorporation on immunofluorescence staining of Ctls and ALS patient IPSCs-derived MNs. (**, P < 0.01; ***, P < 0.001, and ****, P< 0.0001, Kruskal-Wallis test and Dunn`s multiple comparisons, n= 12 each). **e.** Correlation between the percentage of FUS localized in the nucleus and the relative intensity of puromycin incorporation in each sample tested.

To determine whether either of these hypotheses are true, we examined FUS localization in the presence of translation-modulating agents. We found that inducing translation in control MNs promoted wild type FUS localization into the cytoplasm, whereas inhibition nor induction of translation altered the localization of FUS in ALS patient-derived MNs. Interestingly, treatment with a splicing inhibitor did promote localization of mutant FUS into the nucleus of ALS patient-derived MNs. Possibly, mutant FUS fails to be cleared from spliced RNAs and is therefore transported towards the cytoplasm with the (aberrantly) spliced RNA after which it interferes with the translation machinery when translation is initiated.

In summary, we in this study have shown that both FUS mislocalization and concomitant reduced protein synthesis are features of MNs differentiated from iPSCs that are derived from ALS6 or other familial ALS patients. Future work should determine whether the identified phenotypes can be exploited for the development of new therapies for this devastating disease, for which currently there is no effective treatment.

4- METHODS

Cellular reprogramming and motor neuron differentiation

After informed consent, fibroblasts were isolated from all individuals (N=4, 2 affected and 2 controls), and were used for reprogramming using CytoTune™-iPS 2.0 Sendai Reprogramming Kit as manufacturer recomendation. Induced pluripotent stem cells (iPSCs) were then obtained for such individuals. Expression of pluripotency markers *SSEA4* and *OCT4 Nanog* and *SOX2* was checked by immunofluorescence (Supplementary Figure 1 B). Differentiation into motor neurons (MNs) was performed as previously published(Du et al., 2015) (Supplementary Fig. 1 A). Briefly, the iPSCs were grown in Essential 8 medium (Thermo) until reaching 80% of confluency. Then, they were cultivated in NB medium containing DMEM/F12, Neurobasal medium, N2, B27 and Glutamax (all from Thermo) and subjected to a two steps protocol of neural induction/ caudalization and ventralization for obtaining motor neuron progenitors (MNPs). The first phase was achieved after cultivating iPSCs for six days in NB containing Dorsomorphin (2 μM), SB431542 (2 μM), CHIR99021 (3 μM) and Ascorbic acid (0.1 mM). The following step, which also lasted 6 days, consisted of cultivating the cells in NB medium and Dorsomorphin (2 μM), SB431542 (2 μM), CHIR99021 (1 μM), retinoic acid (0.1 μM), Ascorbic acid (0.1 mM) and Purmorphamine (0.5 μM). After obtaining the MNPs, the cells were seeded in 60 mm2 plates containing Matrigel (Corning) and subjected to motor neuron differentiation by cultivating them for 6 days in NB medium containing retinoic acid (0.5 μM), Purmorphamine (0.1 μM) and Ascorbic acid (0.1 mM). A further step of neural maturation was also carried out by adding Compound E (0.1 μM) to the same medium used for motor neuron induction.The presence of β-tubulin, MAP2, Hb9 and ISL1 was confirmed by IF (Supplementary Figure 1 C).
Differentiation towards motor neurons were made 3 different times for each individual to rule out batch-dependent results.

Immunofluorescence

Cells were washed twice, fixed (3.7% formaldehyde RT for 20 minutes) and permeabilized for 30 minutes with 0.1% Triton X-100 and 5% bovine serum albumin in 1× PBS, prior to overnight incubation with the primary antibody (Supplementary Table S1) at 4°C. Cells were then washed 3 times in 1× PBS, incubated with the secondary antibody for 45min (Supplementary Table S1), and washed again 2 times in 1× PBS. Cell nuclei were stained with 1 μg/mL DAPI for 2 minutes and mounted on glass slides and cover slipped with VectaShield. All images were taken in confocal microscope (Zeiss LSM 800). All quantification of images were performed using Cell Profiler 3.0 as previously published(McQuin et al., 2018) .

Western Blot

Cells were harvested by accutase dissociation and lysed in elution buffer (150 mM NaCl, 0.1% NP-40, 5 mM EDTA, 50 mM HEPES pH7.5) containing complete protease inhibitor (Roche) for 15 minutes at 4oC. Then the samples were centrifuged at 300g, at 4°C for 10 min to remove insoluble residues. 20 μg of each sample was loaded on 10% polyacrylamide gels. Proteins were transferred to polyvinylidene difluoride (PVDF) membranes. After blocking in Odyssey blocking buffer (Li-cor Biosciences) at 4°C for 60 min, the membrane was incubated overnight at 4°C with the primary antibody (supplemental materials). Following incubation, the membrane was washed with PBS containing 0,1% Tween 20 (Sigma) three times and incubated in secondary antibody for 1 hour at room temperature. The blots were detected by the Odyssey imaging system (Li-cor Biosciences). The protein bands were quantified with Image studio lite software (Li-cor Biosciences).

Co- immunoprecipitation

Co-immunoprecipitation of FUS from ALS6 and controls NPs was carried out utilizing the Immunoprecipitation Kit Dynabeads Protein a/G (ThermoFisher). The protocol was followed according to the manufacturer's instructions, beginning with the addition of 10 μL of monoclonal anti-FUS antibody (Sigma) or 10 μL of mouse IgG (Santa Cruz Biotechnology) to create the Co-IP bead complex. Cells were washed once with PBS and lysed in 500 μL/well lysis buffer containing 20 mM Tris pH 8.0, 10% glycerol, 135 mM NaCl, 0.5% NP-40, and protease inhibitors (Complete, EDTA-free, Roche) for 15 min on ice. After scraping the cells off, lysates were centrifuged at 16,100 g for 5 min at 4°C to remove cell debris. The input was incubated with the previously prepared beads (ThermoFisher) equilibrated in wash buffer, for 1 hr at 4°C. After washing the beads 3× with wash buffer, beads were taken up in RapiGest (Waters), for 10 min at 65°C.

Sample Digestion

The samples were digested in solution using RapiGest (Waters) as surfactant agent. In this protocol, proteins were reduced with DTT (dithiothreitol), alkylated with iodoacetamide, and digested with trypsin proteomic level in an enzyme: protein ratio of 1:50.

Sample processing and protein profile analysis by liquid chromatography coupled to tandem mass spectrometry

The samples were processed by a nanoACQUITY system comprising a binary pump, an auxiliary pump and a sampler. Peptides were captured, desalted and concentrated in a capture column Symmetry C18(20 nm ×180mm, 5 um) using a mobile phase composed of water with 0.1% trifluoroacetic acid at a flow rate of 15uL/ min for 5 minutes. Then, the peptides were separated on an analytical column HSSC18 (75 μm × 150 mm, 1.7 μm) by eluting with a linear gradient of 2% DMSO in water with 0.1% formic acid and 5% DMSO in acetonitrile with 0.1% formic acid. The proportion of the organic solution was increased from 0 to 60% in 80 minutes.

The chromatographic system is directly coupled to a hybrid quadrupole orbitrap tandem mass spectrometer Q-Exactive (Thermo Scientific), equipped with a Nano Flex source. The acquisition of spectral data were obtained by the data dependent top-15 method in which the spectrometer chooses dynamically the most abundant not-yet sequenced precursor ions from a survey scan from 390 to 1650 m/z (except for the monocharged and those with charges exceeding 7) at 70,000 (at m/z 200) of resolution and AGC target 5 e 6. Sequencing was achieved dissociating the precursor ion with normalized collision energy of 35, resolution equal to 17,500 and AGC target of 5 e 4.

The acquired data were processed by MaxQuant 1.4.0.8 proteomics data analysis workflow (Cox and Mann, 2008). Protein identification was performed by Andromeda search tool using the database of the human proteome UniProtKB (SWISSPROT November 2014). The following criteria were applied to protein identification: allowed maximum of two incomplete cleavages by trypsin, fixed modification by carbamidomethylation of cysteines and variable modification by acetylation of the N-terminal portion and methionine oxidation. Quantification was based on the LFQ (Cox et al., 2014) label-free method.

Puromycin incorporation assay

Cells were incubated for 10 min in media with or without puromycin (Invitrogen) (20 μM). Cells were then either fixed for immunofluorescence or harvested for protein extraction and western blot.

Subcellular fractionation

To separate the cytoplasmic fraction we performed an adaptation of a protocol previously published. Briefly, 3×10^6 cells were dissolved in 200 μL of cold hypotonic buffer (10 mM HEPES−NaOH (pH 7.9) containing 10 mM KCl, 1.5 mM MgCl2, 1 mM DTT, and protease

and phosphatase inhibitor cocktails), and the cell suspensions were incubated on ice for 30 min, mixing for 10 s every five min. After centrifugation at 400g for 10 min at 4 °C, the supernatants were collected as cytoplasmic fractions. After wash three times with cold hypotonic buffer, the pellets were dissolved in cold 100 mM Tris-HCl (pH 9.0) containing 12 mM SDC, 12 mM SLS, and protease and phosphatase inhibitor cocktails and collected as nuclear fraction. The fractions were submitted to SDS-page and western blot.

EU Labeling

Cells were incubated with 10 μM EU (5-ethynyl-uridine; Click-It EU Alexa Fluor 488 Imaging Kit; Life Technologies) for 30 min. Cell nuclei were stained with DAPI at a concentration of 5 $\mu g \cdot mL^{-1}$ for 5 min. All images were taken in confocal microscope (Zeiss LSM 800). All quantification of images were performed using Cell Profiler 3.0 as previously published(McQuin et al., 2018) .

RNA staining

Rna staining using Syto Select (Invitrogen) was performed as manufacturer's instructions. Briefly, Syto was added to cultured media and cells were kept in 37oC for 15min, then washed and fixed for detection using confocal microscope (Zeiss LSM 800).

Statistical analysis

All experiments were performed in triplicate or more replicates as stated in the figures, and three independent experiments were carried out. Data were analyzed by one-way and two-way ANOVA followed by Bonferroni post hoc test. The t test with two-tailed unpaired test was used for pairwise comparison. Graphpad Prism software was used to perform all statistical analysis (version 6.0 GraphPad Software Inc.). Quantification of data is represented as mean ± SEM, and P value threshold was as follows: *, 0.05; **, 0.01; ***, 0.001; and ****, 0.0001.

5- ACKNOWLEDGEMENTS

This work was supported by the Fundação de Amparo à Pesquisa do Estado de São Paulo (FAPESP), Conselho Nacional de Desenvolvimento Científico e Tecnológico (CNPq) and an Abel Tasman fellowship to AA awarded by the University of Groningen.

6- CONFLICT OF INTEREST DISCLOSURE

No financial interest/relationships with financial interest relating to the topic of this article have been declared.

7- REFERENCES

1. Charcot, J.-M. *Deux cas d'atrophie musculaire progressive : avec leÌ• sions de la substance grise et des faisceaux anteÌ• rolateÌ• raux de la moelle eÌ• pinieÌ€ re*. (Masson, 1869).

2. Mathis, S., Goizet, C., Soulages, A., Vallat, J.-M. & Masson, G. Le. Genetics of amyotrophic lateral sclerosis: A review. *J. Neurol. Sci.* **399**, 217–226 (2019).

3. Vance, C. *et al.* Mutations in FUS, an RNA processing protein, cause familial amyotrophic lateral sclerosis type 6. *Science (80-.).* **323**, 1208–1211 (2009).

4. Morlando, M. *et al.* FUS stimulates microRNA biogenesis by facilitating co-transcriptional Drosha recruitment. *EMBO J.* **31**, 4502–4510 (2012).

5. Dichmann, D. S. & Harland, R. M. fus/TLS orchestrates splicing of developmental regulators during gastrulation. *Genes Dev.* **26**, 1351–63 (2012).

6. Deng, Q. *et al.* FUS is phosphorylated by DNA-PK and accumulates in the cytoplasm after DNA damage. *J. Neurosci.* **34**, 7802–7813 (2014).

7. Kim, H. J. Cell fate control by translation: MRNA translation initiation as a therapeutic target for cancer development and stem cell fate control. *Biomolecules* **9**, (2019).

8. Kamelgarn, M. *et al.* ALS mutations of FUS suppress protein translation and disrupt the regulation of nonsense-mediated decay. *Proc. Natl. Acad. Sci. U. S. A.* **115**, E11904–E11913 (2018).

9. López-Erauskin, J. *et al.* ALS/FTD-Linked Mutation in FUS Suppresses Intra-axonal Protein Synthesis and Drives Disease Without Nuclear Loss-of-Function of FUS. *Neuron* **100**, 816-830.e7 (2018).

10. Zappulo, A. *et al.* RNA localization is a key determinant of neurite-enriched proteome. *Nat. Commun.* **8**, 583 (2017).

11. Rogelj, B. *et al.* Widespread binding of FUS along nascent RNA regulates alternative splicing in the brain. *Sci. Rep.* **2**, (2012).

12. Deshpande, D. *et al.* Synaptic FUS Localization During Motoneuron Development and Its Accumulation in Human ALS Synapses. *Front. Cell. Neurosci.* **0**, 256 (2019).

13. Aviner, R. The science of puromycin: From studies of ribosome function to applications in biotechnology. *Comput. Struct. Biotechnol. J.* **18**, 1074 (2020).

14. RM, B., HW, L., H, J., RH, G. & MS, C. Cell-specific Profiling of Nascent Proteomes Using

Orthogonal Enzyme-mediated Puromycin Incorporation. *ACS Chem. Biol.* **11**, 1532–1536 (2016).

15. Halliday, M. *et al.* Partial restoration of protein synthesis rates by the small molecule ISRIB prevents neurodegeneration without pancreatic toxicity. *Cell Death Dis.* **6**, e1672–e1672 (2015).

16. Schneider-Poetsch, T. *et al.* Inhibition of eukaryotic translation elongation by cycloheximide and lactimidomycin. *Nat. Chem. Biol.* **6**, 209–217 (2010).

17. Lo Bello, M. *et al.* ALS-Related Mutant FUS Protein Is Mislocalized to Cytoplasm and Is Recruited into Stress Granules of Fibroblasts from Asymptomatic FUS P525L Mutation Carriers. *Neurodegener. Dis.* **17**, 292–303 (2017).

18. Tyzack, G. E. *et al.* Widespread FUS mislocalization is a molecular hallmark of amyotrophic lateral sclerosis. *Brain* (2019). doi:10.1093/brain/awz217

19. S, N. *et al.* TDP-43 transports ribosomal protein mRNA to regulate axonal local translation in neuronal axons. *Acta Neuropathol.* **140**, 695–713 (2020).

20. Oliveira, D. *et al.* Different gene expression profiles in iPSC-derived motor neurons from ALS8 patients with variable clinical courses suggest mitigating pathways for neurodegeneration. *Hum. Mol. Genet.* **29**, 1465–1475 (2020).

21. Cestra, G., Rossi, S., Di Salvio, M. & Cozzolino, M. Control of mRNA Translation in ALS Proteinopathy. *Front. Mol. Neurosci.* **0**, 85 (2017).

22. Lee, C. S. *et al.* Human DDX3 functions in translation and interacts with the translation initiation factor eIF3. *Nucleic Acids Res.* **36**, 4708–4718 (2008).

23. He, J. Z. *et al.* Enhanced translation of heme oxygenase-2 preserves human endothelial cell viability during hypoxia. *J. Biol. Chem.* **285**, 9452–9461 (2010).

24. Song, P., Yang, F., Jin, H. & Wang, X. The regulation of protein translation and its implications for cancer. *Signal Transduct. Target. Ther. 2021 61* **6**, 1–9 (2021).

25. Du, Z.-W. *et al.* Generation and expansion of highly pure motor neuron progenitors from human pluripotent stem cells. *Nat. Commun.* **6**, 6626 (2015).

26. McQuin, C. *et al.* CellProfiler 3.0: Next-generation image processing for biology. *PLOS Biol.* **16**, e2005970 (2018).

27. Cox, J. & Mann, M. MaxQuant enables high peptide identification rates, individualized p.p.b.-range mass accuracies and proteome-wide protein quantification. *Nat. Biotechnol.* **26**, 1367–72 (2008).

28. Cox, J. *et al.* Accurate proteome-wide label-free quantification by delayed normalization and maximal peptide ratio extraction, termed MaxLFQ. *Mol. Cell. Proteomics* **13**, 2513–26 (2014).

SUPPLEMENTARY FIGURES:

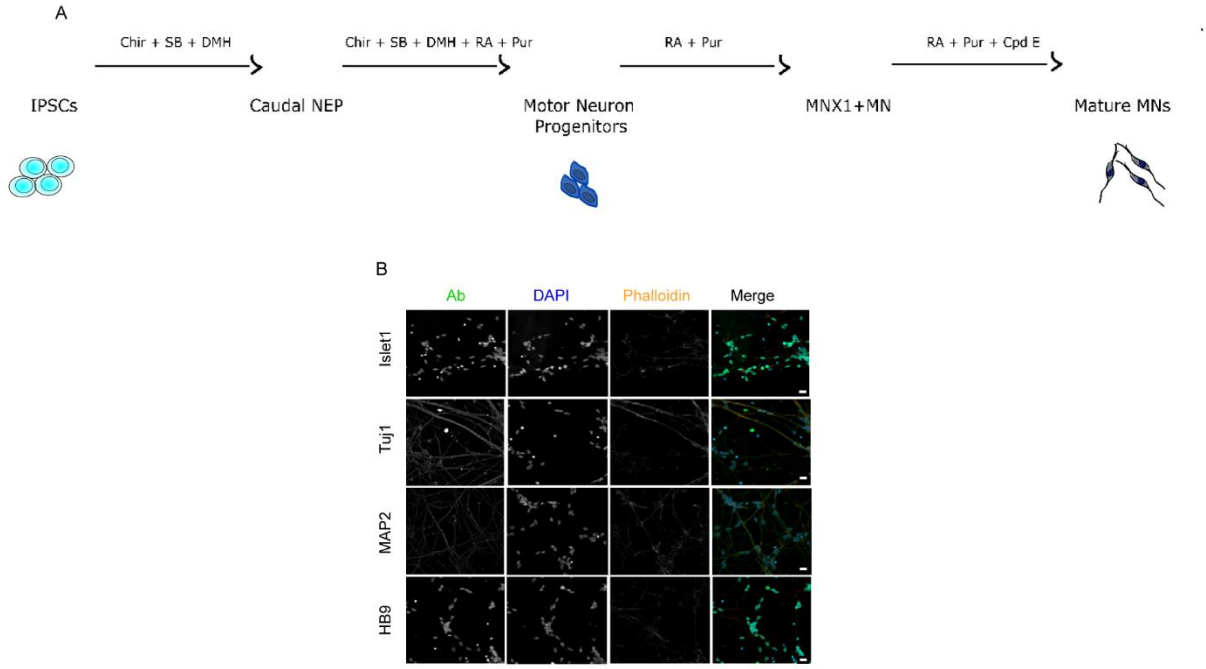

Supplemental Figure 1: Differentiation and characterization of MNs. a. Schematic representation of the differentiation protocol used to obtain motor neurons. **b.** Representative immunofluorescence staining for characterization of the motor neurons obtained after the differentiation protocol. (Scale bar 20µm).

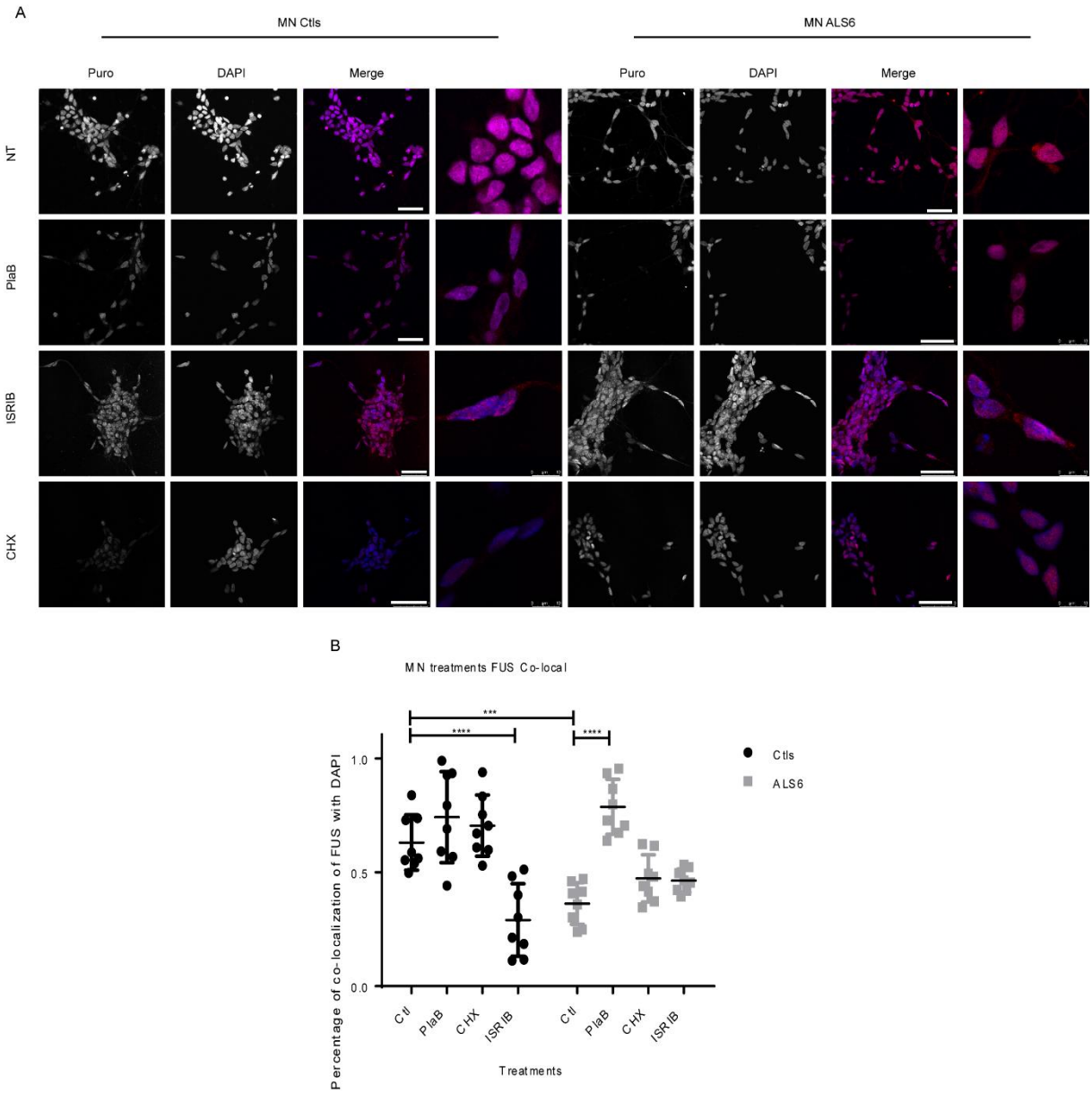

Supplemental Figure 2: FUS localization in MNs treated with compounds regulating translation or splicing. a. Representative images of immunofluorescence staining of FUS to observe its localization on Ctls and ALS6 in IPSCs-derived MNs from Ctls and ALS6 patients treated with different compounds. Scale bar 50 µm. **b.** Quantification of FUS localization by immunofluorescence staining with the anti-FUS antibody in Ctls and ALS6 IPSCs-derived MNs treated with different compounds. (*, $P < 0.05$; two-way ANOVA with Sidak`s multiple comparison test; n = 8 per group).

SUPLEMMENTARY TABLE:

Table 1: List of the proteins found to interact with only controls, both controls and ALS6 or only ALS6 cells in the shotgun proteomics experiments.

Samples	Number of proteins	Protein Gene name				
Controls and ALS6	25	YBX1	IGF2BP3	ACTG1	HNRNPA1	HNRNPC
		RPS2	SYNCRIP	HNRNPU	PABPC1	RPL4
		RPS18	HIST1H4A	ELAVL1	HIST1H2BM	HIST1H2AJ
		HNRNPH1	RPS3	RPS16	UPF1	DHX9
		FUS	VIM	RPS9	IGF2BP1	RPL31
ALS6	58	H2AFY2	HNRNPA0	NES	LMNB1	RPL7A
		RPS17	IGF2BP2	EEF1A1	RPS4X	RALY
		RPS3A	RPL6	PTBP1	PRPF8	MSI2
		FXR1	GNB2L1	EIF3A	KHDRBS1	HNRNPA3
		DDX5	RPL3	RPL13	HNRNPM	ILF2
		RPSA	ILF3	SAFB	RBMX	SFPQ
		HNRNPR	RPS14	RPS8	HIST1H1B	DHX15
		H3F3A	RPL27	HNRNPK	HIST1H1C	LMNB2
		G3BP1	NONO	RPL23A	MATR3	G3BP2
		HNRNPA2B1	RPS7	H2AFY	XRCC6	RPS10
		HNRNPD	HIST2H2BE	SF3B3	NPM1	HSPA8
		RPLP0	CAPRIN1	RPS19		
Controls	5	RPS25				
		RPL17				
		RPS6				
		RPL18				
		RPS20				

Chapter 3

IFNy protects ALS MNs from oxidative stress by enhancing global protein synthesis rates

Amanda Faria Assoni [1,2], René Wardenaar[2], Danyllo Oliveira[1], Petra Bakker [2], Valdemir Melechco Carvalho [3], Oswaldo Keith Okamoto[1] Mayana Zatz [1], Floris Foijer [2]

1 Instituto de Biociências, Universidade de São Paulo, São Paulo 05508-900, Brazil.

2 European Research Institute for the Biology of Ageing, University of Groningen, Groningen, 9713 AV, the Netherlands.

3 Division of Research and Development, Fleury Group, São Paulo 04344-070, Brazil.

ABSTRACT

ALS is a late-onset progressive neurodegenerative disease that leads to respiratory failure in patients within 3-5 years of symptom onset. Currently there is no cure and therefore the only possible treatment is to relieve symptoms. ALS comes in several subtypes and inflammation is one of the few features shared between these subtypes. Furthermore, viral infections, exogenous triggers of inflammation, are known to adversely affect ALS pathogenesis. As inflammation can also be modulated by therapy, it provides an interesting feature that could be exploited to develop new treatments. One of these inflammation-modulating molecules that is also differentially expressed between ALS patients and healthy controls is interferon-gamma (IFNy). We investigated the effect of modulating the inflammatory response in induced pluripotent stem cell-derived motor neurons (MN) from ALS6 patients and healthy controls. ALS6 (with mutations on the Fused in Sarcoma gene) is the type of ALS with the earliest mean disease onset age. We find that INFy - a pro-inflammatory molecule - does not cause a decrease in cell viability in either controls or patient MNs. Instead, IFNy treatment of ALS6 MNs prevents these cells from going into apoptosis when exposed to oxidative stress. We find that this protection is due to upregulation of the translation rate in ALS6 MNs. Overall, our results show that IFNy treatment restores the sensitivity of ALS6 MNs to oxidative stress by translocating Fused in Sarcoma (FUS) back into the nucleus and avoiding the inhibitory effect of cytoplasmic FUS on the translational machinery. Our findings therefore suggest that ALS patients with *FUS* mutations would benefit from IFNy treatment to slow down disease pathology.

1- INTRODUCTION

ALS is a late-onset progressive neurodegenerative disease that causes patients to die of respiratory failure within 3-5 years of symptom onset [1]. The first cells to be affected are the motor neurons (MNs), which leads to symptoms like muscle twitching, spasms and stiffness [2]. There are two types of ALS: familial (in which inherited mutations increase the likelihood of developing symptoms) and sporadic (in which the causes of symptoms are either unknown or the mutation causing the phenotype was a *de novo* event). The familial forms are classified according to the mutated genes. ALS is highly heterogeneous in terms of causes, age and location of symptom onset, and disease progression, further complicating the search for new therapies. Currently, there is no cure, and for most patients the main treatment is to relieve symptoms [3].

Even though ALS -driving mutations have been identified over the past years, the exact molecular mechanism that causes motor neuron degeneration is still unclear. Generally, MNs of ALS patients exhibit defects in nuclear cytoplasmic transport, mitochondria metabolism, vesicular transport, DNA repair, stress granule dynamics, as well as higher markers of oxidative stress and neuroinflammation [4,5].

One of the common features between different types of ALS are abnormalities in the inflammatory response, including neuroinflammation in the brain and spinal cord and alterations of T lymphocytes, monocytes, complement and cytokines in the peripheral blood. Given that there are several therapeutic strategies to modulate inflammation, this feature could potentially be used to develop ALS treatments [6]. However, there is no clear consensus on the role that the immune system plays in ALS, as a combination of excessive inflammation, autoimmunity and inefficient immune responses can be observed simultaneously in ALS patients. Clinical trials in which ALS patients and other neurodegenerative diseases were treated with different anti-inflammatory agents showed no protection against neuronal decline [1]. In such cases, immunosuppression could limit neuroprotective responses and also be a trigger and/or modifier of this disease[7].

Even though inflammation is a hallmark feature of ALS, the role of the immune system in ALS pathology is still largely unclear. It appears that the initial immune response to aggregated proteins or similar stressors promotes neuroprotection, but that when the damage becomes unmanageable, the response transitions into increased neuroinflammation and neurotoxicity[6]. Another important indication that the immune system plays a major role in ALS pathogenesis is the fact that viral infections are a key risk factor for the onset of ALS pathogenesis[10]. Interferon-gamma (IFNy) is a pleiotropic cytokine with important role in both innate and adaptive immunity, therefore, it is an antiviral mediator that plays a fundamental role in the elimination of viruses from the CNS. Both its antiviral and immunomodulatory functions are critical during viral infection, as it restricts viral replication and elicits an appropriate antiviral immune response, while also negatively regulating this response to minimize tissue damage[11]. However, the role of IFNy in ALS is still controversial. For

instance, IFNy concentrations were reported to be decreased in plasma samples from patients with ALS compared to controls[12]. Conversely, others have shown that IFNy concentrations were increased in cerebral spinal fluid (CSF) and serum from hSOD1(G93A) transgenic mice and of ALS patients[13] and that the expression of IFNy receptors was increased in symptomatic hSOD1(G93A) transgenic mice[14].

ALS6 is one of the most aggressive types of ALS, leading to the earliest onset of the disease among all ALS sub-types[15]. ALS6 is associated with mutations in the FUS gene, a DNA/RNA-binding protein involved in many cellular functions, including DNA damage repair, splicing, and RNA transport[16]. Currently, more than 50 different mutations in FUS were detected in ALS6 cases. There are mutations in the disordered N terminal region, as well as in the Rgg and RRM region, but most of the mutations are found in the NLS domain. The majority of mutations in the FUS gene result in cytoplasmic mislocalization of FUS, but the mutations on the NLS make this phenotype more intense. FUS mislocalization also occurs in MNs of other familial forms of ALS and also in sporadic cases where FUS itself is not mutated[17].

In this study, we investigate the relationship between mutant FUS-driven ALS6 and interferon signaling in patient-derived Induced Pluripotent Stem Cells (IPSCs), neural progenitor cells and motor neurons. For this, we used IPSCs from a family with two individuals with a R521H mutation within the FUS gene and two relatives without this mutation that are phenotypically healthy. Since iPSC (-derived) cells can lose important properties of aged cells that are relevant to recapitulating the disease phenotype, we exposed our cells to oxidative stress induced by Sodium Arsenite (SA) and compared the responses between patient and control-derived cell types. Indeed, we find that SA induces apoptosis more in ALS6 MNs than in MNs of unaffected controls. Surprisingly, we observed that concomitant IFNy treatment partly rescued apoptosis of ALS6 MNs to similar levels as observed in MNs generated from control individuals. Intriguingly, IFNy treatment had no effect on SA-treated control MNs. Furthermore, we find, in agreement with others that translation rates are decreased in ALS6 MNs and that IFNy treatment also rescues this back to translation levels observed in control cells. Finally, we observe that IFNy treatment rescues mutant FUS mislocalization in the cytoplasm making it more localized in the nucleus. Together, our observations suggest that IFNy treatment could benefit ALS6 patients by preventing FUS mislocalization and rescuing protein translation defects.

2- RESULTS

2.1- iPSC-derived MNs from ALS6 patients are more susceptible to apoptosis when exposed to oxidative stress and INFy treatment rescues Motor-Neuron viability on sodium arsenite-burden

Induced pluripotent stem cells (iPSCs) lines derived from patients with genetic diseases are a powerful tool for disease modeling and drug discovery. Therefore, to investigate the role of IFNy in ALS6, we made use of IPSCs from a family with two patients with a R521H mutation in the FUS gene and of two relatives who did not carry the mutation and were phenotypically healthy. To study the impact of IFNy treatment in the most relevant cell type for ALS, we differentiated the iPSCs into motor neurons according to published protocols(Du et al., 2015). One limitation of modelling ageing-associated disease with iPSCs and differentiated progeny is that reprogramming erases age-associated damage to cells. Therefore, to assess age-associated phenotypes, cells need to be artificially 'aged'[19]. For this purpose, we compared three drivers of ageing, i.e. inflammation, oxidative stress, and DNA damage, which all are elevated in symptomatic ALS MNs[21]. To mimic inflammation, we chose IFNy, to mimic oxidative stress we chose sodium arsenite (SA), and neocarzinostatin (NCS) was used to induce DNA damage. To test the viability of the motor neurons following treatment, we performed MTS assays. 24h of treatment with each compound. We found that only SA treatment resulted in in a differential response between motor neurons from ALS and controls (Fig. 1A). Furthermore, we found that INFy treatment only modestly reduced viability of patient and control MNs (Fig. 1A). We conclude that MNs derived from ALS patients are more sensitive to oxidative stress than those of healthy controls.

To better understand the role of IFN signaling in stressed MNs, we next combined SA and IFNy treatment on ALS patient- and control-derived MNs. Intriguingly, here we found that IFNy increased the viability of ALS6 MNs treated with SA back to levels similar to those of control MNs (Fig. 1B), suggesting that IFNy somehow rescues the detrimental effect of the FUS mutation in ALS cells. Quantification of apoptotic cells confirmed this: while SA treatment increases the number of cleaved Caspase 3/7 positive cells dramatically in both control and ALS patient-derived MNs, the latter cells showed most apoptotic cells. Importantly, also here, IFNy treatment reduced apoptosis specifically in the ALS-derived MNs back to apoptosis levels observed in control-derived MNs. (Fig. 1C and D). These observations suggest that IFNy treatment can improve the survival of ALS-patient-derived MNs that are exposed to oxidative stress.

To better understand these results, we analyzed the transcriptomes by RNA sequencing of control- and ALS-patient derived MNs that were treated or not with either SA or IFNy or a combination of both.

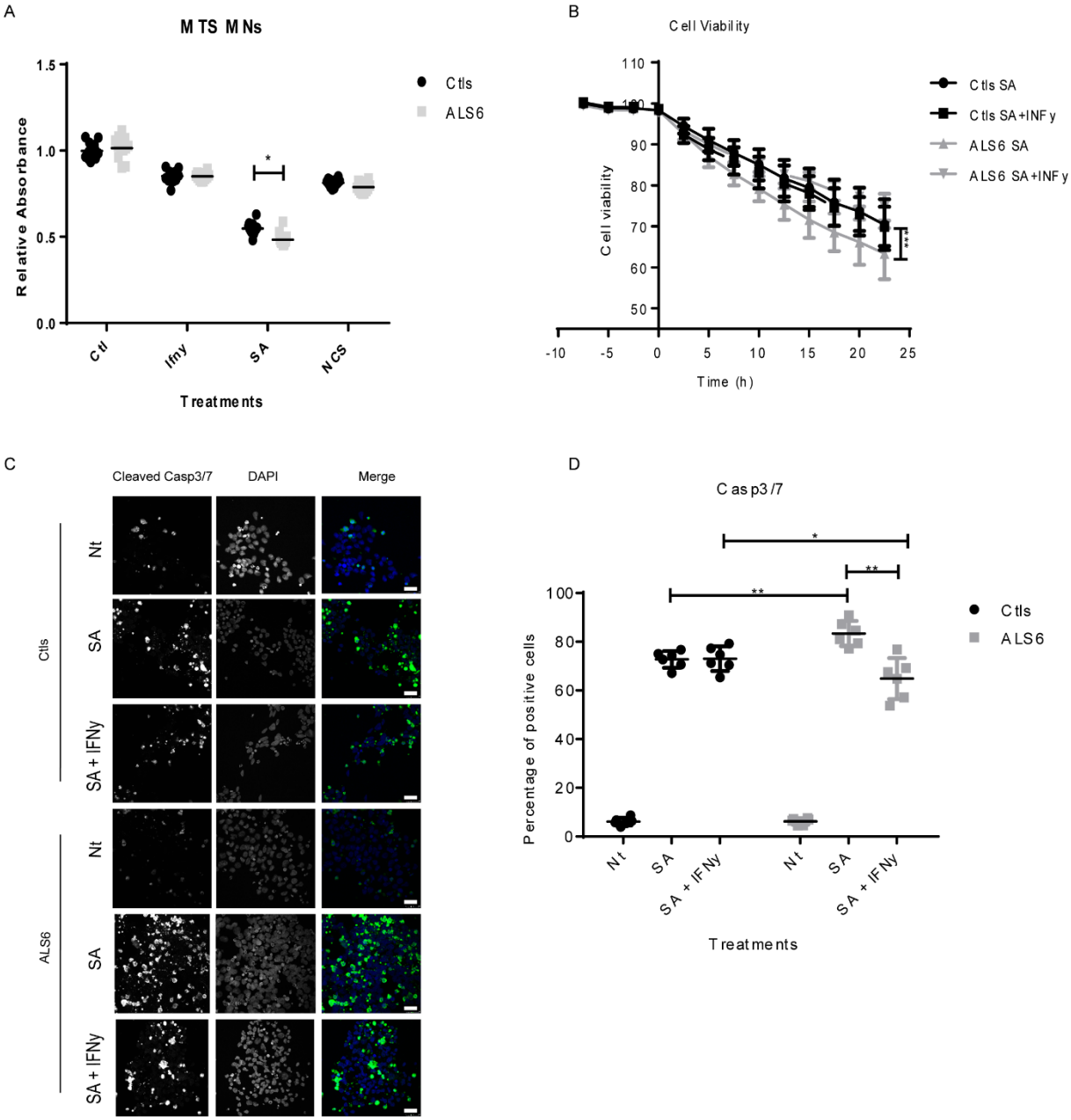

Fig 1. INFy treatment rescues ALS6 MN decreased viability caused by oxidative stress induced apoptosis. a. MTS assay after 24h of treatment of MNs with each compound. (*, $P < 0.05$; ordinary two-way ANOVA with Bonferroni multiple comparison test; $n = 8$ per group). **b.** Kill curve using impedance-based xCELLigence real-time cell analysis system at MN, treated with SA or SA plus IFNy for 24 hours. (***, $P < 0.001$, two-way ANOVA with Tukey multiple comparison test; $n = 8$ per group). **c.** Representative immunofluorescence staining with anti-caspase3/7 of MN untreated (Nt) or treated with SA or SA plus IFNy for 24 h. Scale bar 25 um. **d.** Quantification of the percentage of caspase 3/7-positive MNs treated for 24 h. (*, $P < 0.05$; **, $P < 0.01$; and ***, $P < 0.001$, two-way ANOVA with Tukey multiple comparison test; $n = 8$ per group).

In general, it is observed that gene expression of MNs shifts depending on whether they are stressed or not (Fig. 2A and B). The larger differences in gene expression are due to the

treatments to which the cells are subjected, rather than the presence of the mutation. Another observation was that fewer genes were differentially expressed in the treated ALS6 cells compared to not treated across all conditions, suggesting that they are unable to show a complete response to the compounds (Fig. 2C).

Interestingly, when we compared the effect of SA treatment between ALS patient-derived MNs and control-derived MNs, we found that ALS patient-derived MNs failed to induce genes that are associated with translational initiation and mitochondrial homeostasis (Supplementary table1, Fig. 2 D and E).

However, because IFNy treatment specifically rescued the viability of ALS6 MNs, we focused on identifying the genes that were differentially expressed on ALS6 neurons treated with SA alone or SA plus IFNy (Supplementary table 2, Fig. 2 F and G). Those genes that rescued ALS6 MNs from entering the apoptotic process due to oxidative stress were upregulated, and in addition to downstream IFNy effectors, the genes were associated with translational initiation (Fig. 2 F and G).

In conclusion, we find that ALS6 MNs are more susceptible to oxidative stress-induced apoptosis than MNs derived from unaffected controls. Surprisingly, treatment with IFNy had a protective effect on the viability of ALS6-MNs exposed to oxidative stress, which correlated with a specific upregulation of translation-related genes in ALS6 MNs.

2.2 - IFNy increases translation rates on ALS6 MNs by avoiding mislocalization of FUS to the cytoplasm

As our previous analyses suggested a role for deregulated translation in ALS patient-derived MNs we next investigated whether IFNy treatment, combined or not with SA, influenced translation rates. For this, we made use of a puromycin-incorporation assay, a well-established method to quantify translation rates(RM et al., 2016; Aviner, 2020) . In agreement with earlier findings, we found that translation rates are significantly lower in ALS patient MNs compared to MNs from unaffected relatives(Kamelgarn et al., 2018; López-Erauskin et al., 2018). Furthermore, SA treatment reduced translation rates in control MNs, but not in ALS patient MNs (SA even moderately increased translation), while IFNy treatment increased translation in ALS patient MNs, but not in controls. In line with our previous findings, we also found that while IFNy did not change translation rates of SA-treated control MNs, it significantly increased translation rates in ALS patient MNs almost to the level comparable to untreated control MNs (Fig. 3A, B).

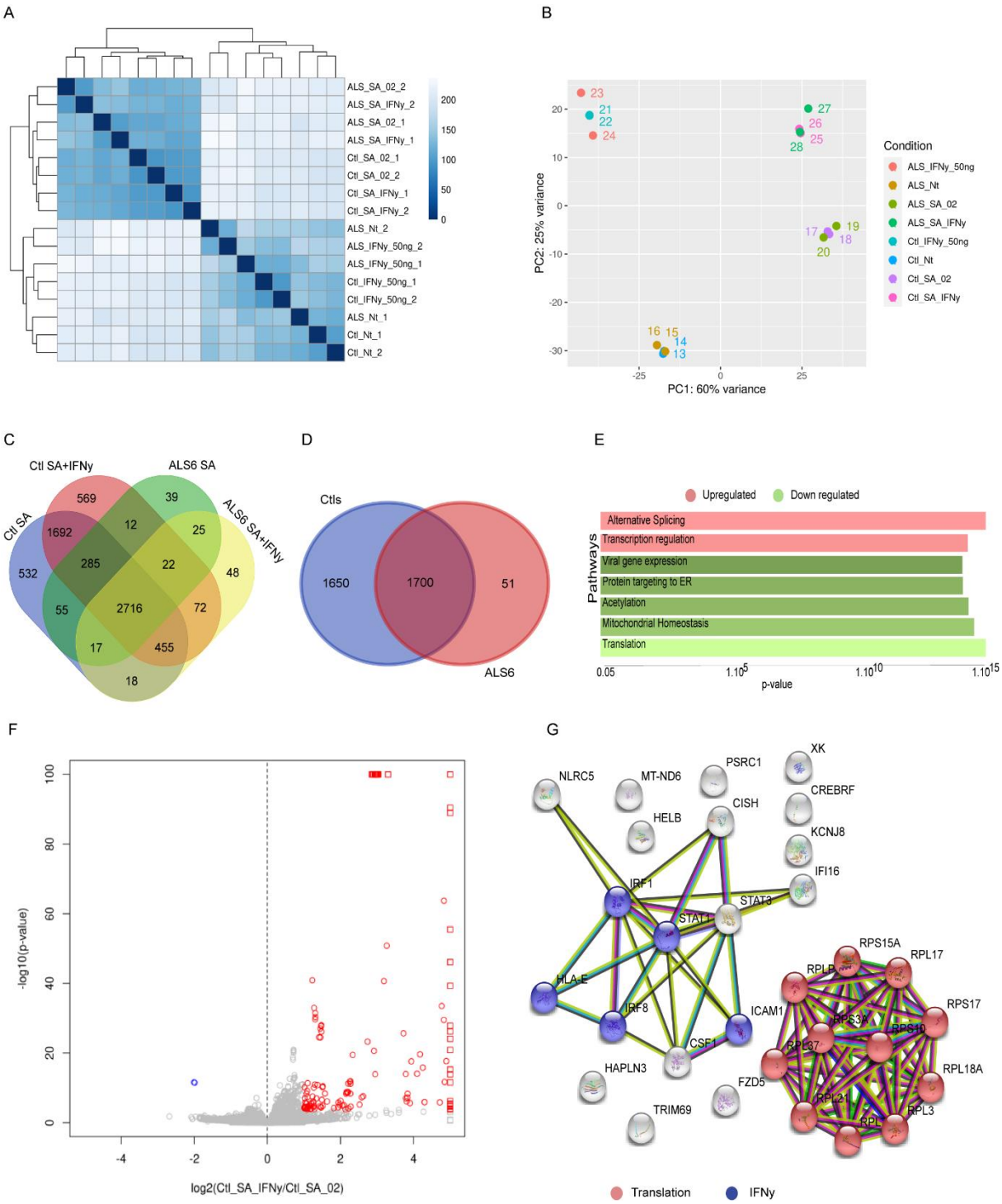

Fig 2. RNA sequencing uncovers translation regulation by SA and IFNy. a. Hierarchical clustering of gene expression profile of controls and ALS6 MN with different treatments. **b.** PCA of gene expression profile of controls and ALS6 MN with different treatments. **c.** Venn diagram of genes differentially expressed with each treatment compared to non-treated MNs. **d.** Venn diagram of genes differentially expressed with SA treatment compared to non-treated MNs. **e.** Summary of cellular functions of enriched pathways differentially expressed with SA treatment in ALS6 MNs. **f.** Volcano plot of genes significantly differentially expressed between ALS6 MN treated with SA only and SA plus IFNy. **g.** String association of genes significantly differentially expressed between ALS6 MN treated with SA only and SA plus IFNy.

Beyond translation, our previous analyses also reveal differences in genes associated with mitochondrial homeostasis in the ALS MN. When assessing mitochondrial length, we found, in agreement with findings of others (Cui et al., 2012; Deng et al., 2018; Nakaya and Maragkakis, 2018) that MNs show mitochondrial shortening when exposed to oxidative stress. As observed for translation, also here we found that treatment with IFNy prevented mitochondrial shortening specifically in SA-treated ALS6 MNs (Fig. 3 C and D).

As mutant FUS has been reported to mislocalize into the cytoplasm (Chapter 2), we next wanted to determine whether IFN treatment of ALS6 MNs would alter this, given the beneficial effects of IFNy treatment. Indeed, we found that IFNy treatment resulted in a significantly increased fraction of ALS patient-derived MNs with only nuclear FUS to a level similar as observed for control MNs (Fig. 3 E and F).

Altogether, our work indicates that ALS-patient derived MNs are more sensitive to oxidative stress induced by SA, and that IFNy treatment rescues this sensitivity. This rescue coincides with increased translation rates and decreased cytoplasmic localization of mutant FUS. Although future work will be required to resolve the molecular mechanism, our findings suggest that ALS6 patients could benefit from IFNy treatment to decrease MN death and thus to potentially delay disease progression.

3- DISCUSSION

In this study, we demonstrate for the first time a protective role of IFNy in motor neurons from ALS patients. ALS is a very heterogeneous disease for which pathogenesis includes many cellular phenotypes such as increased DNA damage, nucleocytoplasmic transport defects, mitochondrial metabolic problems, increased oxidative stress and inflammatory markers [5,23–25]. We hypothesized that DNA damage, oxidative stress, and inflammation are markers that increase with ageing and that would contribute to pathogenesis in ALS patients. Therefore, we generated MNs from control- and ALS patients-derived iPSCs and tested the response to these compounds on these cells. We found that ALS6 MNs display decreased cell viability index and increased levels of cleaved caspase 3/7 (Cas3/7) compared to control MNs only after oxidative stress induced by sodium arsenite.

Because the immune system may play a dual role on the response to the initial ALS pathogenic phenotypes[6], we then investigated whether IFNy treatment along with SA would prevent or increase the proportion of cells entering apoptosis. Intriguingly, we found that IFNy treatment did not significantly alter the survival of control MNs, but restored the viability of ALS6 MNs to the level of control cells.

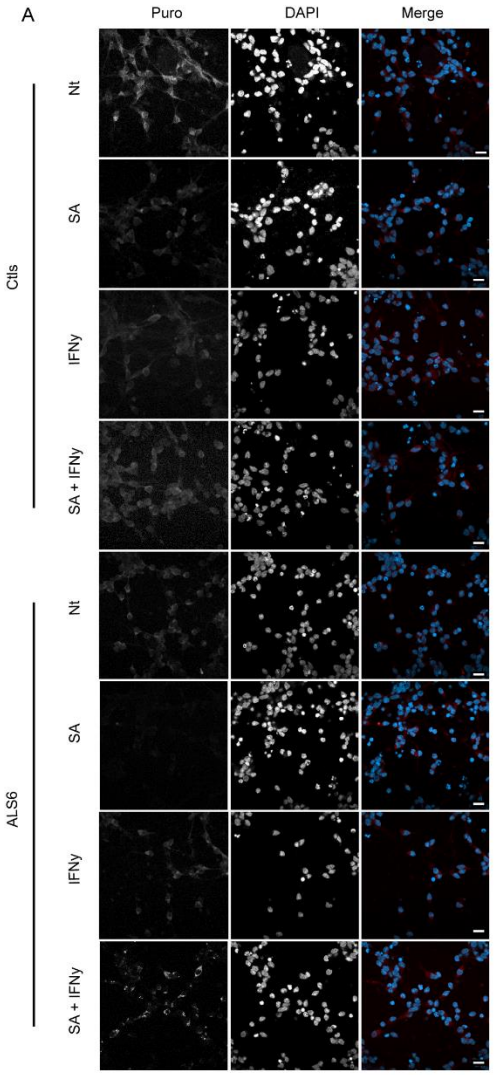
A
Puro
DAPI
Merge
Ctls
ALS6
Nt
SA
IFNy
SA + IFNy

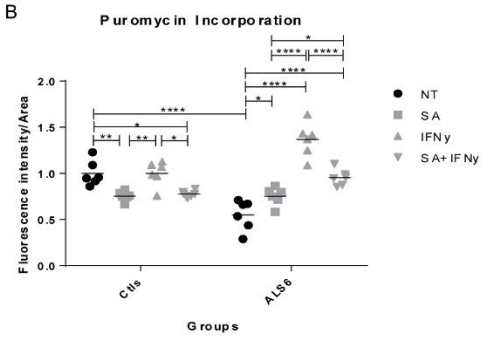
B
Puromycin Incorporation
Fluorescence intensity/Area
Ctls
ALS6
Groups
NT
SA
IFNy
SA+ IFNy

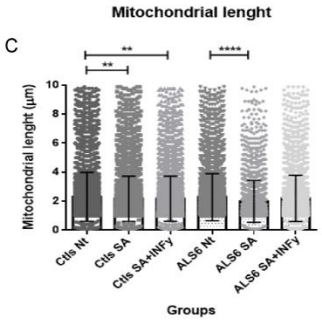
C
Mitochondrial lenght
Mitochondrial lenght (µm)
Ctls Nt
Ctls SA
Ctls SA+INFy
ALS6 Nt
ALS6 SA
ALS6 SA+INFy
Groups

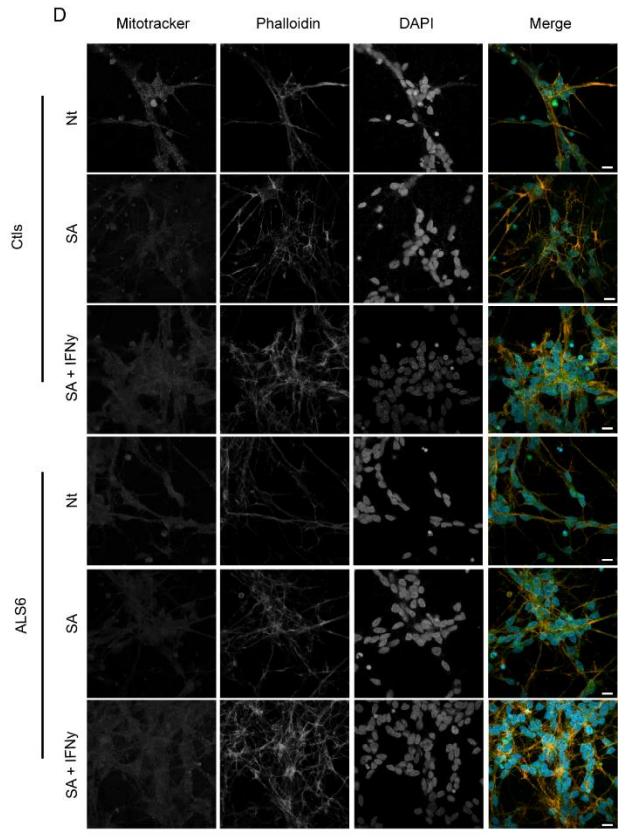
D
Mitotracker
Phalloidin
DAPI
Merge
Ctls
ALS6
Nt
SA
SA + IFNy

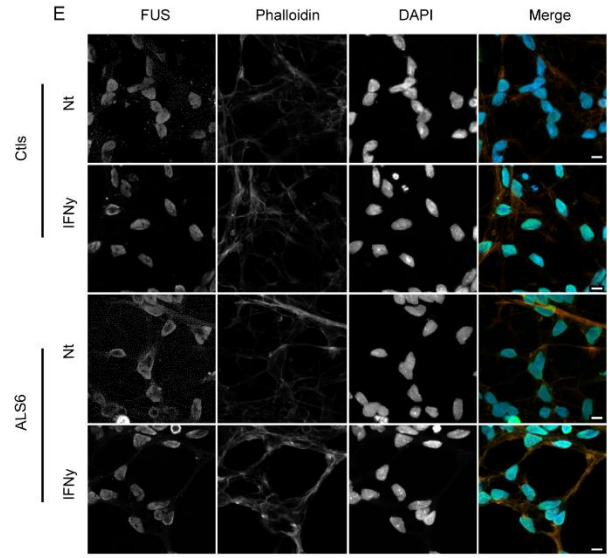
E
FUS
Phalloidin
DAPI
Merge
Ctls
ALS6
Nt
IFNy

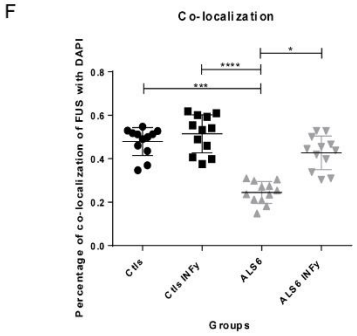
F
Co-localization
Percentage of co-localization of FUS with DAPI
Ctls
Ctls INFy
ALS6
ALS6 INFy
Groups

Fig 3. INFy rescues the defective cellular features observed in ALS6 MNs. a. Representative images of immunofluorescence staining with anti-puromycin antibody in MN in the four treatments: nt, IFNy, SA, and SA + IFNy. Scale bar 20 um. **b**. Quantification of the relative intensity of puromycin incorporation in immunofluorescence staining with the anti-puromycin antibody in MN in the four treatments: nt, IFNy, SA, and SA + IFNy. (*, $P < 0.05$; **, $P < 0.01$; and ***, $P < 0.001$, two-way ANOVA with Tukey multiple comparison test; $n = 8$ per group). **c.** Quantification of the length of mitochondria in MNs with the treatments: nt, SA and SA + IFNy. (*, $P < 0.05$; **, $P < 0.01$; and ***, $P < 0.001$, two-way ANOVA with Tukey multiple comparison test; $n = 30$ fields from each treatment in 4 different experiments). **d.** Representative images of immunofluorescence staining with mitotracker on MNs with the treatments: nt, SA and SA + IFNy. Scale bar 10 um. **e.** Representative images of immunofluorescence staining with anti-FUS antibody in MNs treated or not treated with IFNy. Scale bar 10 um. **f.** Quantification of FUS localization in immunofluorescence staining with the anti-FUS antibody in MNs treated or not treated with IFNy. (*, $P < 0.05$; **, $P < 0.01$; and ***, $P < 0.001$, two-way ANOVA with Tukey multiple comparison test; $n = 8$ per group)

When assessing the transcriptomes of control- and ALS patient-derived MNs, we found that SA treatment significantly decreased expression of translation-related genes both in ALS6 and control MNs, and furthermore lead to decreased expression of mitochondria-related genes specifically in ALS6 MNs. IFNy treatment rescued this downregulation and instead led to upregulation of protein synthesis-related genes, especially in ALS6 MNs. In line with these results, we found that IFNy treatment indeed functionally increased protein translation rates in ALS6 MNs as assessed by a puromycin incorporation assay and furthermore prevented mitochondrial length shortening in MNs treated with SA.

Our findings might be relevant for other types of ALS as well as deregulation of translation has been observed in many models of ALS, including those with mutations in the TDP43[26] , FUS [27], VAPB[28] and SOD1[29] genes. Overall, the findings from these models are suggesting that persistent translational suppression may impair neuronal viability and contribute to the pathogenic mechanisms of ALS. Therefore, it would be interesting to test the effect of IFNy treatment in MNs derived from patients suffering from other subtypes of ALS.

While this study does not fully reveals the molecular mechanism underlying the beneficial effect of IFNy, we find, in agreement with others (Ito et al., 2011; Deng et al., 2015; Blokhuis et al., 2016; Kamelgarn et al., 2016; López-Erauskin et al., 2018; de la Fuente and Emc, 2020; Tsai et al., 2020), that translational inhibition and mitochondrial shortening coincide with mislocalization of the FUS protein to the cytoplasm, as also discussed in the previous chapter of this thesis, Chapter 2. Importantly, we find that IFNy treatment not only rescues the translation defect and prevented mitochondrial shortening promoted by oxidative stress, but also caused FUS to relocate back to the nucleus. While the exact mechanism responsible for this localization rescue requires more work, it does suggest that IFN-γ operates upstream of the process that causes mutant FUS to mislocalize.

Relevant for potential use of our findings, it is important to note that IFNγ is already used in the clinic to treat leukemia and chronic granulomatosis [31], and therefore provides a safe molecule that can also be used to treat other diseases.

However, it is also important to note that our work was performed on newly differentiated MNs that probably mostly represent the features of presymptomatic MNs. Also in that respect, our results are in agreement with literature that refers to the neuroprotective effect of the immune system in the early stages of the disease(Evans et al., 2009; Celeste and Miller, 2018b; Chen et al., 2019; de Munter et al., 2020) .

Overall, our results show that IFNy treatment rescues the increased sensitivity of ALS MNs to oxidative stress and suggest that this is due to translocating FUS back into the nucleus thus avoiding the inhibitory effect of cytoplasmic FUS on the translational machinery. Future work is required to further disentangle the molecular mechanism underlying this rescue and test whether (prophilactic) INFy treatment can prevent or delay symptoms in ALS(6) patients.

4- METHODS

Cellular reprogramming and motor neuron differentiation

After informed consent, fibroblasts were isolated from all individuals (N=4, 2 affected and 2 controls), and were used for reprogramming using CytoTune™-iPS 2.0 Sendai Reprogramming Kit as manufacturer recomendation. Induced pluripotent stem cells (iPSCs) were then obtained for such individuals. Expression of pluripotency markers *SSEA4* and *OCT4 Nanog* and *SOX2* was checked by immunofluorescence (Supplementary Figure 1 B). Differentiation into motor neurons (MNs) was performed as previously published(Du et al., 2015) (Supplementary Fig. 1 A). Briefly, the iPSCs were grown in Essential 8 medium (Thermo) until reaching 80% of confluency. Then, they were cultivated in NB medium containing DMEM/F12, Neurobasal medium, N2, B27 and Glutamax (all from Thermo) and subjected to a two steps protocol of neural induction/ caudalization and ventralization for obtaining motor neuron progenitors (MNPs). The first phase was achieved after cultivating iPSCs for six days in NB containing Dorsomorphin (2 μM), SB431542 (2 μM), CHIR99021 (3 μM) and Ascorbic acid (0.1 mM). The following step, which also lasted 6 days, consisted of cultivating the cells in NB medium and Dorsomorphin (2 μM), SB431542 (2 μM), CHIR99021 (1 μM), retinoic acid (0.1 μM), Ascorbic acid (0.1 mM) and Purmorphamine (0.5 μM). After obtaining the MNPs, the cells were seeded in 60 mm2 plates containing Matrigel (Corning) and subjected to motor neuron differentiation by cultivating them for 6 days in NB medium containing retinoic acid (0.5 μM), Purmorphamine (0.1 μM) and Ascorbic acid (0.1 mM). A further step of neural maturation was also carried out by adding Compound E (0.1 μM) to the same medium used for motor neuron induction.The presence of β-tubulin, MAP2, Hb9 and ISL1 was confirmed by IF (Supplementary Figure 1 C).
Differentiation towards motor neurons were made 3 different times for each individual to rule out batch-dependent results.

MTS assay

Motor neurons were plated (15000 cells per well) at day zero. After 24h of plating, the compounds were added to the media and kept at 37^0C for 20 hours. Measurements were made according to manufacturer's instructions. Briefly, 10 µl of MTS reagent was added directly to the wells and cell plates were incubated at 37°C for 4 hours. Absorbance was measured at 490 nm on a SpectraMax Plus384 reader (Molecular Devices; Sunnyvale, CA). Background absorbance was first subtracted using a set of wells containing medium only, then normalized to and expressed as a relative percentage of the plate-averaged DMSO control.

Cell viability assay- Kill curves were determined by the impedance-based xCELLigence real-time cell analysis system (ACEA Biosciences, San Diego, CA, USA). Briefly, 50 µL of cell culture media was added to each 96 well of the E-Plate 96 PET (ACEA Biosciences) for background reading. Subsequently, 50 µL of cell suspension containing 15000 cells was added to each well and the plate was placed on xCELLigence station inside the incubator. Twenty-four hours later, cells were treated with each compound as described next and impedance reflecting cell adhesion and death changes was measured every 15 min for 24 hours. Data are expressed as changes of impedance ('Cell Index') over time, according to the manufacturer's instruction.

Compound treatments

IFNy: All treatments were made at a concentration of 50ng/ml for the time stated at each figure.

SA: All treatments were made at a concentration of 5µM for the time stated at each figure.

NCS: All treatments were made at a concentration of 100ng/ml for the time stated at each figure.

Immunofluorescence

Cells were washed twice, fixed (3.7% formaldehyde RT for 20 minutes) and permeabilized for 30 minutes with 0.1% Triton X-100 and 5% bovine serum albumin in 1× PBS, prior to overnight incubation with the primary antibody (Supplementary Table S1) at 4°C. Cells were then washed 3 times in 1× PBS, incubated with the secondary antibody for 45min (Supplementary Table S1), and washed again 2 times in 1× PBS. Cell nuclei were stained with 1 µg/mL DAPI for 2 minutes and mounted on glass slides and cover slipped with VectaShield. All images were taken in confocal microscope (Zeiss LSM 800). All quantification of images were performed using Cell Profiler 3.0 as previously published(McQuin et al., 2018) .

Western Blot

Cells were harvested by accutase dissociation and lysed in elution buffer (150 mM NaCl, 0.1% NP-40, 5 mM EDTA, 50 mM HEPES pH7.5) containing complete protease inhibitor (Roche) for 15 minutes at 4oC. Then the samples were centrifuged at 300g, at 4°C for 10 min to remove insoluble residues. 20 µg of each sample was loaded on 10% polyacrylamide gels. Proteins were transferred to polyvinylidene difluoride (PVDF) membranes. After blocking in Odyssey blocking buffer (Li-cor Biosciences) at 4°C for 60 min, the membrane was incubated overnight at 4°C with the primary antibody (supplemental materials). Following incubation, the membrane was washed with PBS containing 0,1% Tween 20 (Sigma) three times and incubated in secondary antibody for 1 hour at room temperature. The blots were detected by the Odyssey imaging system (Li-cor Biosciences). The protein bands were quantified with Image studio lite software (Li-cor Biosciences).

Puromycin incorporation assay

Cells were incubated for 10 min in media with or without puromycin (Invitrogen) (20 µM). Cells were then either fixed for immunofluorescence or harvested for protein extraction and western blot.

RNA Sequencing

Following RNA extraction according to manufacturer instructions (Qiagen).Quality and quantity of the total RNA was assessed by the 2100 Bioanalyzer using a Nano chip (Agilent, Santa Clara, CA). Total RNA samples having RIN>8 were subjected to library generation. Strand-specific libraries were generated using the TruSeq Stranded mRNA sample preparation kit (Illumina Inc., San Diego, RS-122-2101/2), according to the manufacturer's instructions (Illumina, Part #15031047 Rev. E). Briefly, polyadenylated RNA from intact total RNA was purified using oligo-dT beads. Following purification, the RNA was fragmented, random primed and reverse transcribed using SuperScript II Reverse Transcriptase (Invitrogen, part #18064-014) with the addition of Actinomycin D. Second strand synthesis was performed using Polymerase I and RNaseH with replacement of dTTP for dUTP. The generated cDNA fragments were 3′-end adenylated and ligated to Illumina Paired-end sequencing adapters and subsequently amplified by 12 cycles of polymerase chain reaction. The libraries were analysed on a 2100 Bioanalyzer using a 7500 chip (Agilent, Santa Clara, CA), diluted and pooled equimolar into a 10 nM sequencing stock solution. Illumina TruSeq mRNA libraries were sequenced with 50 base single reads on a HiSeq2000 using V3 chemistry (Illumina Inc., San Diego). The resulting reads were trimmed using Cutadapt (version 1.12) to remove any remaining adapter sequences, filtering reads shorter than 20 bp after trimming to ensure efficient mapping. The trimmed reads were aligned to the GRCm38 reference genome using STAR (version 2.5.2b). QC statistics from Fastqc (version 0.11.5) and the above-mentioned tools were collected and summarized using Multiqc (version 0.8). Gene expression counts were generated by featureCounts (version 1.5.0-post3), using gene definitions from Ensembl GRCm38 version 76. Normalized expression values were obtained by correcting for

differences in sequencing depth between samples using DESeq median-of-ratios approach, and subsequent log-transformation the normalized counts.

Statistical analysis

All experiments were performed in triplicate or more replicates as stated in the figures, and three independent experiments were carried out. Data were analyzed by one-way and two-way ANOVA followed by Bonferroni post hoc test. The t test with two-tailed unpaired test was used for pairwise comparison. Clinical and pathologic parameters were analyzed by the Fisher exact test. Graphpad Prism software was used to perform all statistical analysis (version 6.0 GraphPad Software Inc.). Quantification of data is represented as mean ± SEM, and P value threshold was as follows: *, 0.05; **, 0.01; ***, 0.001; and ****, 0.0001.

5- ACKNOWLEDGEMENTS

This work was supported by the Fundação de Amparo à Pesquisa do Estado de São Paulo (FAPESP), Conselho Nacional de Desenvolvimento Científico e Tecnológico (CNPq) and an Abel Tasman fellowship to AA awarded by the University of Groningen.

6- CONFLICT OF INTEREST DISCLOSURE

No financial interest/relationships with financial interest relating to the topic of this article have been declared.

REFERENCES

1. Petrov, D., Mansfield, C., Moussy, A. & Hermine, O. ALS clinical trials review: 20 years of failure. Are we any closer to registering a new treatment? *Frontiers in Aging Neuroscience* **9**, 68 (2017).

2. Charcot, J.-M. *Deux cas d'atrophie musculaire progressive : avec leÌsions de la substance grise et des faisceaux anteÌrolateÌraux de la moelle eÌpinieÌre*. (Masson, 1869).

3. van den Berg, L. H. Therapy of amyotrophic lateral sclerosis remains a challenge. *The Lancet Neurology* **13**, 1062–1063 (2014).

4. Van Damme, P., Robberecht, W. & Van Den Bosch, L. Modelling amyotrophic lateral sclerosis: Progress and possibilities. *DMM Disease Models and Mechanisms* **10**, 537–549 (2017).

5. Taylor, J. P., Brown, R. H. & Cleveland, D. W. Decoding ALS: From genes to mechanism. *Nature* **539**, 197–206 (2016).

6. Béland, L.-C. *et al.* Immunity in amyotrophic lateral sclerosis: blurred lines between excessive inflammation and inefficient immune responses. *Brain Commun.* **2**, (2020).

7. Vériène, J., Fossouo, L. & Parker, J. A. Neurodegeneration in C. elegans models of ALS requires TIR-1/Sarm1 immune pathway activation in neurons. *Nat. Commun.* **6**, 7319 (2015).

8. A, E. Amyotrophic lateral sclerosis is a multifactorial disease. *Muscle Nerve* **18**, 741–752 (1995).

9. Logroscino, G. *et al.* Incidence of amyotrophic lateral sclerosis in Europe. *J. Neurol. Neurosurg. Psychiatry* **81**, 385–390 (2010).

10. D, C.-V., P, B.-V., A, S.-P. & J, R. Infectious agents and amyotrophic lateral sclerosis: another piece of the puzzle of motor neuron degeneration. *J. Neurol.* **266**, 27–36 (2019).

11. AJ, L. & AA, A. The Dual Nature of Type I and Type II Interferons. *Front. Immunol.* **9**, (2018).

12. Lu, C.-H. *et al.* Systemic inflammatory response and neuromuscular involvement in amyotrophic lateral sclerosis. *Neurol. - Neuroimmunol. Neuroinflammation* **3**, e244 (2016).

13. Liu, J., Gao, L. & Zang, D. Elevated Levels of IFN-γ in CSF and Serum of Patients with Amyotrophic Lateral Sclerosis. *PLoS One* **10**, e0136937 (2015).

14. R, W., B, Y. & D, Z. Activation of interferon signaling pathways in spinal cord astrocytes from an ALS mouse model. *Glia* **59**, 946–958 (2011).

15. Kwiatkowski, T. J. *et al.* Mutations in the FUS/TLS Gene on Chromosome 16 Cause Familial Amyotrophic Lateral Sclerosis. *Science (80-.).* **323**, 1205–1208 (2009).

16. Sama, R. R. anjit. K., Ward, C. L. & Bosco, D. A. Functions of FUS/TLS from DNA repair to stress response: implications for ALS. *ASN neuro* **6**, (2014).

17. Tyzack, G. E. *et al.* Widespread FUS mislocalization is a molecular hallmark of amyotrophic lateral sclerosis. *Brain* (2019). doi:10.1093/brain/awz217

18. Shelkovnikova, T. A. *et al.* Antiviral Immune Response as a Trigger of FUS Proteinopathy in Amyotrophic Lateral Sclerosis. *Cell Rep.* **29**, 4496-4508.e4 (2019).

19. Studer, L., Vera, E. & Cornacchia, D. PROGRAMMING AND REPROGRAMMING CELLULAR AGE IN THE ERA OF INDUCED PLURIPOTENCY. *Cell Stem Cell* **16**, 591 (2015).

20. Vera, E., Bosco, N. & Studer, L. Generating Late-Onset Human iPSC-Based Disease Models by Inducing Neuronal Age-Related Phenotypes through Telomerase Manipulation. *Cell Rep.* **17**, 1184–1192 (2016).

21. Barber, S. C. & Shaw, P. J. Oxidative stress in ALS: Key role in motor neuron injury and therapeutic target. *Free Radic. Biol. Med.* **48**, 629–641 (2010).

22. Deshpande, D. *et al.* Synaptic FUS Localization During Motoneuron Development and Its Accumulation in Human ALS Synapses. *Front. Cell. Neurosci.* **0**, 256 (2019).

23. Wang, H. & Hegde, M. L. New Mechanisms of DNA Repair Defects in Fused in Sarcoma–Associated Neurodegeneration: Stage Set for DNA Repair-Based Therapeutics? *J. Exp. Neurosci.* **13**, 117906951985635 (2019).

24. Baron, D. M. *et al.* Amyotrophic lateral sclerosis-linked FUS/TLS alters stress granule assembly and dynamics. *Mol. Neurodegener.* **8**, 30 (2013).

25. Ilieva, H., Polymenidou, M. & Cleveland, D. W. Non–cell autonomous toxicity in neurodegenerative disorders: ALS and beyond. *J. Cell Biol.* **187**, 761–772 (2009).

26. S, N. *et al.* TDP-43 transports ribosomal protein mRNA to regulate axonal local translation in neuronal axons. *Acta Neuropathol.* **140**, 695–713 (2020).

27. López-Erauskin, J. *et al.* ALS/FTD-Linked Mutation in FUS Suppresses Intra-axonal Protein Synthesis and Drives Disease Without Nuclear Loss-of-Function of FUS. *Neuron* **100**, 816-830.e7 (2018).

28. Oliveira, D. *et al.* Different gene expression profiles in iPSC-derived motor neurons from ALS8 patients with variable clinical courses suggest mitigating pathways for neurodegeneration. *Hum. Mol. Genet.* **29**, 1465–1475 (2020).

29. Cestra, G., Rossi, S., Di Salvio, M. & Cozzolino, M. Control of mRNA Translation in ALS Proteinopathy. *Front. Mol. Neurosci.* **0**, 85 (2017).

30. Miller, C. H. T., Maher, S. G. & Young, H. A. Clinical Use of Interferon-γ. *Ann. N. Y. Acad. Sci.* **1182**, 69 (2009).

31. Marciano, B. E. *et al.* Long-Term Interferon-γ Therapy for Patients with Chronic Granulomatous Disease. *Clin. Infect. Dis.* **39**, 692–699 (2004).

Supplementary table 1: List of the transcripts that were significantly differentially expressed between ALS6 motor neurons treated with SA only and SA+IFNy.

Group	Total number of genes	Gene Names				
ALS6 Ctls	170	RPS11	CTU2	ZNF512B	BCL9L	SPNS2
		ELMO2	MDH2	MARCKSL1	TUSC2	GINS4
		MMP2	TXNL4A	SPSB4	RPSA	IRF2BP1
		CMTR2	DHCR7	SCAF1	HOXD4	SPTLC2
		ZHX3	SRRD	SLC2A4RG	TTBK2	HES6
		UTP20	AC005670.3	HCN4	CTXN1	SEMA6C
		CYP26A1	AIF1L	UNC5D	MT-CYB	DAB2IP
		GCSH	C2orf69	APH1B	AHCY	AL365361.1
		H2AZ2	VAT1	FAM168A	TSHZ2	RAB3D
		BYSL	AD000090.1	FAM214B	POGK	FADD
		PFKP	SF3B5	MGAT3	NRAS	AC024075.2
		PDCL3	COG8	ZC3H4	RPL22L1	NIN
		SNHG16	KCTD2	SEMA4F	CHRNB4	SDC1
		GFOD2	NATD1	NUDCD3	HOXA3	ZNF322
		SALL1	DNAAF5	CENPB	APLP1	FUT9
		SLC25A3	ASB1	NREP	TMEM165	ENY2
		H3-3A	SUPT16H	NDRG4	IREB2	CALU
		TMSB10	TOMM22	GJC1	RPS8	HSPA5
		G3BP1	SOCS3	USP5	TUBA1B	CMPK1
		RAB1B	POP4	ABCA2	PDCD7	LINC00654
		CCDC177	NLGN3	MESD	PBRM1	OGFOD3
		PPP1R14A	ACAA2	HRC	UHMK1	TP53INP1
		DDB1	DAG1	CCDC71L	SSR3	TUBB6

Group	Total number of genes	Gene Names				
		KLHL14	TMEM132A	CELSR2	FAM171A1	SSH1
		TPRG1L	MAPK8IP2	LZIC	TADA3	ENSA
		PAIP1	TMEM121B	DCAKD	MSI1	H6PD
		TAF9B	POU3F2	PCDHGB6	AC135050.6	CAD
		C2orf49	CHPF2	GUK1	ZBTB43	IGDCC4
		CCNB1	RPLP2	FAM210B	PCLO	KCNQ2
		CLUH	DPY19L2P2	STAMBP	ZNF778	SPOCK2
		TMX4	RPL27	HILPDA	TM2D3	LINC00461
		CD2BP2	RPL24	PREPL	BHLHE22	MED1
		AATK	MAVS	ADAT1	FLOT2	PABPC4
		FGFR1	VCP	ZNF737	EARS2	DDX6
		FXYD6	KNOP1	EIF4H	AASDHPPT	PPP2R1A
		CERK	ABT1	SRM	MCM3	TMEM245
		AP3S2	ZNF710-AS1	LAP3	MAP10	ENDOD1
		HOXA1	RAVER1	TUBB4B	RPS2	COL2A1
		TNS3	LFNG	IDH1	FAM110A	DPH2
		RPS5	PIP5K1C	XRCC5	C17orf75	PCDHB10
		LRRN1	KIF1B	COL26A1	RCOR2	KCTD6
		IGSF3	GSK3B	SELENON	NRBP1	DIAPH1
		PIKFYVE	POU2F2	IMP3	SLC25A22	LAMTOR1
		C4orf3	GPD1L	CUTALP	TLNRD1	ZDHHC5
		TMEM132E	C6orf120	CNIH1	LEPROT	TRAF4
		ANP32E	PIGT	SNX12	WDR24	RRM2
		NAT10	ARL8A	OIP5-AS1	YJU2	C19orf12
		SYN3	TSPAN14	VMA21	PRR14L	ST8SIA3
		CXADR	PDK4	ASTN1	C11orf71	MDK
		PCYT2	PANK3	CD164	DYNLL2	METRNL
		HEIH	WDR82	AREL1	NHP2	MT-ND3
		INSIG1-DT	TMEM134	H3-3B	SLC9A7	RASSF2
		HSD11B2	HMGXB4	ARHGAP35	CDK6	HNRNPAB
		CDC25B	CBX2	CAPN15	HMX2	TOP2A
		EFNB1	HYAL2	TMEM167B	AP2A1	PPIL2
		BSN	ALDH5A1	MFAP1	SMPD1	VPS18
		BAHCC1	SEC61A1	NEK9	FZD7	SLC27A4
		TRIQK	AC018647.2	PLEKHG1	MARVELD1	FEN1
		COL9A2	EPHB1	NEURL1B	CRB2	UBA52
		LMNB2	SSBP2	TOMM40	EFCAB14	IGF1R
		TBL3	TK2	SP8	SOX12	PGAP3
		RPL35	NME4	CPE	SLC16A9	ANKRD50
		MT-ATP6	AC074117.1	DCHS1	ARL10	IPO7
		SMC3	STMN1	UST	GSN	SCARB2
		PDIA3	PEX11B	PTPRU	ZNF587B	IQSEC1
		GAREM2	MEGF6	SILC1	TMEM8B	NAV1

Group	Total number of genes	Gene Names				
		ASB13	REEP1	BTD	MED11	JARID2
		CEP350	DLL4	RBM15B	ZBTB45	THNSL1
		CES2	SLC2A1	BEX3	ST8SIA1	STK4
		LTBP4	LSAMP	CWC15	SMIM12	RETREG3
		KCNC1	MMP24	APEX2	ANKRD46	ATPAF1
		TMEM250	ADCY1	SMIM10L2A	DGKZ	IRX2
		SPTSSA	CKS2	SNRNP200	TCP11L1	PLAGL2
		PPIL1	INTS5	NCAN	LRATD1	FIGNL2
		GOLGA3	BSG	CNNM3	ANK2	FBXO41
		SCUBE3	EFR3B	SOBP	TIMM10B	CELSR1
		STK17A	SLC25A15	RPN2	RIMS3	TMEM164
		NAT8L	PES1	SDF2L1	ARPP19	FGFR1OP2
		LAMTOR2	WFS1	MPRIP	LARP1	COQ8A
		METTL2B	TBC1D16	SFT2D2	ZBTB16	PLEC
		SMUG1	ZNF608	HOXA6	PSMB2	PCDHB16
		DNAJC5	TRIP11	C16orf70	CALR	TMEM109
		PABPC5	PABPN1	SREBF1	AL161772.1	SLC25A6
		EMC1	CACNA2D2	GSE1	HIGD1A	PRSS23
		PPM1F-AS1	DOCK6	ZNF703	SNRPD1	PAFAH1B2
		NRARP	MAGEF1	ARMC5	MEPCE	LINC00205
		GRB2	HMGCR	UBTF	BZW1	UBAP2L
		ATXN7L3B	URB2	AC093525.7	SMIM7	CASZ1
		LCOR	LRFN4	PHB	RRAGA	TMEM177
		CHST15	MCF2L	SEMA6B	TMEM35A	PCDH8
		CDK1	STK24	LIN7C	BTBD2	HSP90B1
		RPS28	TBC1D24	PCNX3	PCDHB2	MOB1A
		THAP12	HOXB1	CACNG6	PCNA	NOL6
		AP001372.2	CHGB	POU2F1	RBBP4	PDZRN4
		PLXNA1	FAM20B	GAPDH	LZTS1	TIMM8B
		ATOH8	HES2	MLLT11	MAML3	ST6GAL2
		SORT1	FAM3C	COX7C	XKR7	SOX21-AS1
		YWHAQ	COL9A1	RRP15	SCD	CTDSP1
		FAM98B	VPS35	GPX1	ASIC1	CDK5R1
		OTUD3	PLBD2	PYCR2	NYNRIN	CHD4
		CRELD2	BRI3BP	GNA12	B4GALT2	NEUROG2
		CHMP1B	VAC14	LIMK1	TTC5	RASD1
		SERPING1	SOGA1	RTL6	FEM1A	DBN1
		EIF1AX	SIKE1	AKAP11	HS6ST2	BEX1
		INTS1	NUTF2	LYRM7	TTBK1	MIR600HG
		RPLP1	HNRNPH1	BRD3	GM2A	AP3D1
		MMP16	COL4A2	MOCS2	DENND4B	SMIM14
		FZD9	ZFP62	LDOC1	C11orf95	DDX54
		SON	GFPT1	ADAM11	PHC2	TMEM170B
		SH2B2	GGACT	ATP6V0E2	STK32A	JPT2

Group	Total number of genes	Gene Names				
		ABHD2	BMF	SLC35E2A	ROBO1	LINC00909
		QPRT	NECTIN1	AUTS2	ARSB	MED28
		MZT1	PFAS	TCN2	MYH10	PTPRA
		COL18A1	NUCKS1	TMEM88	CTBP1	GOLIM4
		ERLIN2	RPLP0	RPRM	CYP7B1	DST
		FAXC	MKNK2	MRPL30	ALDH1B1	BAP1
		PDZRN3	SEC16A	EPHB2	MPP2	NIPBL-DT
		TMEM151E	EFNA5	ACTG1	POMK	MSH2
		C14orf132	H2AZ1	CALM1	PRKX	NPPC
		FUS	MRAS	SLC25A23	ANKRD11	HIF1AN
		TF	LMNB1	POMGNT2	NDUFA4	PET100
		MMP15	PCDHB14	C8orf33	PCNX4	MED9
		ELAC2	NCBP2AS2	HNRNPU	TBC1D20	NEUROD4
		ADRA2A	BPNT1	NME1	KIF5A	ZNF180
		IPP	CD276	SCAP	PLPPR3	ETAA1
		NIPBL	PUM2	RHOBTB1	SEZ6L2	SLC46A1
		DDX18	IL17RD	BAIAP2-DT	FAM168B	TSC22D4
		NCDN	PIK3C2B	PRCC	STX7	STK35
		ZNF24	C6orf89	AC010491.2	MYO5A	CAPN5
		MFN2	C7orf50	EPM2AIP1	MEGF8	RRM1
		RANBP6	LSM14B	SYT16	AC093297.2	C2CD2
		RAB5B	HECTD1	PAX5	ADAM10	RPL13
		CAPN1	VKORC1L1	NTN3	SPEN	PRDX2
		CRIPT	SDSL	RTL8B	GALC	SALL4
		PCDH18	MARCHF9	PEBP1	MT-CO3	RRP12
		ZBED1	INSM1	RPL14	CHST14	POLR3H
		PHLDA1	FLJ37453	HNRNPA1	FBXO5	SKIDA1
		NUDT12	RPS6	GIGYF1	IER5L	CYREN
		ZBTB18	PPP5C	GEMIN5	N6AMT1	PAIP2B
		FGFR3	HS3ST3B1	MYBBP1A	IRX1	CTBP1-DT
		DYNC1H1	AC139530.1	HSBP1	TGFBR1	ACER2
		TMEM33	FAM102A	ARL5A	WDR4	CYP26B1
		CLSTN2	HMGN2	EDEM3	SZRD1	CALM3
		GLIS2	AC090114.2	MRTFB	CDC42	KCNC4
		ATF7	PFKFB2	EPHB4	FRAT2	SRSF2
		CNTN2	PNMA2	C4orf46	GRK2	DISP2
		VPS25	AGRN	INSIG1	ZBTB26	CEP41
		CST3	CNPY3	REPIN1	LINGO1	SDHC
		WDR6	ATP9A	RCN2	POMGNT1	GBF1
		CHRNB2	TSKU	STARD7	RRS1	UBTD2
		TP73-AS1	G3BP2	SMIM13	TECPR2	ACVR2B
		FUT4	CHD7	SOX2	TUB	TCF3
		VASH1	PPP1R14B	SCO1	CYB5D2	IRGQ
		SAPCD2	NHLRC2	AP1S1	LINC00667	NEUROG1

Group	Total number of genes	Gene Names				
		ECEL1	SBF1	COX10-AS1	ARRB1	MAP3K4-AS1
		GLG1	LRP1	VGLL4	NR6A1	ACVR1B
		MTND2P28	BIRC6	SPC24	SCAMP5	PCDHB3
		ZNF70	RFT1	BRWD1	NEUROD1	CENPV
		HGH1	FLJ16779	NRXN2	SUMF2	TSPAN6
		FAM234A	USP46	APC2	DCAF7	PRELID1
		ULBP3	PSD	ACKR3	CLCN7	CPTP
		ARAP1	PDCL	FAM171A2	DIRAS2	LLPH
		UBE2L6	GNAZ	NCR3LG1	RNFT2	CYTH3
		AGGF1	NAE1	PSD3	RIMKLB	ORAI2
		TSN	DHX8	ISCA2	DDA1	PLEKHA8
		GSTP1	EID1	PIGM	KIAA2026	MLEC
		GMFB	UBE3B	CKAP4	PPIB	LMTK3
		IGDCC3	NLK	HMGB1	RND3	SLITRK1
		NR2C2	CD99L2	UCK2	RRBP1	MBD3
		CHMP7	EID2B	PGK1	ATP5MC2	RPL13A
		LONRF2	ATG2A	LZTS2	PRDX5	AMOTL1
		VWA1	HOXB4	ANKS1A	VDAC1	IER3IP1
		NFYA	ICMT	DBNL	PPIA	SLC38A1
		FUBP1	DAZAP2	CLPB	EIF3F	KIAA2013
		MT-ND2	CYB5B	RPTOR	TRIB1	PAICS
		NDNF	ARHGAP1	VAMP2	ERLEC1	MMD
		MTR	CARD10	MAP4	DHX37	RAB11A
		FAM126B	MEX3A	TBCB	RALGDS	SNX1
		DHFR	ZNF268	EIF4EBP2	PRMT6	ARHGEF17
		MAD2L1	ZNF706	RTL8A	ARFGAP2	WSB2
		CAMSAP1	TFAP4	DHCR24	LYPLA2	MT-CO2
		IRX3	MAPKAPK3	DIO3	GABPB1-IT1	ARHGDIA
		NMNAT2	UNC5C	CCNA1	TMEM129	RBM8A
		PSMF1	TIAM2	PRTG	RRP1B	HNRNPA3
		IGSF8	LRFN1	RPL10A	PPP1R26	CETN2
		HNRNPUL2	TMEM203	LRP3	PFKM	TOR1AIP2
		PGM2L1	CHD2	PANX1	DKC1	IARS2
		ANKRD52	POLR2F	EIF6	CENPBD1P1	NRCAM
		KLHL9	EMC10	MACF1	MANEAL	RHOBTB3
		GAA	BNIP1	TBC1D14	CXXC5	HIPK2
		ZNF747	USF3	GTF2A1	NELFB	HMX3
		PRDM12	RPL15	POLR1C	GID8	ZMIZ1
		PAQR4	ERBB2	SETD2	GRAMD4	TKFC
		OPA3	RMDN1	KIF7	MRPS26	DAP
		TRAF7	RPS3A	ZNF783	IPO5P1	QSOX1
		MOB1B	KCNA3	ZBED3	RBPMS2	FSTL3
		SNN	GPRIN1	HMGB3	NFIC	PTPN3

Group	Total number of genes	Gene Names				
		C6orf62	BAZ2B	CCDC12	PFDN5	FAM217B
		SH3D19	LRP8	FAM234B	PPT1	PKDCC
		MICALL1	ZNRF3	RO60	MIAT	SCAMP2
		YIPF6	BRD7	NDUFAF3	ZBTB39	EIF4A2
		SFRP2	MIR99AHG	NAXE	SEMA4B	CIRBP
		POLD2	TMEM181	FLJ12825	BEX4	ZC3H10
		DCX	PFDN1	NDST1	ARRDC4	SHROOM2
		STRIP1	ALDH16A1	DPYSL2	LONP2	POFUT1
		AC055839.2	EYA3	SOX4	TADA1	LYSMD1
		CHMP6	RPL34	C5orf24	TXLNA	SNRPD3
		NCOA3	BOD1L1	MSN	RAB31	PPM1F
		SPCS3	HS6ST1	RAB3C	SLC35E2B	TSR1
		POLRMT	BLCAP	AC026748.3	DHRS3	CXXC4
		MANF	GNE	NR2F1	GTF3C2	RGMA
		EIF4E2	SKI	LYRM2	ANKRD9	H1-0
		FAM86C1P	TNKS1BP1	B4GALNT4	MRPS30	CAMKK2
		ENTPD7	RPL18A	PKD1	PRRC1	PHETA1
		CCDC113	ATXN7L3	DDOST	CEP89	ARF3
		TNRC18	LIPG	FASN	MT-ND1	PEX19
		MIR9-3HG	CTPS1	PRDX6	MIEF1	ERCC6L
		FHDC1	SLC25A11	ILF2	ZNF292	CUX1
		CELSR3	SYNCRIP	FGFBP3	INSYN1	RALGAPA1
		GRWD1	KCNJ12	NGRN	ZNF813	ST8SIA2
		FGD5-AS1	TMEM167A	RGS16	ZNF696	RAD21
		HOXB8	F2R	URB1	HEG1	PRR12
		DNAJC9	RPL3	MECP2	B4GAT1	ANK3
		RAD1	FARSA	PNPLA4	FBXL19	SOX11
		MRTO4	TUBA1C	SOX21	NUDT3	ZBTB44
		C1QBP	H2AX	RXRA	TRIP13	TIMP2
		GANAB	TXNRD1	POU3F4	M6PR	MRPL16
		AL109627.1	TMBIM6	RNF141	MAZ	BMPR1B
		TMEM248	SLC6A8	PKD2	PDCD10	CARF
		GVQW3	WASH5P	BMPR1A	TLE5	SYVN1
		HNRNPA0	SWSAP1	CLDN11	RAP2B	VOPP1
		C1orf198	NFE2L1	RPL29	ZNF629	SEMA5A
		NGFR	NT5DC2	SLC44A2	KIF3B	ARPIN
		MEIS1	FUT11	TMEM127	MCCC2	TTPAL
		NSD1	ARSG	HPS6	AGAP2-AS1	P4HB
		TMED7	ARF5	LYPLA1	CCDC8	SPATA33
		BEX2	SEMA6D	MTHFR	HEATR1	PPP1R14C
		TRIL	CSKMT	PTOV1	EEF1A1	COL6A1
		ITGB1	IKZF4	SCOC	GMEB2	MFSD5
		FAM177A1	MYCN	SMAD3	ADPRS	BLOC1S6
		TUBA1A	MBTPS2	LNPEP	AC005224.3	GPRC5B

Group	Total number of genes	Gene Names				
		COL5A2	TSPYL1	SHISA3	POLR2D	NUMA1
		KIAA0930	NCL	YIPF4	EIF4G1	STRN4
		SNRPC	GSPT1	CDK12	MTATP6P1	CEMIP2
		FGF14-AS2	SSR2	FBN2	C1QL4	SPARC
		SET	EXTL3	ZNF397	ISYNA1	CBX5
		LIMD2	HRH1	RTN4R	BCAS4	EXOSC6
		NTN4	GLDC	SYT2	NUP210	COL5A1
		WFIKKN1	LSM8	AL691432.2	SEL1L	ZNF770
		NAPB	ZNF616	ZNF43	NDUFC2	FZD1
		LAMTOR3	TMEM97	RBBP9	CNOT9	MFNG
		MRPL20-AS1	GDF11	DICER1	EEF1AKNMT	VTI1B
		POLR1A	MCM2	RPL7L1	PARP1	DLAT
		TSHZ1	MRPS16	SSBP4	COPS7B	KIF21B
		SENP8	MFAP2	KATNAL1	FGFRL1	PEG10
		USP9Y	ZDHHC13	APEH	CNEP1R1	KCNK5
		SUSD6	SPTBN2	MAGEE1	BTF3L4	DCTN5
		NSG2	ARPC4	GGA3	MRPL43	NORAD
		MYCL	TOMM70	FYCO1	RPS15	ASCL1
		JRK	ZNF853	DACT3	SLC35A4	ZBTB5
		DGCR5	RAB22A	MFAP3	AGO1	PSME3
		HOXA-AS3	ID2	MINK1	L1CAM	FAM131B
		XIAP	SLC24A1	ARL5B	PDPN	DBR1
		RGS8	ARSD	SLC25A5	DLL3	FUNDC2
		WNT5A	CPLX2	FRRS1L	PHACTR4	BCAT1
		RPS29	CHMP1A	MRPL24	FOXP4	TMSB4X
		GNS	B3GALT6	BTBD17	PTMA	MAGED2
		WIPI2	MT-ND5	SPRN	INAVA	MALSU1
		RANBP1	CNIH4	GRIPAP1	GNL3L	KPNA6
		CBX1	ADAR	GNPDA1	ARHGEF11	PDIA4
		PEX26	PLXNB2	DRAXIN	IVNS1ABP	IGFBPL1
		SLC29A3	HTATSF1	COMMD2	VEZF1	RANBP2
		ACBD7	GRIK3	ABCA1	PRDM8	LIG3
		RAB11FIP4	RNF24	MGAT1	DNAJC14	SHKBP1
		SQLE	PCDHB9	MXD4	ST3GAL2	ADAMTS5
		SEPHS1	GPX8	SLC35B2	GIT1	NOTCH3
		REXO1	TM9SF2	BPNT2	AF106564.1	RBP1
		NEFL	SLC29A1	FNIP1	CLSTN1	ATP2A2
		PARD6G	PSKH1	LRRC58	PRDX3	ONECUT2
		SCRT2	CYB5R3	ZNF8	EPHA3	LGR4
		HOXA5	ZBED4	MGAT5	LMAN2	DMAC1
		ILF3-DT	SETD1B	ULK1	RBM12	PNN
		ATP6V1A	SBK1	FZD2	DHX32	TXNDC17
		TMEM185B	MTPN	LINC00294	MEN1	DGCR2

Group	Total number of genes	Gene Names				
		TGIF2	CANT1	ATP13A3	STN1	HOXB2
		RNF150	SSR1	NOVA2	SMC2	TAOK1
		BTBD9	HEATR6	EFNA4	MED4	KIF3C
		NCSTN	MT-CO1	CSDE1	COTL1	PGD
		ICE1	SOX1	MYH9	PTPN1	UBE2Q1
		RIC8A	TMED10	ANAPC13	GADD45G	FJX1
		CCND1	ODC1	CLPTM1	MARCKS	FGD6
		SC5D	MBNL3	TTYH3	SACS	HSPG2
		IGFBP2	SDC3	MBTPS1	ASPM	NDFIP1
		PRKDC	YIF1A	IDH2	TTLL12	GOLGA4
		SULF2	NR2F6	PACRGL	MN1	CELF4
		AP2B1	MAFB	AGPAT3	PNRC2	G6PC3
		SLC30A7	SEPTIN3	EBLN3P	FBXL15	LRRC14
		KDM6B	PCDH17	LETM1	TBC1D13	FKBP1A
		E2F4	SYNJ2BP	ARHGAP45	HRH3	EIF3G
		UBE2Q2	RC3H2	LIPE	NUS1	TMED4
		KIAA0232	HIP1R	PODXL2	PSAP	GGA2
		SMS	PDE4DIP	RPS3	LRRC55	MIB1
		MAPK7	NACC1	ADCY5	NCS1	AL160006.1
		RTL8C	GAS1	LRFN3	ONECUT1	ADD2
		GIGYF2	AC026471.1	RNF145	BACE1	MAT2A
		CCAR2	GABRB3	FGD4	BCL2L11	TUBB4A
		PRMT1	ENO1	HOXB3	MAPKAPK5	PGPEP1
		TYMS	HOXD3	E2F1	ELK1	TMEM106E
		TMOD2	LRRC20	FRAT1	SERPINE2	PISD
		NA	ATP6AP2	ZMYND8	PIMREG	LRIG2
		FAM199X	ZNF106	EFTUD2	COX6B1	LINC01521
		MAB21L2	SLC35C1	RAB11FIP2	MAPK6	NPTXR
		PPDPF	KIF1A	LRRC4	UBE2R2	PINK1-AS
		NOL4L	COL4A1	NRIP1	CNIH2	GPC1
		CLN6	VCAN	NRP2	LAMB1	ARMCX2
		RPL39	HCG11	ZNF609	NUDT11	APP
		KAT8	PCYOX1L	PRDX1	TASOR2	VHL
		ZBTB47	ASH2L	PTRH1	BLACAT1	LMBR1
		RBM3	FBXL16	CDH2	SNX27	PARM1
		MXRA5	TM9SF3	NACC2	MICOS10	AC073508.3
		FAM160A2	TMEM123	ACP2	FPGS	CENPF
		ANKRD40	TP53	METRN	ID4	IGF2BP1
		H1-10	C18orf32	FLNC	RNF26	BCKDHB
		IBA57	ZFAND5	MARCHF6	SFT2D3	ZNRF1
		EPHB3	BICD2	CCNG2	WIPF2	AL162595.1
		FAM122B	CDH7	ADGRL2	FAM136A	ERCC2
		KMT2B	TMEM115	JAG1	AKAP1	SNX17
		ZKSCAN1	C2orf68	ORMDL3	GOLM2	NDN

Group	Total number of genes	Gene Names				
		RABAC1	STK11	PCDHB11	FOXRED2	ATRN
		YPEL1	RAPGEF5	RHOA	AAMP	PUM1
		SLC48A1	SETD1A	CZIB	ANOS1	XPO5
		FASTKD2	SLC39A10	RRP9	NLN	CCDC88A
		ZNF677	PDIA6	SMC1A	ATRAID	PDE12
		PCBD2	DCXR	DLL1	TFDP1	SLC35B4
		NTPCR	PTGFRN	TP53INP2	SEC24C	ARNT2
		SELENOS	PBXIP1	ANTXR2	AXIN2	SPOCK1
		SF3B2	MED24	CACNG4	AC106820.4	DNAJC10
		EHD1	GUCD1	ZNF407	MGA	DCAF8
Ctls	165	RAB2A	RPL17	AKR1C1	ARF1	SBF2
		FSTL1	PODXL	KIAA1586	GTPBP3	CADM3
		ABCA3	PCDHA12	GTF2I	PACS2	SUV39H1
		PCDHB15	CDK16	CDKN1A	KRAS	SLX4
		CIPC	GAP43	LPL	SIPA1L2	TIMM10
		VPS33A	WDCP	LAMP2	ATP7A	CYP20A1
		TFIP11	AC103702.1	PUDP	BCL2L2	DIP2B
		AC016582.2	SAYSD1	AGAP3	ERAP1	CAPRIN1
		POLR2G	RABL6	GET3	EMG1	POLR2K
		GNL3	LINC00641	TMEM59L	ACTR1A	GUCY1A2
		KLHL13	METTL16	AC016044.1	FBRSL1	TRIM13
		GLT1D1	PHF12	PAK4	BBS10	BRAT1
		COX7A2L	UQCRQ	CNOT8	MMAB	CDK2AP1
		LRRC41	CAND2	KIRREL3	RNF144A	CBL
		CXCR4	RCN1	TENT4A	DCTN3	SP1
		CADM4	ZNF480	ZNF830	LHX5	ZBTB33
		C9orf78	MAP3K6	JMJD8	CIAO2B	LHX3
		ADAM12	ERH	CHRNA3	MYO10	LSM5
		PXYLP1	SOCS4	TMEM186	SMYD5	RPS15A
		HSD17B10	MAP6	UBE2D4	LINC02693	EIF4A1
		NUP155	SREBF2	ISLR2	RPS13	TAF1
		GAS5	TRUB1	FAT1	LDAH	SKOR1
		ESYT1	TRIM14	FAM219B	MYL6	CIC
		MSL1	ENPP2	NCBP3	RBM19	SAMD14
		RPL19	PIK3CD	PDZD11	FADS2	MTURN
		TLN1	PITPNM2	CPS1	AC144831.1	MAP3K2
		GNAL	ZBTB41	PIAS4	CENPO	CEP97
		RTN1	CDS2	GATA2	MTTP	PCDH19
		HS3ST3A1	AHCTF1	BNIP3L	MGAT5B	SLC9A6
		KIRREL1	ITGA2	CFLAR	SLC12A2	HTT
		HIC2	CEP68	WDR48	PPTC7	RAB3B
		MON1B	SCARF2	GPC3	ESRRG	TPGS2
		STK32C	MAN2C1	SV2A	EFNB3	FOXA1
		REEP6	ENOPH1	EBNA1BP2	ZDHHC24	SDK1

Group	Total number of genes	Gene Names				
		IMP4	MPDU1	TRAK1	CSTF2T	AP5B1
		ANKRD13E	SLC5A3	HELZ	TOM1L2	ZNF286A
		USP47	PSEN2	C22orf39	STOX2	TDG
		TCF25	PCDHB13	TMEM50A	GRSF1	ANKFY1
		FAT4	UBE2L3	AL138762.1	CNR1	MYCBP2
		DIRAS1	NRXN1	KLHL20	KIAA1549L	CHRNA4
		CCDC97	BLOC1S5	MAPK8IP3	PHOX2B	APH1A
		PDE1C	SAR1A	NEXMIF	MPND	ENTPD4
		SLC4A8	TMEM259	NOVA1	HECTD4	THAP7
		LINC00665	EVX1	FZD3	GOLGA1	WNT7A
		THRAP3	CCNA2	ETFB	DYRK2	TSHZ3
		INIP	PLS3	NMT1	PIK3R3	DCTPP1
		NINL	RUVBL2	NMU	MAP2K6	CCDC80
		WSCD1	GTSE1	ASXL1	PROSER1	FDXACB1
		GRM2	PIANP	RPL8	PFN2	RHOB
		CASTOR2	ISCA1	CHURC1	TMPO	CKAP2
		RNF185	TPST2	TIMM50	TM7SF2	INTS9
		OSBPL8	MT-ND6	RND2	ARHGAP28	RPS12
		LONP1	EPN1	KLC2	OXCT1	GNPTAB
		MED13L	CKMT2-AS1	SMARCAD1	SH3BGRL	ACAT2
		DUS2	CALM2	RNMT	NR2C2AP	NTN1
		B3GAT1	SP4	ZHX1	ARPC5	RPA1
		SUSD2	MOSMO	PCDHGC3	CKS1B	GLUL
		ARL6IP1	FBXO25	ZNRD2	VPS51	ZNF71
		TUBA5P	PSRC1	LDB1	UBR5	ANAPC16
		HMGN1	RESF1	GFRA1	PEAK1	ELOVL6
		FRY	ZNF74	MIA3	MRPS7	COPS8
		AC012306.3	PIAS1	TMEM131L	CUEDC2	AKAP9
		UBA1	ADCYAP1R1	DUS1L	FABP3	NCBP2
		LBX1	CDH20	NSG1	SLC27A1	SLC20A1
		CACNG5	PPP4R1	KDM2B	CDC42SE1	AP4S1
		MAPKAPK2	CNOT2	NHLH1	AP2M1	NR5A2
		LHFPL2	MAN1A2	UBFD1	RAB11B-AS1	MRPS23
		SHC1	AC012618.3	KCND2	ANXA6	SPTB
		GPR153	IGFBP5	GNB1	RRP36	SNX30
		ARL4A	FKTN	RPL23A	CSK	ABAT
		ARHGAP21	COLEC12	C5orf22	KIAA1217	TSG101
		CCDC34	CDCA5	TIMM17B	ABTB2	HECTD3
		DAD1	SLIT1	IGF2R	VBP1	GTF3C4
		BRCA1	LINC00662	ADNP	RPL7	MAPK3
		TMEM19	UBE2T	TIGD3	MOCS3	PATZ1
		GINS1	GALNT10	SNRPB2	CHL1	SHROOM3
		PRKCB	CRNDE	ST6GAL1	VANGL2	AC008124.1

Group	Total number of genes	Gene Names				
		SDAD1	SPAST	ZBTB3	RHNO1	FAM32A
		CAND1	PTGER4	UBE3A	SUB1	MICAL3
		CLCC1	GHDC	CCDC144NL-AS1	AKAP10	SRPRB
		TENM4	NLRX1	TLE4	ZNF281	ATP5PB
		SEC14L5	UBE2QL1	ITGA7	SMARCA5	NCAPD2
		MAP3K20	BANF1	ZNF207	WWC1	DNAJB9
		KPNA2	RPS6KA2	TOLLIP	GLB1L2	EDC4
		COL1A1	UCP2	DNAL1	SPON1	WBP2
		OGDH	DAAM2	ALMS1	LMBRD2	RPL18
		ISL1	EFEMP1	LRRC57	AKR7A2	PPM1L
		ZFP14	RFK	PCDHB5	RIF1	KRR1
		RBM17	PCSK1N	JMJD7-PLA2G4B	ST20-AS1	C1D
		SIX5	DNAJB11	UBAP2	SOX3	SLF2
		MANEA	CC2D1B	RAB18	GATAD1	KIAA1191
		BX284668.2	PLXNA4	BEND3	SLC1A2	HOXB6
		KPNA3	NAP1L1	CDKN2AIPNL	SUGT1	USB1
		BIRC5	ECT2	DEXI	VIM	CD81
		ZNF529	FKBP8	ZNF91	PCDHGC4	SCRN3
		ALDH3A2	KIF23	POU3F3	PHOX2A	TRIM44
		GNAS	COX6A1	MORF4L1	LGALS3BP	RELA
		ATP5MC1	PPARD	APC	TMEM209	TRRAP
		ARHGEF9	KDM4A	CCDC152	MRFAP1L1	TRIM71
		BORCS7	EI24	IFRD2	KIF21A	SLC45A4
		ARHGAP39	CARHSP1	SEC61B	MMACHC	SCAMP1
		PGAP4	FH	KCNMB4	REV3L	WNK3
		C1orf174	AAAS	GALNT1	PTK7	RPL27A
		PLEKHO1	INPP5F	ADNP2	RHBDL3	MAP2
		GLE1	VASH2	STX6	PRKAR1A	KHSRP
		CHRAC1	INPPL1	B4GALT5	CSNK1G2	DDC
		AC254633.1	BUB3	ZBTB25	AP1M1	ZFYVE26
		TMEM63C	COPB2	MAP1S	PRELID3B	VSX1
		CTDSP2	PTTG1IP	MAGED1	SARM1	PPP4C
		RMND5B	ZNF664	XKR4	RPL22	ADSL
		SSU72	LINC00900	CRAMP1	FAM229B	DR1
		TRUB2	PAM	AC133552.5	YDJC	KMT2A
		UFM1	WDTC1	STMN2	COX20	WSCD2
		AP3M2	SRCAP	TNPO2	CACUL1	MGAT4A
		FBXO11	GLO1	AC023794.2	RAB6B	USF1
		ST8SIA4	NLGN4X	MGRN1	SHANK1	JMJD1C
		RNF4	POLR3A	MINAR1	NR1H2	EIF4E3
		ING5	TMEM68	PLEKHA6	DBX1	BRINP2
		TRIM41	NXN	SAMD4B	LIN7A	PA2G4
		QDPR	ADA2	SFXN5	SLC38A2	EIF2AK4

Group	Total number of genes	Gene Names				
		PLEKHG4	KMT2D	CHCHD2	DCAF1	THOC6
		AL358473.1	SLC29A4	MAP3K11	PCDHB4	MFSD12
		TPM3	ZMYND19	CSNK2A1	ZSCAN29	TMX1
		SLC6A15	EIF5B	SIVA1	CLVS2	RUSC2
		FPGT	CENPE	FAM222A	GPR176	MIR124-2HG
		SIPA1	DMAC2L	CEBPZOS	DPYSL5	NKX1-2
		TMPO-AS1	UTP25	TMOD3	DIPK1B	PTPRO
		POLR2B	NIBAN2	TP53RK	MT-ND4	DOP1A
		EP400	TELO2	ZNF697	TAFA5	THUMPD1
		TRIM2	CRABP2	SF3B3	CAP1	ZSWIM5
		ADH5	AAR2	KMT2C	PCYOX1	DMAP1
		P2RX3	TFAM	NUDT21	KIF2C	LYNX1
		FABP5	SRP14	XPO7	ZC3HAV1L	CMBL
		USP7	BRCA2	ARID1A	SIPA1L3	RPL23
		MEIS2	RALGAPB	ACSL4	ATXN3	B4GALT7
		PCBP4	ALG10B	HSPA12A	PRPS1	ANKRD12
		TMEM120E	CHMP2A	NKIRAS2	LIPA	NSMCE3
		SCP2	FAM8A1	MLYCD	OXR1	PI4KAP2
		PTP4A2	UNC119B	UQCRH	PPP2R2C	MKRN3
		PPP1R9A	ZDHHC7	NCLN	MRC2	CCDC61
		CDCA4	ZPR1	AC005863.1	MIDN	ITFG1
		NPM1	TLN2	SPHK2	LRPPRC	FYTTD1
		LIMD1	SFXN1	XYLT1	HIRIP3	SUFU
		TSR3	FOXN3	PIP4P1	SEPTIN9	ZNF587
		CXorf56	MIER2	ADAMTS7	SALL2	AC010931.1
		CLCN4	KIDINS220	AL161910.1	PPP1R16A	FAAP100
		PSMD11	KIAA0513	PCDHA6	ACO1	PRPF38A
		CELF1	CYRIA	RHBDD1	NOC2L	ILVBL
		USP42	PXMP4	MT-TL1	SCAI	ROBO2
		CDC42BPA	RTN2	GOLPH3L	ATF5	RNF40
		RGS4	FNIP2	ZNF22	TULP4	NOL9
		CNOT1	UQCR10	RNPEPL1	TSNAX	PDCD11
		UQCRC1	WDFY3	CPSF2	MYO18A	RABL3
		ADAM23	PYGB	AP1AR	MADD	NHSL1
		LSM4	RPS10	ZADH2	PRRC2C	INSR
		MRPL34	OARD1	EFS	KLF12	CHRD
		NUCB1	DKK3	TMTC2	ARHGEF18	UBXN6
		ESRRA	MIR1915HG	METTL1	PFKFB3	SRGAP3
		LDHB	API5	LBR	SIN3A	TBC1D10B
		GNA11	ZNF793	RNASEH1	CENPA	AKAP13
		MMP24OS	MARCHF5	DARS2	TXNL1	WWTR1
		RHBDF1	ATP13A2	FZR1	OTP	MARK4
		LTBP1	CCNJ	KHNYN	JPH4	GAS7

Group	Total number of genes	Gene Names				
		UNC13B	MMP14	B3GNT5	CABLES2	RASAL2
		USP19	TUT4	RFLNA	ISG20L2	MEST
		KDM5A	RBM14	ERGIC1	TNFAIP8L1	RGP1
		RASSF5	MDM2	ARHGEF10L	PGAP6	TOMM40L
		AL031985.3	CAPNS1	ERBB4	ESD	ANGPTL2
		ABI2	COPE	CCDC25	PNRC1	ATP5F1B
		EML3	YRDC	ATRX	MAT2B	TMEM30A
		HINT3	KLHDC3	CHST8	PYGO2	PKM
		KDM4B	THSD7A	BID	E2F5	RPS7
		ABCF2	RPGRIP1L	FAN1	MRPL50	VSX2
		GDAP1L1	PTPRF	RGMB	STYX	GPD2
		OPRK1	LHX4	POLR2L	DOK6	HOXB9
		UBN2	RAB2B	MRPL4	WRAP73	CDV3
		COL7A1	VPS4B	CHRDL1	ERI2	ZFR
		ASNSD1	SLC25A4	MED20	CTSD	MYCBP
		SLC35A5	BOK	TOMM20	NHEJ1	MFSD4B
		KIF2A	SESN1	ZDHHC2	NSUN5P1	QSER1
		HPS4	ENTPD1-AS1	PTEN	SEC22B	SLC35E3
		ARL2BP	TNPO1	ADGRB2	ARHGAP19	CCND2
		CD99	MYLK	LINC01963	TWNK	CUL4A
		OCRL	RRP1	SUSD5	RPL6	TIMM13
		FANCC	AFAP1	TRIO	CAMK2N1	CHERP
		MAFA	CHML	MEX3B	ELP3	ZNF462
		IMMT	LINC02525	ROGDI	AK2	AKT1
		CBFA2T2	FSCN1	MATR3	KAT6A	PCP4
		AGPS	BCR	UGGT1	RAB36	CDC42BPB
		HP1BP3	ZFP36L1	AC005696.4	CMTM6	CYB561D1
		PCCB	PUS3	PACSIN2	NSUN3	NOP14-AS1
		BRD8	CAPN2	SMARCC2	MED16	NDUFS5
		TMED9	SEC22C	MID1IP1	FBN1	USP22
		WDR12	GPR161	USF2	RPL30	TMX2
		SF3A3	AKAP6	MMRN2	PLOD3	SYT14
		PNPLA6	MTMR4	TUG1	NUP50	CRTAC1
		C11orf68	DCLRE1A	ZNF248	DRG1	HSD17B12
		AC092279.1	LNPK	PTPRE	CUX2	GMNN
		AHCYL1	PLCD1	PTK2B	PUS7L	SUDS3
		CPAMD8	POLDIP2	PELP1	B3GLCT	EFNA3
		AC007406.4	GLT8D1	EXOC5	DCAF16	FDXR
		STMP1	CFL2	RNF41	HOXD1	NES
		ARMC6	TARS2	TSPAN3	PYM1	ALG10
		PPP1R37	LPIN2	EIF3B	PBK	KSR2
		RPL4	FCF1	FBXW8	EXOSC5	TMTC4
		LACTB2	CFL1	SERINC3	HSDL1	SNRPB

Group	Total number of genes	Gene Names				
		EIF4A3	METTL2A	L3MBTL2	LAMA5	ENC1
		ASH1L	TAGLN3	NRP1	COA1	PNMA8A
		PHACTR1	CEP55	MCRS1	ABHD17C	GTF3C6
		ACO2	TENM3	CDH13	SEH1L	CABLES1
		RTCB	OPCML	RAB8B	WDFY1	MORC2
		LOXL1	WDR7	GTF2E1	RAPGEF4	ZNF714
		UBE2N	AKAP12	CCDC50	SIGMAR1	FAM160B2
		WAPL	SGTA	TAF7	SNTB2	CERS2
		UBQLN2	LINC02606	CHSY1	PRR11	ANAPC15
		TAB1	PLEKHB2	LAPTM4A	TTC3P1	FOXD1
		YWHAZ	COPG2	RFC3	TMEM41B	CERCAM
		RBBP6	AP1B1	GPR83	LAMC1	TMEM254
		SCHIP1	ARHGEF4	ZNF219	SRP9	SETX
		RPL10	MPP6	TTF2	ERG28	TMEM199
		DNAJC30	UBE2O	EXT2	ZBTB8A	UBE2V2
		TMEM25	SZT2	ABL2	ZNF260	DERL1
		PROX1	SLC35E1	FARSB	GRAMD1A	AGAP1
		LSM3	SCARA3	CRY2	HMGB2	DDR1
		MOGS	MFN1	GPX7	PTBP1	DCC
		ACOT2	CBX7	PTPRZ1	PTAR1	EIF4G2
		SSRP1	DNAAF2	TCAF1	MARCHF2	GTF3C1
		AL117334.1	SNX11	ACTL6A	ONECUT3	ZNF385A
		ASXL2	STAR	SLC23A2	CSRNP3	HOXC6
		ZNF146	GOLGA2	DNAJC22	RAN	AC016876.2
		NDUFA13	PHF2	STAG2	MED23	NUDT15
		HOXB5	TAL1	LYSMD4	CPT2	KPNB1
		SOX9	RFC1	RGS3	PCNX1	ZNF12
		CRABP1	MTAP	EIF3J-DT	ATF7IP	BRD3OS
		PCDHGB4	ARMCX1	ARHGEF12	MIR217HG	PHF10
		SLC35F1	TTI1	BIN3	TEF	CLNS1A
		FAU	AL627230.1	RPS23	LIMK2	UHRF1
		ZNF107	ABL1	SCYL1	HMGA2	ING1
		BCKDK	PTPRG	AARS1	TMEM94	WNK1
		BOD1	NCOR1	GABPB2	C1orf109	DNER
		PHB2	EIF4ENIF1	PTPN11	TRPM4	AC022211.1
		UMPS	AFDN	EML1	ARHGEF40	AP003119.3
		DCTN1	TNFRSF21	KDM5C	RNF165	TMED1
		TTC3	RASL11B	YARS2	ZCCHC14	SPRYD3
		CHAMP1	CALN1	NAPG	UBE2D1	PMM2
		AC092718.3	LRP2	TAGLN2	MVB12B	AC011297.1
		PGAM1	MYDGF	SEPTIN11	RAB11B	EMILIN3
		SEC13	LMBR1L	NDUFA11	FAM120C	VPS13C
		PAQR3	SYNE1	DCBLD2	RANBP3	HMGA1
		NHLH2	ZNF573	MRPL19	B3GAT2	ATCAY

Group	Total number of genes	Gene Names				
		HDGFL3	RBM5	PRKAR2A	PPAN	SERBP1
		PDGFD	PSMG3-AS1	BTG1	ELOC	COA3
		CACNA1H	PSMD10	DPH3	FAAP20	GTF2H3
		FYN	PPP1R9B	ARMCX5	YWHAB	PDHB
		CNDP2	GUF1	SKP1	NNT-AS1	NAGK
		PSD2	LIG1	PGRMC2	SIAH1	ECI1
		NKX1-1	ADCY10P1	PCDHA4	EIF4B	AC008060.4
		PARK7	GCN1	MEIS3P1	NCKAP1	ATIC
		ELAVL2	MED21	CAPZA2	TNFAIP1	NF2
		FAM160B1	SYT11	KCNA2	KCTD20	CAST
		DDI2	SOCS1	ZNF749	MAGEH1	STRN
		KIF4A	MCM4	PLTP	CLDN12	TTK
		H2BC19P	DARS1	SRPRA	PSMA4	SNHG14
		LINC01597	SPA17	MYO6	JAG2	MTMR3
		ZNF726	SLC26A2	UBQLN4	NXPH4	NUP62
		FAM120A	C22orf24	PCMT1	SHD	SCAF11
		PCDHGA1(	CAMK4	MYO1C	ZC3H13	EPB41L5
		AURKAIP1	EGLN2	GON4L	RTN4	CDH4
		GTF2IP1	KANSL3	FAM89B	NAPA	ITPRIP
		NUP85	CHST12	RIC1	ZDHHC18	POLR3D
		EIF2S1	TARDBP	PI4KA	WBP1L	E2F3
		DPYSL4	TRIM28	PRTFDC1	RPL26	RPL26L1
		SLC39A9	CSPG5	PRPF19	UHRF1BP1	NUDCD1
		TM9SF4	PTPRN	R3HDM4	SIGIRR	AC092198.1
		TNFRSF1A	SLC15A3	BTRC	GLUD1	FLNA
		SHISAL1	PDE10A	RPL12	AC074135.1	NDC1
		PANK1	THRA1/BTR	SLC25A16	EPPK1	NOTCH1
		FBN3	CCDC85C	WIZ	LINC01128	FDPS
		MCFD2	SRC	AC126773.4	SREK1IP1	DUSP9
		KALRN	MRPL27	SMARCB1	SLC11A2	LRPAP1
		LINC00863	FBXW7	CEP170B	INSIG2	PNPO
		ENO2	ZNF720	CKB	AL009178.2	NCOA4
		NF1	CRMP1	ARFGEF3	ADSS2	SUOX
		CCDC90B	TIMELESS	KIF11	DFFA	MIR4458HG
		ADAMTSL4	GNG7	PARVA	FUT1	DAAM1
		TAOK2	ZER1	COPG1	KIF26A	SCML4
		ARFGEF2	PLIN5	FEM1B	RNF220	SELENBP1
		SPG7	PDE4B	USP24	CARM1	MROH1
		TMEM176A	INTS2	KIF5B	PTPRS	AMD1
		NUP133	KIF13A	MRPS17	SESN3	TRIB2
		GALNT2	C12orf45	DCAF12	ZC3H7B	PCDHGB1
		CTNNB1	TMEM14B	SLC12A6	UROD	TRAF3IP1
		CHROMR	WAC-AS1	CIAO3	PDE2A	HIPK1

Group	Total number of genes	Gene Names				
		NAV2	PTGES2	URI1	COMMD4	URM1
		COX7B	SCG3	RAP1GAP	DDX28	SEMA4C
		XXYLT1	ASIC4	QARS1	FOXO3B	AL353796.1
		FAM78A	SEC62	SOS2	EZH1	SKA2
		AL353748.3	UBE2Z	NEFM	ZYG11B	RNF44
		VEZT	RNPS1	NNAT	TMEM65	TRIM8
		DNMT3A	CKAP2L	SCML2	RACK1	DPYSL3
		CNOT7	SEZ6L	ADAMTS9	PLXNA2	EVX2
		CD200	AL358613.2	BCL9	CD24	DPY19L1
		NCKAP5L	CDC42EP4	GPCPD1	ATP6V1B2	PAK2
		ITGA6	AL356123.2	STMN3	SLC22A17	ATP2B1
		THAP5	ZDHHC21	RAB14	PGRMC1	PRKAG1
		GK5	MKI67	CACNG7	ZNF512	SMAD5
		NOTCH2	BRMS1L	GRK3	MLLT1	INCENP
		LRCH4	FNDC10	STIM1	AL135925.1	WASF2
		NOL11	GLI2	KCNH2	MRPL3	LANCL1
		PSMD2	RNF139	FOXD3	ZFP91	AC000093.1
		TOR2A	ZNF594	PLXNB1	BMPR2	ELAVL3
		ARMH4	CLSPN	RPS4X	B3GALNT1	FRMD4B
		TTC28-AS1	SHPK	NIPSNAP1	KLF7	AL109615.4
		IPO5	MNT	LINC01686	ZNF428	N4BP3
		ANP32A	RAB40C	CHD3	NUP188	TRAPPC6B
		ACLY	SH3BGRL3	RPS27A	RAI1	ATP5MC3
		NACA	CBX3	PI4K2A	SUMO2	RAB8A
		GLOD4	PURB	TEX261	MYRF	SHISA5
		CDK4	MAP4K2	SGCB	BPTF	SNRPD2
		DVL1	SYPL1	GDI1	KNL1	SLC39A6
		MCM5	FIZ1	MEAK7	DENR	RPS27
		CSNK2A2	PPP4R2	PDXK	RPL21	RNF169
		ZNF681	UNC80	ARHGEF2	RARRES2	CDCA8
		RABGGTB	LAMB2	BNIP2	PHF6	AL157392.3
		DICER1-AS1	KIF3A	CPSF7	JKAMP	MRPL54
		HMBOX1	ACP1	EPHA5	SMARCD2	INA
ALS6	5	CLMP	KCNH1	LPCAT1	TMEM230	RAMAC
		AC009812.1	HERC1	EEF2KMT	C4orf48	SEMA4G
		COX8A	NDUFB7	CPLANE2	AUXG010000581	SRSF9
		PTMS	FZD8	THNSL2	MRPS33	SETBP1-DT
		TAF10	SEC14L6	BLOC1S4	GABRB2	EPB41L4A-DT
		CDH8	TOMM5	TXNDC15	CHASERR	LYRM4
		NPIPB5	AL355001.2	SLC16A7	FRMD8	AC112220.2
		PSIP1	SLC30A3	SLC25A1	HCN2	DUSP15
		GPX4	RPL38	HDDC3	GRIK5	MFSD14A
		TIMM8A	RPS16	CENPVL3	SLC16A13	RPS14

Supplementary table 2: List of the transcripts that were significantly differentially expressed between ALS6 motor neurons treated with SA only and SA+IFNy. (Transcript ID; log fold change and p-value).

Transcript_id	log2FoldChange	p-value
ENST00000592686	7,90	6,57E-07
ENST00000588645	7,62	2,52E-06
ENST00000439555	7,28	1,13E-25
ENST00000493208	7,11	2,08E-15
ENST00000463784	6,60	3,17E-20
ENST00000264832	6,56	3,47E-23
ENST00000613424	6,46	2,06E-59
ENST00000459982	6,44	5,42E-48
ENST00000472045	6,42	6,95E-95
ENST00000437654	6,32	2,60E-48
ENST00000476613	6,31	1,33E-24
ENST00000405885	6,25	3,07E-92
ENST00000563180	6,21	7,99E-11
ENST00000423829	6,07	1,60E-13
ENST00000245414	6,07	2,41E-105
ENST00000458069	5,89	1,01E-42
ENST00000545081	5,45	7,44E-06
ENST00000357302	5,34	1,33E-05
ENST00000564803	5,27	7,07E-26
ENST00000443093	5,21	3,64E-05
ENST00000564617	5,21	1,23E-15
ENST00000527192	5,20	4,27E-07
ENST00000564056	5,20	2,19E-16
ENST00000569607	5,20	8,48E-15
ENST00000268638	5,17	2,17E-48
ENST00000566369	5,16	1,69E-28
ENST00000262510	5,14	6,71E-07
ENST00000436936	5,14	6,71E-07
ENST00000539144	5,14	6,71E-07
ENST00000562492	5,07	8,54E-19
ENST00000526001	4,99	2,06E-06
ENST00000525659	4,84	1,52E-07
ENST00000420111	4,63	8,44E-14
ENST00000562889	4,40	3,25E-08

Transcript_id	log2FoldChange	p-value
ENST00000359595	3,99	3,70E-10
ENST00000329608	3,94	9,88E-49
ENST00000558770	3,94	7,30E-10
ENST00000369801	3,94	1,65E-18
ENST00000488198	3,91	9,70E-13
ENST00000369802	3,67	1,41E-23
ENST00000376630	3,56	2,13E-63
ENST00000493699	3,54	5,39E-32
ENST00000484194	3,36	9,94E-13
ENST00000657855	3,19	5,01E-05
ENST00000452281	3,14	4,80E-60
ENST00000673885	3,14	3,27E-59
ENST00000673841	3,13	1,79E-60
ENST00000392322	3,13	8,81E-61
ENST00000673859	3,13	3,26E-51
ENST00000674153	3,13	2,26E-59
ENST00000673638	3,12	5,40E-44
ENST00000392323	3,12	3,23E-60
ENST00000674080	3,12	1,12E-61
ENST00000415035	3,12	4,28E-61
ENST00000673777	3,11	3,55E-72
ENST00000673952	3,11	1,20E-60
ENST00000673816	3,11	2,09E-60
ENST00000540176	3,11	6,33E-71
ENST00000673847	3,11	6,21E-60
ENST00000361099	3,11	6,75E-71
ENST00000409465	3,11	7,57E-62
ENST00000673942	3,11	6,96E-72
ENST00000673858	3,11	4,84E-71
ENST00000674081	3,10	3,05E-71
ENST00000674028	3,10	2,26E-63
ENST00000338264	3,10	1,33E-05
ENST00000673762	3,10	1,36E-66
ENST00000424722	3,10	2,23E-43
ENST00000673734	3,10	1,71E-71
ENST00000423282	3,09	1,50E-65
ENST00000673832	3,08	3,65E-66
ENST00000673863	3,08	4,58E-68
ENST00000454414	3,00	2,08E-24
ENST00000432058	3,00	1,60E-17
ENST00000329464	2,86	1,59E-06
ENST00000560442	2,81	5,54E-05
ENST00000464072	2,81	2,69E-19
ENST00000558173	2,81	3,11E-06
ENST00000359709	2,73	4,84E-06
ENST00000295809	2,62	4,07E-06
ENST00000368131	2,62	4,07E-06

Transcript_id	log2FoldChange	p-value
ENST00000368132	2,62	4,89E-06
ENST00000483916	2,59	5,18E-06
ENST00000493884	2,59	5,18E-06
ENST00000340979	2,56	6,87E-06
ENST00000448393	2,53	3,04E-05
ENST00000295417	2,29	1,34E-11
ENST00000559390	2,22	5,32E-07
ENST00000542394	1,70	6,84E-06
ENST00000440906	1,69	7,43E-06
ENST00000247815	1,66	8,27E-06
ENST00000545134	1,65	7,41E-06
ENST00000560141	1,55	2,89E-07
ENST00000361681	1,51	2,53E-06
ENST00000585360	1,48	1,50E-05
ENST00000418914	1,47	3,67E-07
ENST00000429031	1,46	4,07E-08
ENST00000369904	1,46	1,29E-13
ENST00000369909	1,46	2,46E-14
ENST00000409267	1,45	3,26E-14
ENST00000369907	1,45	3,32E-14
ENST00000492431	1,44	2,62E-13
ENST00000375641	1,43	4,44E-05
ENST00000375635	1,43	4,15E-05
ENST00000409138	1,42	1,74E-13
ENST00000369903	1,42	1,26E-13
ENST00000375633	1,40	4,68E-05
ENST00000491847	1,40	4,52E-06
ENST00000348721	1,39	5,64E-06
ENST00000443053	1,37	7,26E-06
ENST00000498330	1,33	4,33E-05
ENST00000462286	1,30	2,96E-07
ENST00000459765	1,30	5,29E-05
ENST00000585517	1,22	2,20E-10
ENST00000264657	1,21	3,67E-11
ENST00000389272	1,19	2,79E-09
ENST00000404395	1,19	2,06E-09
ENST00000588969	1,19	1,32E-09
ENST00000396467	1,18	2,84E-07
ENST00000344700	1,16	3,37E-09
ENST00000638356	1,12	1,48E-13
ENST00000487500	1,12	8,25E-08
ENST00000644700	1,12	1,27E-08
ENST00000352983	1,12	9,12E-08
ENST00000296953	1,03	1,32E-05
ENST00000648437	0,98	1,50E-07
ENST00000464218	0,98	1,61E-07
ENST00000467531	0,98	1,61E-07

Transcript_id	log2FoldChange	p-value
ENST00000621356	0,98	1,54E-07
ENST00000575669	0,96	4,55E-06
ENST00000581373	0,94	1,77E-06
ENST00000584364	0,94	1,86E-06
ENST00000618619	0,94	1,78E-06
ENST00000580261	0,94	2,06E-06
ENST00000618613	0,93	2,25E-06
ENST00000579248	0,93	2,57E-06
ENST00000574723	0,92	6,87E-06
ENST00000579408	0,90	3,46E-06
ENST00000511787	0,87	6,53E-07
ENST00000576436	0,86	2,39E-05
ENST00000647841	0,83	1,28E-06
ENST00000473638	0,82	2,01E-06
ENST00000272274	0,81	1,03E-05
ENST00000326092	0,81	1,12E-05
ENST00000600147	0,80	1,65E-06
ENST00000509877	0,79	5,23E-06
ENST00000319826	0,77	2,08E-05
ENST00000461690	0,77	3,17E-05
ENST00000311549	0,76	3,98E-05
ENST00000274065	0,75	1,48E-06
ENST00000222247	0,73	7,89E-06
ENST00000464182	0,73	1,81E-05
ENST00000515792	0,70	1,11E-05
ENST00000512690	0,70	1,08E-05
ENST00000514682	0,69	1,11E-05
ENST00000509736	0,69	1,14E-05
ENST00000560274	0,67	1,63E-05

Chapter 4

VAPB is required to normal cell cycle progression of medulloblastoma cells and downregulates β-catenin expression

Amanda Faria Assoni[1,2], Thiago Giove[1], René Wardenaar[2], Raiane Ferreira[1], Elisa Helena Farias Jandrey[1] Gabriela Novaes[1], Isabela Fonseca[1], Petra Bakker[2], Carolini Kaid[1], Valdemir Melechco Carvalho[3], Mayana Zatz[1], Floris Foijer[2], Oswaldo Keith Okamoto[1*].

1. Human Genome and Stem Cell Research Center, Institute of Biosciences, University of São Paulo, Cidade Universitária, São Paulo 055080-090, Brazil.

2. European Research Institute for the Biology of Ageing, University of Groningen, Groningen, 9713 AV, the Netherlands.

3. Division of Research and Development, Fleury Group, São Paulo 04344-070, Brazil.

ABSTRACT

Although the Vesicle-associated membrane protein-associated protein B/C (VAPB) has been widely studied in the context of neurodegenerative diseases such as ALS, its role in cancer has only recently been investigated and needs further research. VAPB participates in the endoplasmic reticulum unfolded protein response (UPR) and is involved in cellular calcium homeostasis regulation. Medulloblastoma is the most common type of malignant embryonic brain tumor in children up to four years of age and accounts for approximately 18% of all pediatric brain tumors. It arises from undifferentiated primitive cells during neuronal development, involving signaling pathways relevant to nervous system development. Therefore, medulloblastoma is an interesting model to investigate the possible relationship between VAPB and tumorigenesis. We generated VAPB knockouts (KOs) using the CRISPR-Cas9 system and isolated single cell clones from two medulloblastoma cell lines: DAOY and USP13-med. Here we show that the ALS-related protein VAPB plays an important role in cellular proliferation in medulloblastoma by regulating cell progression through the cell cycle. We demonstrate that high VAPB expression in medulloblastomas correlates with lower overall patient survival. Consistent with this clinical correlation, we find that VAPB is required for proper proliferation of medulloblastoma cells, as knockout of VAPB impaired progression through the cell cycle and arrested cells in G0/G1. Analyzing RNA sequencing data, we observe that transcript levels of many WNT-related proteins, including CTNNB1, were decreased in VAPB KOs. Our results reveal a novel pro-oncogenic function of VAPB in medulloblastoma cells that involves modulation of the WNT pathway, a known regulator of neurodevelopment.

1- INTRODUCTION

Neurodegenerative diseases and cancer are very different pathologies, but there is a growing body of evidence suggesting that both have overlapping deregulated mechanisms, besides that each are highly debilitating diseases for patients that still await for good treatment alternatives (Driver, 2014).

Epidemiology data indicates that neurodegenerative diseases occur less frequently in cancer survivors and vice versa (Houck et al., 2018). While this inverse correlation is already well-established in some neurodegenerative conditions such as Alzheimer's and Parkinson's diseases, when it comes to amyotrophic lateral sclerosis (ALS), there is still no clear consensus (Fang et al., 2013; Freedman et al., 2013, 2014).

ALS is the most frequent late-onset motor neuron disease. It is characterized by death of upper and lower glutamatergic motor neurons. Genetically, mutations in more than 40 different genes were already correlated with the risk of ALS development (Cook and Petrucelli, 2019). In ALS sporadic cases, few genes were described as deregulated. The Vesicle-Associated membrane Protein B (*VAPB*) is one example of a gene differentially expressed independently of the specific mutation. *VAPB* mRNA levels were found to be decreased in the spinal cord of sporadic ALS patients compared to healthy controls (Anagnostou et al., 2010). Moreover, *VAPB* gene is also associated with one of the familial forms of ALS, in which a single missense mutation causes motor neuron degeneration that leads to the phenotype of ALS8 (Nishimura et al., 2004; Mitne-Neto et al., 2011). Interestingly, in addition to familial and sporadic ALS, *VAPB* differential expression was already reported in cancer. A genome-wide microarray analysis of 50 human breast cancer cell lines and 145 clinical specimens revealed that *VAPB* is often amplified or overexpressed in breast cancer (Neve et al., 2006; Rao et al., 2012).

Although VAPB is widely studied in the neurodegenerative context, its role in cancer has only been recently addressed and still needs further understanding. Medulloblastoma is the most common type of malignant embryonic brain tumor in children up to four years of age, accounting for about 18% of all pediatric brain tumors. It originates from undifferentiated primitive cells during neural development, involving signaling pathways relevant to the nervous system development (Northcott et al., 2012a). Thus, medulloblastoma is an interesting model to investigate the possible relationship between VAPB and tumorigenesis.

Functionally, VAPB is a highly conserved type II integral membrane protein that belongs to the VAP protein family and localizes to the endoplasmic reticulum (ER) and cis-Golgi (Skehel et al., 1995; Weir et al., 1998). It is implicated in a diverse array of cellular processes such as the regulation of neurotransmitter release, vesicle trafficking, lipid binding, maintenance of ER/Golgi architecture, and the unfolded protein response (UPR) (Soussan et al., 1999; Skehel et al., 2000; Gkogkas et al., 2008). These findings support a possible mechanism by which VAPB can influence both neurodegeneration and tumor development, particularly in the Central Nervous System (CNS).

Here, we show that proliferation is decreased in VAPB-KO cells due to a cell-cycle arrest in G0/G1. We observed that these cells have different transcript levels of many WNT pathway genes, a well- known pathway of neurodevelopment. In summary, we report a novel function of VAPB protein in the proliferation medulloblastoma cells and its underlying mechanism involving WNT/β-catenin signaling modulation.

2. RESULTS

2.1 VAPB knockout in Medulloblastoma cell lines decreases cell proliferation and CSC maintenance

The role of VAPB in cancer is poorly-understood. Therefore, to explore its functions in medulloblastoma, we generated VAPB knockouts (KOs) using CRISPR-Cas9 system and isolated single cell clones of two medulloblastoma cell lines: DAOY and USP13-med (PB et al., 2016). The controls were generated by expressing the same lentiviral construct expressing Cas9, but lacking the guide RNA, on the mixed population followed by isolation of single cell clones. The resulting clonal cell lines were used for all subsequent experiments.

The loss of VAPB protein expression was confirmed by western blot for each single cell clone (Fig. 1A). One characteristic of the VAPB-KO clones in the USP13-med line was that the morphology of the cells remarkably changed, as they became bigger and more elongated (Suppl. 1A). However, no morphological alterations were observed in the DAOY VAPB-KO cells.

Functionally, the VAPB-KOs in both cell lines were less proliferative than the control lines, as assessed by the kinetics of *in vitro* cell growth (Fig. 1B). As a first assessment of the tumorigenic potential of VAPB-KOs in a 3D model, we performed a sphere formation assay (SFA), which estimates the stem cell population residing in tumors, or cancer stem cells (CSC), which are considered to be responsible for the poor prognosis of cancer patients. This assay revealed that VAPB-KO cells were less capable of forming spheres (Fig. 1C and D and Suppl. 1B and C). Together, results suggest that VAPB inactivation might reduce CSC characteristics.

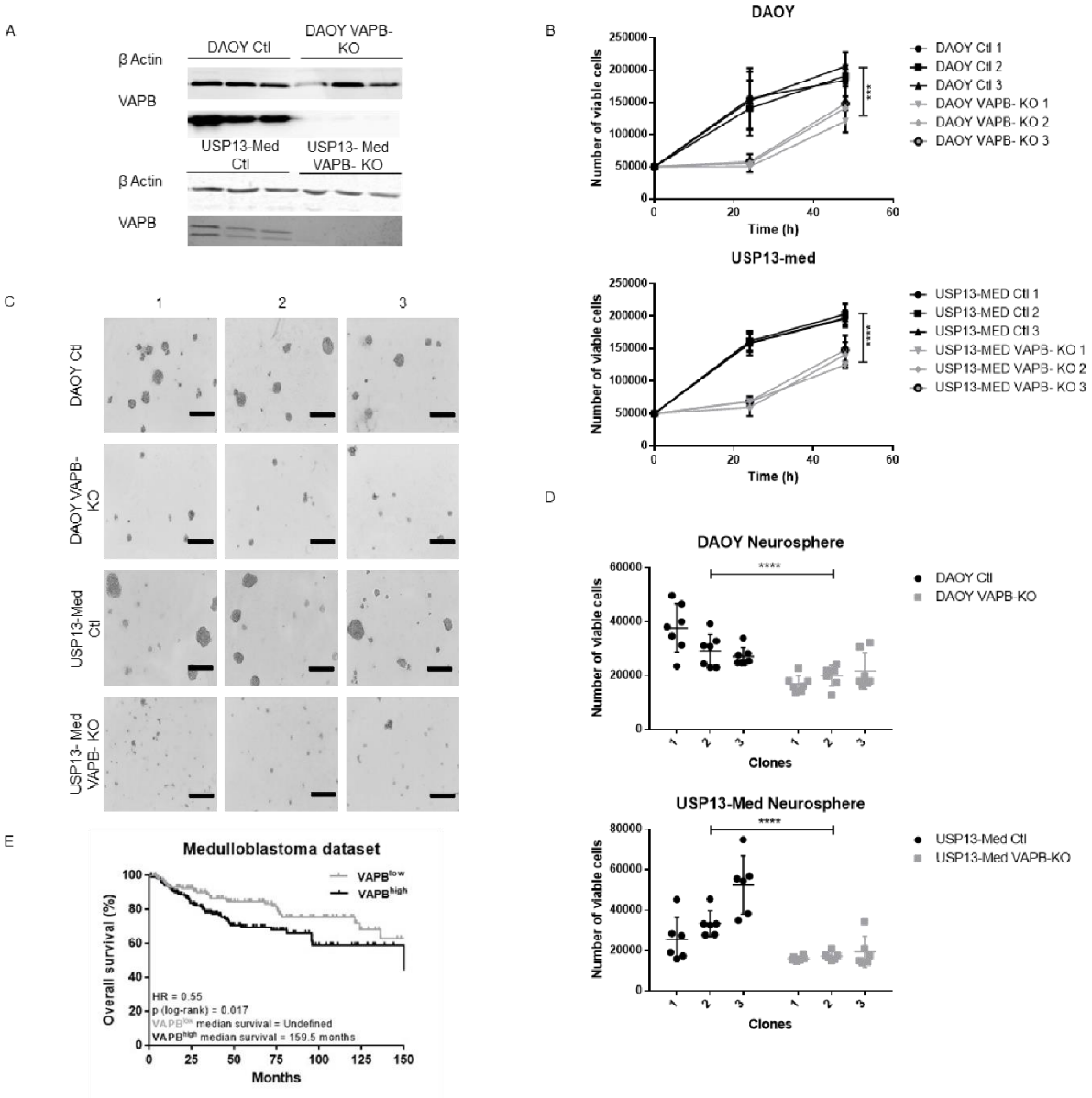

Fig. 1: VAPB knock-out decreases cell proliferation and CSC in medulloblastoma cell lines. a. Western blot against VAPB and -βactin proteins on the isolated single cell clones of DAOY and USP13 cell lines with knockout of VAPB protein and controls. **b**. Cell count of DAOY and USP13 single cell clones of VAPB-KO and Controls at 24h and 48h (*, $P < 0.05$; **, $P < 0.01$; and ***, $P < 0.001$, one-way ANOVA with Tukey multiple comparison test; n = 3 per group). **c**. Representative phase contrast images of tumorspheres at 144 hours post cell plating. Scale bar, 400 μm. **d**. Quantification of the number of viable cells after dissociation of tumorspheres at 144h post cell plating (*, $P < 0.05$; **, $P < 0.01$; and ***, $P < 0.001$, one-way ANOVA with Tukey multiple comparison test; n = 7 per group). **e**. Impact of *VAPB low* or *high* expression on the survival of patients with medulloblastomas in Cavalli's dataset.

We next set out to validate these findings *in vivo*. For this, control and VAPB-KO clonal cell lines were injected subcutaneously in nude mice in the right or left flank, following which we followed mice for tumor development. While the USP13-med clones did not initiate tumors in this setting (data not shown), the DAOY clonal lines were tumorigenic. Importantly, we found that, also in vivo, VAPB-KO cells were impaired in forming tumours as mice receiving

VAPB-KO cells developed no tumors or much smaller tumors compared to mice receiving VAPB-WT DAOY cells (Suppl. 1D and E).

To determine the relevance of our findings for human patients, we evaluated the impact of VAPB expression in the overall survival of medulloblastoma patients from Cavalli's dataset (FMG et al., 2017). Indeed, increased VAPB expression ($VAPB^{high}$) in tumor tissue was significantly correlated with poor overall survival in comparison with VAPB lower-expression ($VAPB^{low}$) patients (Fig. 1E). We conclude that VAPB expression is an important parameter for medulloblatoma outcome and therefore set out to better understand the molecular role of VAPB in medulloblastoma biology .

2.2. Reconstitution of VAPB expression in VAPB-KO medulloblastoma cells restores cell proliferation in a dose-dependent fashion

To confirm whether the reconstitution of VAPB expression would recover proliferation of the VAPB-KO medulloblastoma cells *in vitro*, we overexpressed HA-tagged VAPB under control of a Tet-On (i.e., doxycycline-sensitive) promoter. We added increasing concentrations of doxycycline (0.15-0.9 µM) to the culture media and confirmed restoration of VAPB protein expression by assessing the levels of HA-VAPB by western blot (Fig. 2A).

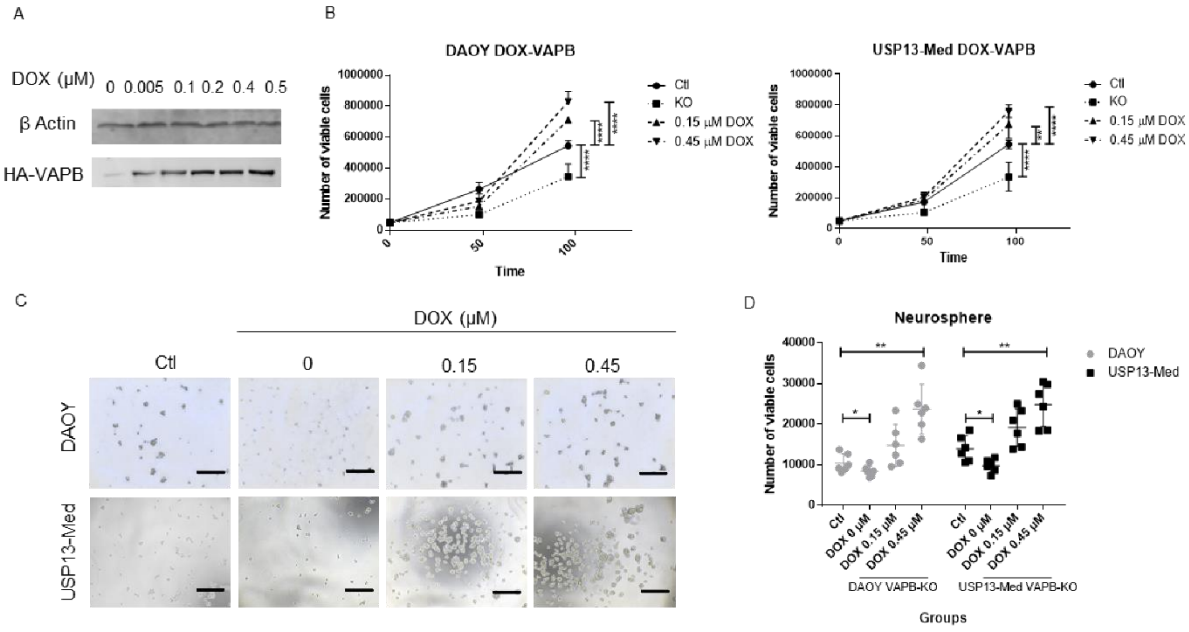

Fig. 2: VAPB re-expression restores proliferation and tumor sphere formation ability in medulloblastoma cell lines in a dose-dependent way. a. Representative western blot against HA-tag and β-actin on one VAPB-KO clone with HA-tagged VAPB under control of a **Tet**-On (i.e., doxycycline-sensitive) promoter and addition of different concentration of doxycycline: 0 µM, 0.15 µM, 0.3 µM, 0.45 µM, 0.6 µM and 0.9 µM. **b.** Cell count of DAOY and USP13 single cell clones of VAPB-KO with **Tet**-On HA-tagged at 48h and 96h after addition of DOX (*, $P < 0.05$; **, $P < 0.01$; and ***, $P < 0.001$, one-way ANOVA with Tukey multiple comparison test; n = 3 per group. **c**.

Representative phase contrast images of tumor spheres of one DAOY and one USP13 clone with **Tet**-On HA-tagged and different concentrations of DOX at 48h hours post cell plating. Scale bar, 400 µm. **d**. Quantification of the number of viable cells after dissociation of tumor spheres at 96h post cell plating and addition of different DOX concentrations (*, P < 0.05; **, P < 0.01; and ***, P < 0.001, two-way ANOVA with Tukey multiple comparison test; n = 6 per group).

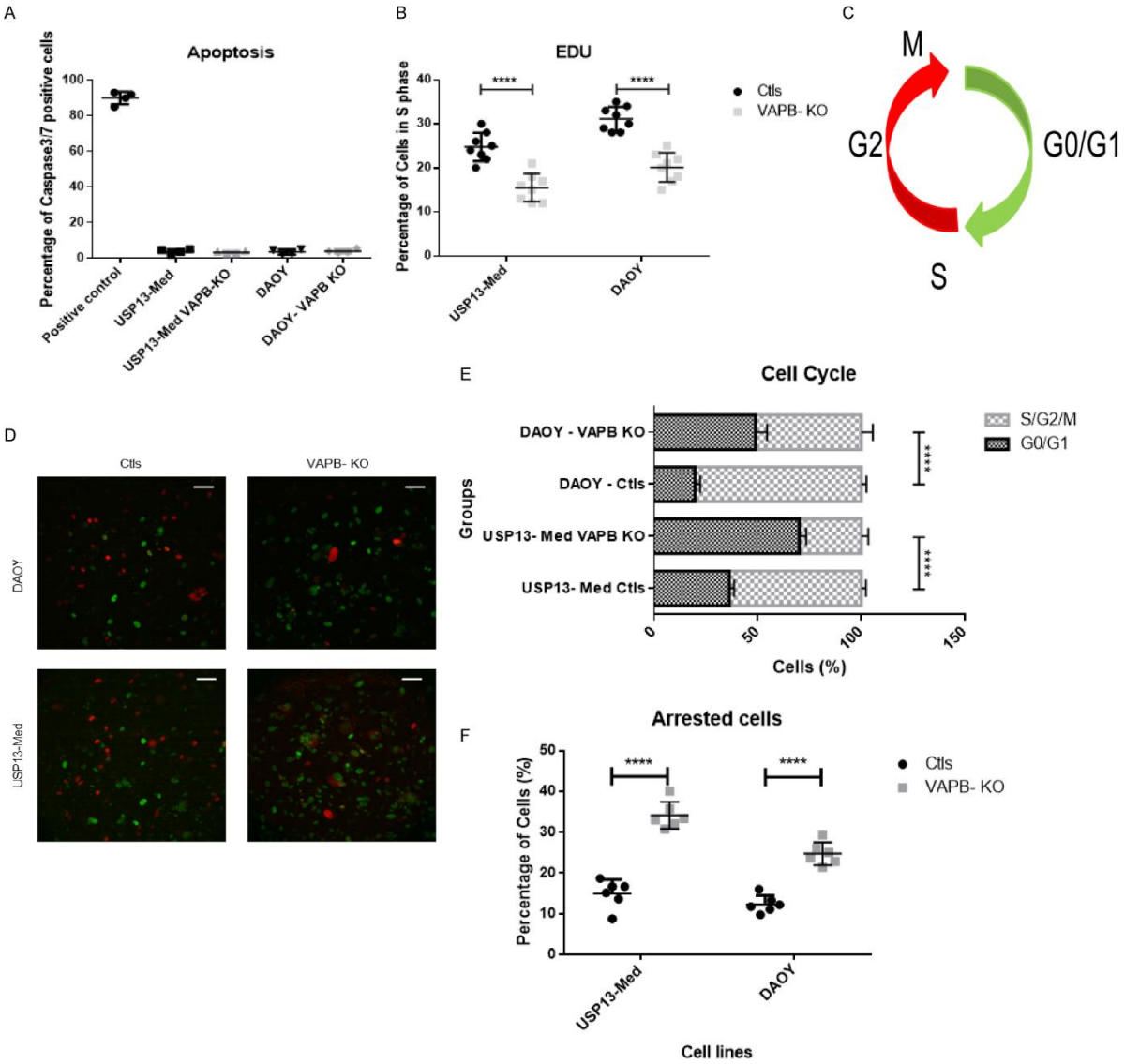

Fig. 3: VAPB-KO causes cell cycle arrest in G0/G1. a. Quantification of the number of cells with active Caspase 3/7 on a positive control treated with H_2O_2 for 24 hours and on the DAOY and USP13 single cell clone controls and VAPB knockout. **b**. Quantification of tumor cell proliferation based on positive EdU incorporation of DAOY and USP13 single cell clones of controls and VAPB-KO. Data are expressed as mean ± SEM (*P < 0.05, **P < 0.01, ***P < 0.001, ****P < 0.0001, two-way ANOVA multiple comparison test). **c**. Representation scheme of the FUCCI system with GFP-cdt1 and RFP-geminin. **d**. Quantification of the percentage of cells in different cell cycle stages (G1/GO or S/G2/M) incorporation of DAOY and USP13 single cell clones of VAPB-KO and Controls. Data are

expressed as mean ± SEM (*P < 0.05, **P < 0.01, ***P < 0.001, ****P < 0.0001, two-way ANOVA multiple comparison test). **e.** Quantification of the percentage of cells that keep in G1/G0 all throughout the length of the time-lapse imaging record (60h). Data are expressed as mean ± SEM (*P < 0.05, **P < 0.01, ***P < 0.001, ****P < 0.0001, two-way ANOVA multiple comparison test). **f**. Representative images of immunofluorescence staining of DAOY and USP13 single cell clones of VAPB-KO and Controls expressing the FUCCI system with GFP-cdt1 and RFP-geminin. Scale bar, 25 μm.

When assessing proliferation rates of control cells and cells with reconstituted VAPB protein expression, we found that VAPB expression significantly recovered the *in vitro* proliferation rates of the tumor cells (Fig. 2B) as well as their ability of generating spheres (Fig. 2C and D). On top of that, the cell proliferation rates were dependent on the amount of VAPB: the more VAPB protein present, the higher the proliferation rate (Fig. 2B-D), underscoring the relevance of VAPB protein to the *in vitro* expansion of medulloblastoma cells. To better understand how VAPB influences cell proliferation we next investigated the consequences of VAPB absence on cell cycle dynamics of our medulloblastoma lines.

2.3 VAPB-KO causes cell cycle arrest in G0/G1

Since VAPB is an endoplasmic reticulum (ER) protein that has not yet been related to the cell cycle, we performed additional cell cycle assays to better understand the decreased proliferation of cells lacking the VAPB protein. First, we observed by EdU (5-ethynyl-2'-deoxyuridine) incorporation that the VAPB-KO clones had fewer cells in S phase (Fig. 3A). Second, by quantifying the number of cells with cleaved Caspase 3/7, we found that the extended doubling time of the VAPB-KOs was not due to increased apoptosis (Fig. 3B), but because of a cell cycle delay. To further explore this phenotype, we introduced the cell cycle marker FUCCI into our VAPB cell lines and performed time-lapse imaging of these cells. The FUCCI cell cycle marker (Fluorescence Ubiquitin Cycle Indicator) combines expression of GFP-tagged CDT1 to label cells in G0/G with expression of RFP-tagged Geminin to label cells in G2.

As shown in Fig. 3C-F, the VAPB-KO cells were mainly arrested in G0/G1 (Fig. 3D and F) and remained arrested throughout the experiment (60h) (Fig. 3E). To clarify the signaling pathways involved in this cell cycle arrest, we next investigated the transcriptomes of VAPB-WT and VAPB-KO clones by RNA sequencing.

2.4 VAPB modulates WNT/β-catenin pathway in medulloblastoma cells

When analyzing the transcriptomes, we noted that the number of differentially expressed between VAPB-WT and VAPB-KO cells was much higher in a USP13-med background than in DAOY cells (Fig. 4A). This data is in agreement with the pronounced morphology change observed in USP13-med VAPB-KOs, an effect that was not detected in the DAOY KO cells.

Nonetheless, when analyzing the subset of differentially expressed genes in both cell lines, we found an overrepresentation of proliferation-related genes in both backgrounds (Supplementary table 1, Fig. 4B and C).

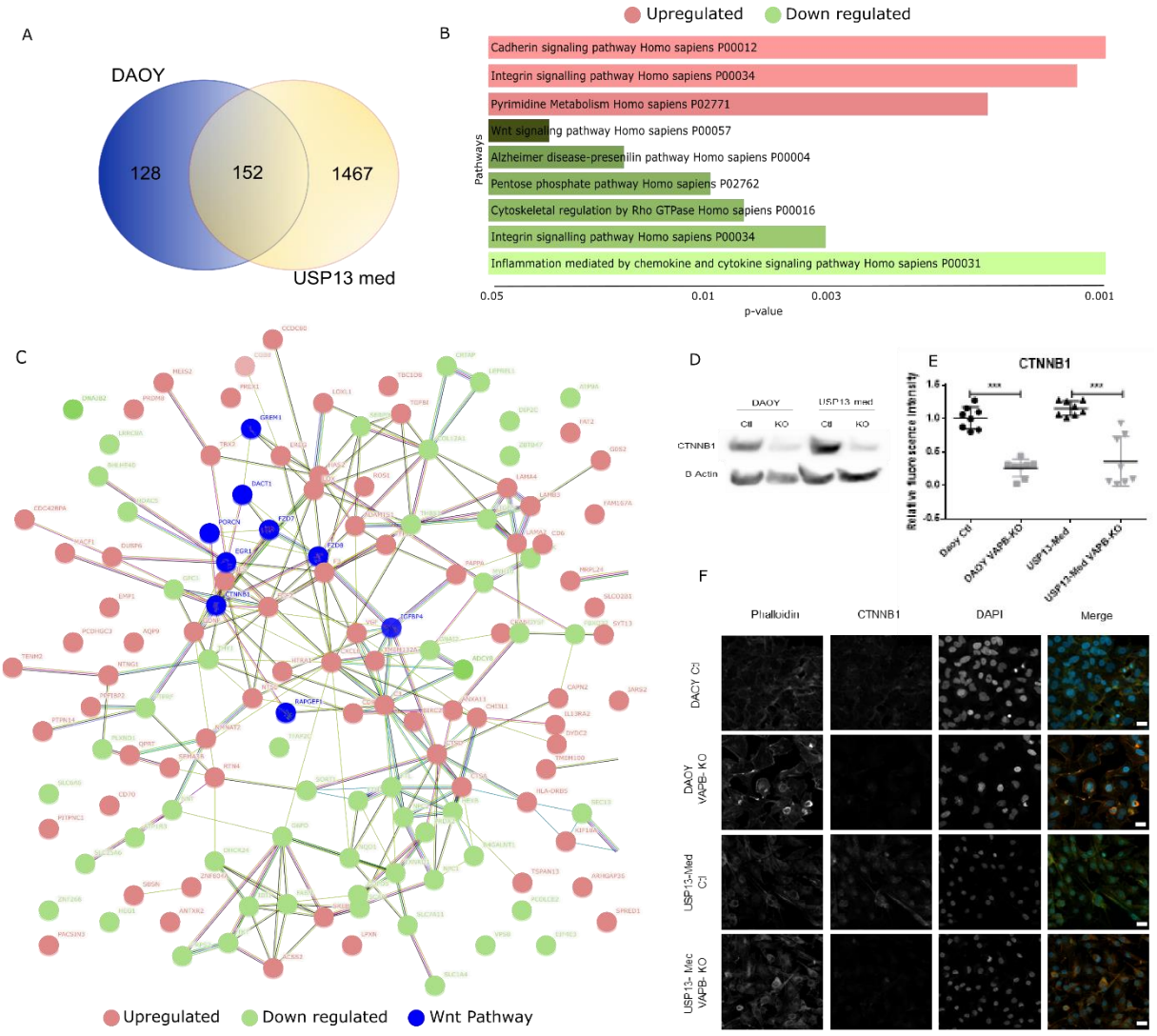

Fig. 4: VAPB absence causes dysregulation of different signaling pathways. a. Venn diagram of differential expressed genes in DAOY and USP13-med VAPB-KO cells. **b.** Enriched pathways of differentially expressed genes in both DAOY and USP13-med VAPB-KO cells. **c.** Interactome mapping of differentially expressed genes in both DAOY and USP13-med VAPB-KO cells, as indicated by RNA sequencing data. **d.** Western blot of DAOY and USP13 single cell clones of VAPB-KO and controls blotted using anti-total b-catenin. **e**. Quantification of the relative intensity of β-catenin on images of immunofluorescence staining of DAOY and USP13 single cell clones of VAPB-KO and controls. **f**. Representative images of immunofluorescence staining using anti-total β-catenin of DAOY and USP13 single cell clones of VAPB-KO and controls.

One pathway that was downregulated in the VAPB- KO cells, was the WNT signaling pathway (Fig. 4C). Indeed, the WNT pathway is well-known for its implication in medulloblastoma development: one molecular subtype of medulloblastoma is characterized by mutations in genes belonging to this pathway (Northcott et al., 2010) and the *CTNNB1* gene is frequently upregulated in most medulloblastoma samples.

We therefore next validated this at the protein level and confirmed by western blot and immunofluorescence that the amount of total CTNNB1 is decreased in the VAPB-KOs compared with controls (Fig. 4D-F), suggesting that the WNT pathway is less active in the KOs of both cell lines. While we did not yet elucidate how VAPB regulates the WNT signaling pathway, we conclude that VAPB is required for the proliferation of medulloblastoma cells by regulating WNT signaling activity.

3- DISCUSSION

Here we show that the ALS-related protein VAPB plays an important role in the proliferation of medulloblastoma cells by arresting cells at G1/0. To our knowledge, this is the first time that VAPB-KO cells have been generated and its functions in human cancer cells have been investigated.

VAPB is a protein that has been studied in depth in the context of neurodegeneration and ALS and has not been previously linked to cell proliferation. Here, we demonstrate that VAPB plays an important role medulloblastoma cell proliferation *in vitro* as well as *in vivo.* Importantly, this decreased proliferation phenotype can be reverted by reconstitution of VAPB expression in a dose-dependent fashion, given the positive correlation between VAPB expression and cell proliferation.

We found that VAPB delays proliferation by arresting cells in the G1 phase of the cell cycle. This finding is consistent with our RNA sequencing results, in which we find that most differentially expressed genes between the VAPB-WT and VAPB-KO relate to proliferation. One of the signaling pathways that was downregulated in the VAPB-KO is the WNT signaling pathway, which is generally associated with cancer aggressiveness(Ellison et al., 2005; Zhan et al., 2016). Moreover, one of the medulloblastoma subtypes is characterized by mutations in this specific pathway(Northcott et al., 2012b).

Even though further work is required to understand what is the relation between VAPB absence and WNT pathway regulation, the effect of VAPB inactivation on cell cycle progression can be well-explained by the decreased β-catenin levels – the main WNT pathway effector (Y et al., 2014)– as found in the VAPB-KO clones. It is known that β-catenin levels increase during S phase and reach a maximum accumulation in late G2/M phase and then abruptly decrease when cells enter a new G1 phase.(Y et al., 2014) Accordingly, a subset of WNT target genes is transcribed by the β-catenin-TCF complex in both S and G2 phases.

Therefore, decreased b-catenin levels may impair cell cycle progression. Indeed, transient inhibition of this complex disrupts both cell survival and G2/M progression(Y et al., 2014).

How would VAPB influence WNT signaling? It has been previously reported that hypoxic ER stress decreases the stability of β-catenin. Increased ER stress during hypoxia was shown to correlate with a decrease in low-density lipoprotein receptor protein 6 (LRP6), and this reduction in LRP6 decreased the accumulation of β-catenin and impaired canonical Wnt/b-catenin signaling(Xia et al., 2019). Therefore, the influence of the VAPB protein on WNT signaling may be related to its ability to form vesicles, its role in the secretory and endocytic pathways, ER homeostasis, and the positive feedback loop that the WNT pathway exerts on itself. However, this needs further investigation.

Indeed, misregulation of the WNT molecular cascade triggers pathological consequences and has been linked to many human diseases, particularly cancer(Zhan et al., 2016). Canonical WNT signaling is directly and indirectly modulated by various stimuli, resulting in a central network in cellular signaling that ultimately coordinates cell proliferation, differentiation, gene expression, and consequently tumorigenesis and neurodegeneration(AJ and R, 2006).

Medulloblastoma is the malignant brain tumor most common in children aged zero to four years (Dolecek et al., 2012). It is a major cause of morbidity and mortality in children, with a significant proportion of patients not responding to available treatments and/or developing motor and cognitive disorders. Therefore, understanding the molecular mechanisms that may reveal new therapeutic targets is of paramount importance. Despite the small number of studies examining the effects of the VAPB protein in cancer, we have found strong evidence that the VAPB protein plays a role controlling proliferation and progression through the cell cycle of cancer cells. Therefore, VAPB - a protein whose function is already well known in the context of neurodegeneration could well be an essential protein in CNS cancers.

4- METHODS

Human and animal samples

The study followed the International Ethical Guideline for Biomedical Research (CIOMS/OMS, 1985) and was approved by the Institutional Animal Experimentation Ethics Committee (CEUA-USP 290/2017).

Cell lines and cultures

Two embryonal CNS tumor cell lines: DAOY (Medulloblastoma, ATCC HTB-186) and USP13-MED (Medulloblastoma, in-house established; ref. 23), one control human-induced

pluripotent stem cell (hiPSC, C2535, in-house reprogrammed) and its derived NPCs were analyzed. Generation and characterization of hiPSCs and NPCs was done as in Oliveira et al. 2020(Oliveira et al., 2020) . DAOY was grown according to ATCC recommendations, and cell authentication was performed by high-resolution karyotype analysis. USP13-MED was isolated and characterized as previously reported(PB et al., 2016). After thawing, all cell lines were cultured under standard conditions (5% CO_2 (g) at 37°C) up to 4 weeks (passages 1–4) and tested for Mycoplasma contamination by PCR (Cat. MP002; Sigma-Aldrich), before use in the described experiments.Two embryonal CNS tumor cell lines: DAOY (Medulloblastoma, ATCC HTB-186) and USP13-MED (Medulloblastoma, in-house established; ref. 23). DAOY was grown according to ATCC recommendations, and cell authentication was performed by high-resolution karyotype analysis. USP13-MED was isolated and characterized as previously reported(PB et al., 2016). After thawing, all cell lines were cultured under standard conditions (5% CO_2 (g) at 37°C) up to 4 weeks (passages 1–4) and tested for Mycoplasma contamination by PCR (Cat. MP002; Sigma-Aldrich), before use in the described experiments.

Impact of *VAPB* expression on the survival of patients with Medulloblastomas

Clinical data on overall survival and Microarray expression of 632 patients with Medulloblastomas were obtained from the Cavalli dataset and viewed by the Gliovis portal (Bowman et al., 2017). The patients were dichotomized in $VAPB^{low}$ (quartile 25^{th}) and $VAPB^{high}$ (quartile 75^{th}) considering the levels of VAPB expression in the dataset. The patients' survival rates were compared using a Kaplan-Meier curve and analyzed by the log-rank test.

Immunofluorescence

Cells were washed twice, fixed (3.7% formaldehyde RT for 20 minutes) and permeabilized for 30 minutes with 0.1% Triton X-100 and 5% bovine serum albumin in 1× PBS, prior to overnight incubation with the primary antibody (Supplementary Table S1) at 4°C. Cells were then washed 3 times in 1× PBS, incubated with the secondary antibody for 45min (Supplementary Table S1), and washed again 2 times in 1× PBS. Cell nuclei were stained with 1 μg/mL DAPI for 2 minutes and mounted on glass slides and cover slipped with VectaShield. All images were taken in confocal microscope (Zeiss LSM 800).

Statistical analysis

All experiments were performed in triplicate or more replicates as stated in the figures, and three independent experiments were carried out. Data were analyzed by one-way and two-way ANOVA followed by Bonferroni post hoc test. The t test with two-tailed unpaired test was used for pairwise comparison. Clinical and pathologic parameters were analyzed by the Fisher exact test. Graphpad Prism software was used to perform all statistical analysis (version 6.0 GraphPad Software Inc.). Quantification of data is represented as mean ± SEM, and P value threshold was as follows: *, 0.05; **, 0.01; ***, 0.001; and ****, 0.0001.

RNA Sequencing

Following RNA extraction according to manufacturer instructions (Qiagen).Quality and quantity of the total RNA was assessed by the 2100 Bioanalyzer using a Nano chip (Agilent, Santa Clara, CA). Total RNA samples having RIN>8 were subjected to library generation. Strand-specific libraries were generated using the TruSeq Stranded mRNA sample preparation kit (Illumina Inc., San Diego, RS-122-2101/2), according to the manufacturer's instructions (Illumina, Part #15031047 Rev. E). Briefly, polyadenylated RNA from intact total RNA was purified using oligo-dT beads. Following purification, the RNA was fragmented, random primed and reverse transcribed using SuperScript II Reverse Transcriptase (Invitrogen, part #18064-014) with the addition of Actinomycin D. Second strand synthesis was performed using Polymerase I and RNaseH with replacement of dTTP for dUTP. The generated cDNA fragments were 3′-end adenylated and ligated to Illumina Paired-end sequencing adapters and subsequently amplified by 12 cycles of polymerase chain reaction. The libraries were analysed on a 2100 Bioanalyzer using a 7500 chip (Agilent, Santa Clara, CA), diluted and pooled equimolar into a 10 nM sequencing stock solution. Illumina TruSeq mRNA libraries were sequenced with 50 base single reads on a HiSeq2000 using V3 chemistry (Illumina Inc., San Diego). The resulting reads were trimmed using Cutadapt (version 1.12) to remove any remaining adapter sequences, filtering reads shorter than 20 bp after trimming to ensure efficient mapping. The trimmed reads were aligned to the GRCm38 reference genome using STAR (version 2.5.2b). QC statistics from Fastqc (version 0.11.5) and the above-mentioned tools were collected and summarized using Multiqc (version 0.8). Gene expression counts were generated by featureCounts (version 1.5.0-post3), using gene definitions from Ensembl GRCm38 version 76. Normalized expression values were obtained by correcting for differences in sequencing depth between samples using DESeq median-of-ratios approach, and subsequent log-transformation the normalized counts.

Edu Labeling

Tumor cells were incubated with 10 μM EdU (5-ethynyl-20-deoxyuridine; Click-It EdU Alexa Fluor 488 Imaging Kit; Life Technologies) for 30 min. Cell nuclei were stained with DAPI at a concentration of 5 $\mu g \cdot mL^{-1}$ for 5 min. All images were taken in confocal microscope (Zeiss LSM 800) and analyzes by particle automated analysis on ImageJ software.

3D tumor spheroid assay

For tumorsphere formation, cells were seeded onto a 96-well ultra-low attachment plate in DMEM/F12 supplemented with B-27, N-2, 20 $ng \cdot mL^{-1}$ EGF, and 20 $ng \cdot mL^{-1}$ bFGF (Invitrogen, Carlsbad, CA, EUA), at an initial density of 1500 $cells \cdot mL^{-1}$. After 7 or 4 days of incubation at 37 °C with 5% CO_2 humidified atmosphere (as stated in each figure), spheres

were dissociated for 20 min on Tryple at 37oC, centrifuged and counted with tripan to assess cell viability.

Cell population growth assay

The manual counting of cells, they were plated on 6 well plates in triplicate. 2ml of cell suspension containing 500000 cells on day 0. Subsequentially, cells were detached and counted using the automated countess (Invitrogen) every other day or as stated on the figure

Plasmids

For CRISPR knockout of VAPB gene, three different guide RNAs were designed aiming the exon 2 of the VAPB gene according to the guide resource tool of the Zhang lab(Ran et al., 2013) and cloned into the lentiCRISPR plasmid as described in Shalem et. al 2014(O et al., 2014). The guide RNA that generated more out of frame sequences was chosen and applied to the cell lines used in this study.

To construct a doxycycline-inducible expression system for HA-VAPB overexpression, full-length cDNA encoding VAPB was inserted between BamHI and EcoRI sites of the retroviral plasmid pRetroX-Tight-BlastR (Puromycin exchanged by Blasticidin.

For transient expression, pEGFPC1-hVAP-B was a gift from Catherine Tomasetto (Addgene plasmid # 104448)

FUCCI plasmids were generated in house by the Foijer Lab.

Time-lapse Imaging

Time-lapse imaging was performed on a DeltaVision microscope (Applied Precision Ltd./GE). A total of 50,000 cells expressing the FUCCI system were pre-seeded in 4-well imaging chambers (LabTech). Images were captured every 7 minutes with a 20X objective lens. Cell cycle changes were partially manually analyzed using softWoRxExplorer (Applied Precision Ltd./GE).

Western Blot

Cells were harvested by trypsinization and lysed in elution buffer (150 mM NaCl, 0.1% NP-40, 5 mM EDTA, 50 mM HEPES pH7.5) containing complete protease inhibitor (Roche) for 15 minutes at 4oC. Then the samples were centrifuged at 300g, at 4°C for 10 min to remove insoluble residues. 20 µg of each sample was loaded on 10% polyacrylamide gels. Proteins were transferred to polyvinylidene difluoride (PVDF) membranes. After blocking in Odyssey blocking buffer (Li-cor Biosciences) at 4°C for 60 min, the membrane was incubated overnight at 4°C with the primary antibody (supplemental materials). Following incubation, the membrane was washed with 1X PBS containing 0,1% Tween 20 (Sigma) three times and

incubated in secondary antibody for 1 hour at room temperature. The blots were detected by the Odyssey imaging system (Li-cor Biosciences). The protein bands were quantified with Image studio lite software (Li-cor Biosciences).

5- ACKNOWLEDGEMENTS

This work was supported by the Fundação de Amparo à Pesquisa do Estado de São Paulo (FAPESP), Conselho Nacional de Desenvolvimento Científico e Tecnológico (CNPq) and an Abel Tasman fellowship to AA awarded by the University of Groningen.

6- CONFLICT OF INTEREST DISCLOSURE

No financial interest/relationships with financial interest relating to the topic of this article have been declared.

REFERENCES

1. Driver, J. A. Inverse association between cancer and neurodegenerative disease: review of the epidemiologic and biological evidence. *Biogerontology* **15**, 547–557 (2014).
2. Houck, A. L., Seddighi, S. & Driver, J. A. At the Crossroads Between Neurodegeneration and Cancer: A Review of Overlapping Biology and Its Implications. *Curr. Aging Sci.* **11**, 77–89 (2018).
3. Freedman, D. M. *et al.* The association between cancer and amyotrophic lateral sclerosis. *Cancer Causes Control* **24**, 55–60 (2013).
4. Freedman, D. M. *et al.* The risk of amyotrophic lateral sclerosis after cancer in U.S. elderly adults: A population-based prospective study. *International Journal of Cancer* **135**, 1745–1750 (2014).
5. Fang, F. *et al.* Amyotrophic lateral sclerosis and cancer: A register-based study in Sweden. *Amyotroph. Lateral Scler. Front. Degener.* **14**, 362–368 (2013).
6. Cook, C. & Petrucelli, L. Genetic Convergence Brings Clarity to the Enigmatic Red Line in ALS. *Neuron* **101**, 1057–1069 (2019).
7. Anagnostou, G. *et al.* Vesicle associated membrane protein B (VAPB) is decreased in ALS spinal cord. *Neurobiol. Aging* **31**, 969–985 (2010).
8. Nishimura, A. L. *et al.* A mutation in the vesicle-trafficking protein VAPB causes late-onset spinal muscular atrophy and amyotrophic lateral sclerosis. *Am. J. Hum. Genet.* **75**, 822–831

(2004).

9. Mitne-Neto, M. *et al.* Downregulation of VAPB expression in motor neurons derived from induced pluripotent stem cells of ALS8 patients. *Hum. Mol. Genet.* **20**, 3642–52 (2011).
10. Rao, M. *et al.* VAMP-Associated Protein B (VAPB) Promotes Breast Tumor Growth by Modulation of Akt Activity. *PLoS One* **7**, e46281 (2012).
11. Neve, R. M. *et al.* A collection of breast cancer cell lines for the study of functionally distinct cancer subtypes. *Cancer Cell* **10**, 515–527 (2006).
12. Northcott, P. A. *et al.* Medulloblastomics: the end of the beginning. *Nat. Rev. Cancer* **12**, 818–34 (2012).
13. Weir, M. L., Klip, A. & Trimble, W. S. Identification of a human homologue of the vesicle-associated membrane protein (VAMP)-associated protein of 33 kDa (VAP-33): A broadly expressed protein that binds to VAMP. *Biochem. J.* **333**, 247–251 (1998).
14. Skehel, P. A., Martin, K. C., Kandel, E. R. & Bartsch, D. A VAMP-binding protein from Aplysia required for neurotransmitter release. *Science (80-.).* **269**, 1580–1583 (1995).
15. Gkogkas, C. *et al.* VAPB interacts with and modulates the activity of ATF6. *Hum. Mol. Genet.* **17**, 1517–1526 (2008).
16. Soussan, L. *et al.* ERG30, a VAP-33-related protein, functions in protein transport mediated by COPI vesicles. *J. Cell Biol.* **146**, 301–311 (1999).
17. Skehel, P. A., Fabian-Fine, R. & Kandel, E. R. Mouse VAP33 is associated with the endoplasmic reticulum and microtubules. *Proc. Natl. Acad. Sci. U. S. A.* **97**, 1101–1106 (2000).
18. PB, S. *et al.* Establishment of a novel human medulloblastoma cell line characterized by highly aggressive stem-like cells. *Cytotechnology* **68**, 1545–1560 (2016).
19. FMG, C. *et al.* Intertumoral Heterogeneity within Medulloblastoma Subgroups. *Cancer Cell* **31**, 737-754.e6 (2017).
20. Northcott, P. A. *et al.* Medulloblastoma Comprises Four Distinct Molecular Variants. *J. Clin. Oncol.* **29**, 1408–1414 (2010).
21. Ellison, D. W. *et al.* β-catenin status predicts a favorable outcome in childhood medulloblastoma: The United Kingdom Children's Cancer Study Group Brain Tumour Committee. *J. Clin. Oncol.* **23**, 7951–7957 (2005).
22. Zhan, T., Rindtorff, N. & Boutros, M. Wnt signaling in cancer. *Oncogene 2017 3611* **36**, 1461–1473 (2016).
23. Northcott, P. A., Korshunov, A., Pfister, S. M. & Taylor, M. D. The clinical implications of medulloblastoma subgroups. *Nat. Rev. Neurol.* **8**, 340–351 (2012).
24. Y, D. *et al.* Enrichment of the β-catenin-TCF complex at the S and G2 phases ensures cell survival and cell cycle progression. *J. Cell Sci.* **127**, 4833–4845 (2014).
25. Xia, Z. *et al.* Hypoxic ER stress suppresses β-catenin expression and promotes cooperation between the transcription factors XBP1 and HIF1α for cell survival. *J. Biol. Chem.* **294**, 13811–13821 (2019).
26. AJ, M. & R, N. Purified Wnt5a protein activates or inhibits beta-catenin-TCF signaling depending on receptor context. *PLoS Biol.* **4**, 570–582 (2006).
27. Dolecek, T. A., Propp, J. M., Stroup, N. E. & Kruchko, C. CBTRUS statistical report: primary brain and central nervous system tumors diagnosed in the United States in 2005-

2009. *Neuro. Oncol.* **14 Suppl 5**, v1-49 (2012).

28. Oliveira, D. *et al.* Different gene expression profiles in iPSC-derived motor neurons from ALS8 patients with variable clinical courses suggest mitigating pathways for neurodegeneration. *Hum. Mol. Genet.* **29**, 1465–1475 (2020).
29. Ran, F. A. *et al.* Genome engineering using the CRISPR-Cas9 system. *Nat. Protoc.* **8**, 2281–2308 (2013).
30. O, S. *et al.* Genome-scale CRISPR-Cas9 knockout screening in human cells. *Science* **343**, 84–87 (2014).

Supplementary table 1: List of genes differentially expressed in both DAOY and USP VAPB-KO compared to controls.

Gene Names					
DIP2C	SORT1	DHCR24	LRRC8A	NMNAT2	TFAP2C
SLCO2B1	MEIS2	TKT	FAT2	FTL	IDI1
GDPD5	LINC02154	MACF1	TENM2	CORO1B	G6PD
TSPAN13	COPG1	LAMA2	CHI3L1	EMP1	THBS1
DYSF	QPRT	UTY	PAPPA	AC109635.5	TXNRD1
NPC2	SLC6A6	AQP9	LPXN	LAMB3	SLC25A6
HDAC5	CD6	HLA-DRB5	ANTXR2	IL13RA2	CD81
MRPL24	PRPS2	GNAI2	CXCL8	FTH1	RPL27A
C3	CDC42BPA	FASN	EGR1	PACSIN3	FZD8
SYT13	TBX2	B4GALNT1	LOXL1	FZD7	KIF18A
RAPGEF1	HAS2	ADCY8	RTN4	PTPRF	HTRA1
SEC13	NT5E	GREM1	CILK1	NQO1	BHLHE40
THY1	HEXB	BIRC2	PRDM8	ZNF268	CD70
TBC1D8	EREG	TMEM132A	MFAP4	MYLK	NTNG1
FAM167A	PTPN14	HEG1	CRABP2	CAPN2	EIF4E3
DYDC2	ZBTB47	CRTAP	DUSP6	SLC1A4	PRDX2
USP9Y	G0S2	VPS8	GDNF	P3H2	DNAJB2
MYH10	CTSD	PLXND1	SERPINE2	CCDC80	PPFIBP2
SPRED1	SEMA3B	TMEM100	ATP9A	PALMD	PORCN
CTNNB1	SLC7A11	ACSS2	ADAMTS1	FGF2	LOX
IARS2	PREX1	SREBF1	CGB8	TGFBI	ANXA11
ARHGAP36	CTSA	F3	TFPI2	ATP1B3	COL12A1
NES	VGF	IGFBP4	PCOLCE2	SCAP	SNHG29
NNT	SBSN	PITPNC1	SNHG14	NPC1	ROS1
PCDHGC3	LAMA4	ZNF804A	FBXO32	ITGB5	DACT1

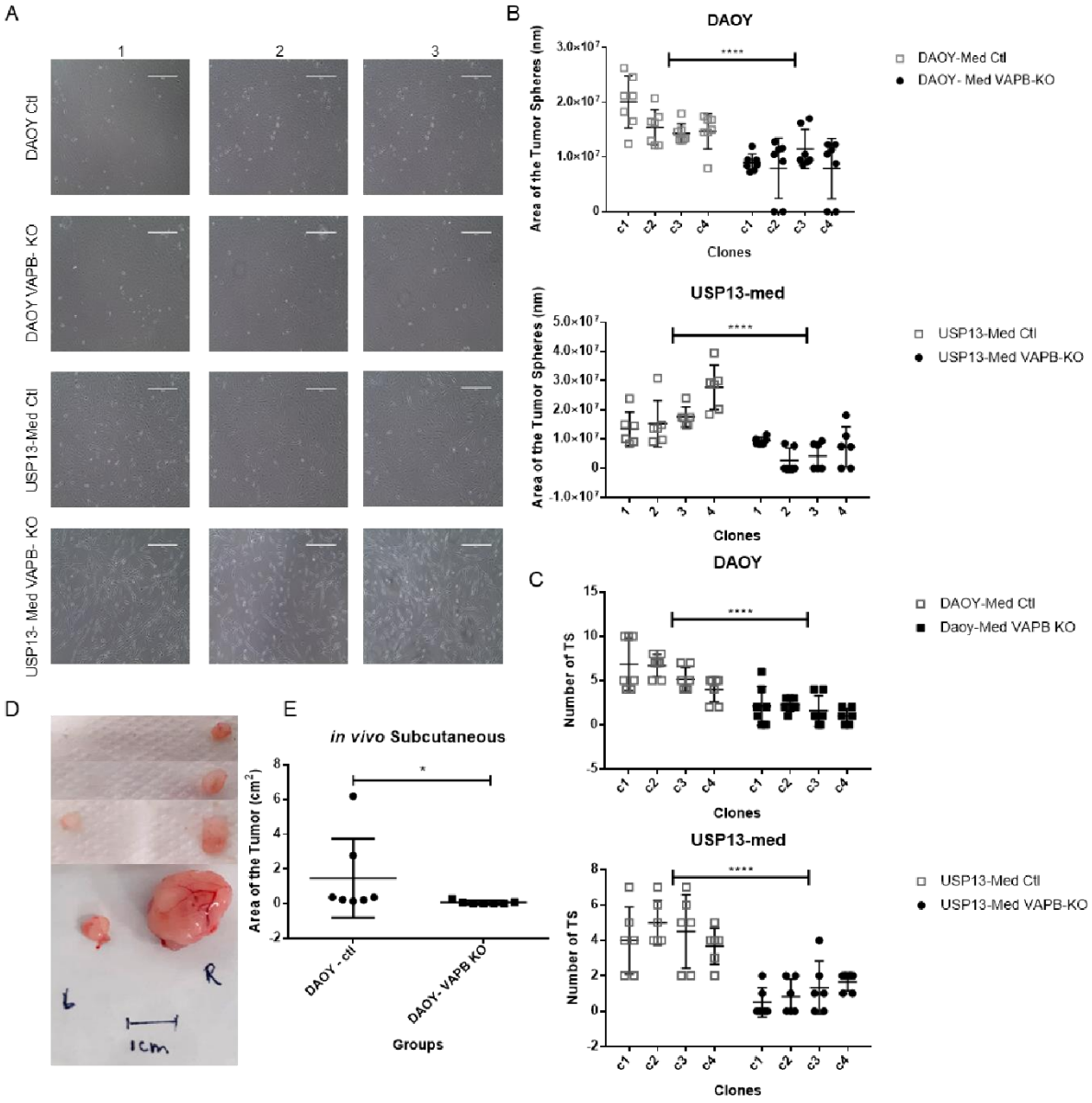

Suppl. Fig. 1: VAPB knock-out changes cell morphology, decreases cell proliferation *in vitro* and tumor growth *in vivo*. a. Representative phase contrast images of VAPB clones from DAOY and USP13-Med controls or VAPB-KO. Scale bar 400 µm. **b**. Quantification of the area of tumorspheres at 144 h post cell plating (*, $P < 0.05$; **, $P < 0.01$; and ***, $P < 0.001$, one-way ANOVA with Tukey multiple comparison test; n = 7 per group). **c**. Quantification of the number of tumorspheres at 144 h post cell plating (*, $P < 0.05$; **, $P < 0.01$; and ***, $P < 0.001$, one-way ANOVA with Tukey multiple comparison test; n = 7 per group). **d**. Representative pictures of tumors formed in nude mice after 4 months of injection of $5*10^5$ DAOY cells controls or VAPB-KO. **e.** Quantification of the volume of the tumors formed in nude mice after after 4 months of injection of $5*10^5$ of DAOY cells controls or VAPB-KO.

Chapter 5

A novel VAPB/EPHA4 axis regulating proliferation of medulloblastoma cells

Amanda Faria Assoni[1,2], Thiago Giove[1], René Wardenaar[2], Elisa Helena Farias Jandrey[1], Gabriela Novaes[1], Petra Bakker[2], Carolini Kaid[1], Mayana Zatz[1], Floris Foijer[2], Oswaldo Keith Okamoto[1*].

1. Human Genome and Stem Cell Research Center, Institute of Biosciences, University of São Paulo, Cidade Universitária, São Paulo 055080-090, Brazil;

2. European Research Institute for the Biology of Ageing, University of Groningen, Groningen, 9713 AV, the Netherlands.

Abstract

EPHA4 is highly expressed in the Central Nervous System and is emerging as a key factor in various nervous system diseases, including cancer. Vesicle-associated membrane protein B (VAPB) is one of the proteins found to bind EPHA4, and its expression is found to be increased in cancer, which correlates with tumor aggressiveness. Therefore, we aimed to understand the regulatory mechanism of cancer stem cells (CSCs) through the VAPB/EPHA4 interaction, with implications for medulloblastoma development. We used two medulloblastoma cell lines (DAOY and USP13) to understand the expression pattern of EPHA4 and how it interacts with VAPB and generates CSCs. Here, we show that the presence of the EPHA4 receptor alone is not responsible for the maintenance of CSCs, but may act as a cell-cell contact molecule that, when downregulated, enhances CSC formation. Also, VAPB binds to EPHA4 in non-transformed neuronal tissues, but not in medulloblastoma cells. However, inactivation of VAPB in medulloblastoma increased EPHA4 phosphorylation, while inhibition of EPHA4 phosphorylation increased cycling of the VAPB-KO cells, recovering their proliferation rate. Therefore, downregulation of VAPB may be an interesting strategy to increase EPHA4 phosphorylation and control proliferation of medulloblastomas.

1- INTRODUCTION

EPH (erythropoietin-producing hepatocellular carcinoma) is a family of receptor tyrosine kinases that plays an important role in tissue organization during development as well as in adult tissue homeostasis(Barquilla and Pasquale, 2015). Ephrin ligands and receptors are highly expressed during Central Nervous System (CNS) development, in which they regulate the spatial organization of cell populations, tissue remodeling, axon alignment, and synaptic formation (Pasquale, 2008). Some members of the family are also highly expressed in the adult nervous system, where they control synaptic structure and function, as well as various aspects of neural and progenitor stem cells (Sheffler-Collins and Dalva, 2012). For example, EPHA4 has been identified as a potential regulator of neurogenesis, and is expressed only by neural stem cells (NSCs) in adult neurogenic niches of mice brain(Khodosevich et al., 2011). EPHA4 expression has also been shown to maintain NSCs in an undifferentiated state. Specifically, EPHA4 knockdown in neurosphere cultures leads to decreased proliferation and premature differentiation of NSCs (Khodosevich et al., 2011). In addition to its role in NSC differentiation, the receptor EphA4 is highly present in the CNS and its expression levels have been reported to be relevant in various nervous system diseases, such as ALS and brain tumors (Eberhart et al., 2000; Genander et al., 2009).

Classical EPH signaling depends on the binding of ephrins, which induce EPH receptor clustering, autophosphorylation and kinase activity. When the ephrin receptor is activated it can undergo endocytosis, proteolytic cleavage, or both, resulting in receptor fragments with different signaling capabilities (Pitulescu and Adams, 2010; Lisabeth et al., 2013). The binding of EPH receptors to ephrins in neighboring cells generates contact-dependent bidirectional signals that regulate cell shape, movement, survival, and proliferation (Batlle et al., 2005; Pasquale, 2005, 2010; Batlle and Wilkinson, 2012). Additionally, interactions between Ephrin and ephrin receptors expressed in the same cell can also attenuate cell-to-cell contact-dependent signals (Wykosky and Debinski, 2008; Beauchamp et al., 2012; Falivelli et al., 2013).

In addition to the classical ephrins ligands, EPH receptors can also bind to proteins from other protein families. Vesicle-associated membrane protein B (VAPB) is one of the proteins found to bind EPHA4 (Tsuda et al., 2008). VAPB is an endoplasmic reticulum (ER) anchored protein with a domain that can be cleaved and secreted, the Major Sperm Protein (MSP) domain. Well known functions of the VAPB protein include tethering between organelles, lipid trafficking, and the unfolded protein response (UPR) (Mao et al., 2019). Functionally, its high expression has been associated with increased breast cancer cell proliferation and decreased patient survival(Rao et al., 2012). Considering that EphA4 and VAPB are related to cancer and can also interact with each other, these observations point to a possible pathway by which the secreted portion of the VAPB protein, the MSP domain, may influence tumor development, particularly in the CNS, by acting on EPHA4 receptors.

CNS tumors are the second most common neoplasm in children (MacDonald et al., 2014). Primary CNS malignancies are clinically relevant because they usually have a high lethality and often leave severe sequelae, including cognitive and motor deficits that significantly affect patients' quality of life (Dolecek et al., 2012). One of these CNS malignancies, medulloblastoma, is a malignant tumor that originates from primitive cells that poorly differentiated during neuronal development.

Alterations in signaling pathways relevant to CNS development are involved in the development of medulloblastoma. In general, medulloblastoma cells exhibit characteristics of primitive cells and often show abnormalities in the activity of proteins belonging to the signaling pathways SHH, NOTCH, WNT and TGFB1(Rodini et al., 2010). From a molecular perspective, medulloblastoma is considered to be highly heterogeneous. Recent research on cancer biology has provided irrefutable evidence of the clinical implications of this inter- and intratumoral heterogeneity (Navin, 2014). Theoretically, tumors arise from the malignant transformation of a single cell, however, at the time of diagnosis, multiple genetically distinct cell populations may be detected (Paguirigan et al., 2015). The existence of highly diverse tumorigenic cancer cell populations with stem cell-like properties that can induce intra-tumor heterogeneity makes the understanding of mechanisms of tumor development more complex (Manoranjan et al., 2013). Such cancer stem cells (CSCs) have been identified in medulloblastoma as well as in several other types of malignant tumors (Singh et al., 2003). Due to their ability to self-renew, these cells are thought to give rise to various cellular progeny during tumor development(Magee et al., 2012).

Little is known about the development and maintenance of CSCs. Given its pathophysiology, medulloblastoma is an interesting model to study this question. Considering that i) medulloblastoma arises from poorly differentiated primitive cells during neural development; ii) medulloblastoma growth is associated with the involvement of signaling pathways relevant to CNS development; iii) cancer cells with NSC properties are present in medulloblastoma and are capable of generating *de novo* tumors. iv) Ephrin receptors such as EPHA4 are important in neurogenesis, regulate neural stem cell differentiation, and are involved in cancer; and v) VAPB is overexpressed in tumors, correlates with tumor aggressiveness, and is able to modulate Ephrin signaling via interaction with EphA4, we explored the hypothesis of a possible novel regulatory mechanism of CSC through the VAPB/EPHA4 interaction, with implications for medulloblastoma development. More specifically, here we show that the presence of the EPHA4 receptor alone is not responsible for the maintenance of CSCs, but may act as a cell-cell contact molecule that, when downregulated, enhances CSC formation. The presence of VAPB inhibits EPHA4 phosphorylation and increases the ability of cells to form tumorspheres.

2- RESULTS

2.1- EPHA4 is downregulated in medulloblastoma patients' samples and its phosphorylation increases CSCs formation

To understand the expression pattern of *EPHA4* gene in medulloblastoma, we evaluated its expression in two cell lines (DAOY and USP13) cultivated in monolayer or in 3D tumorspheres (TS). We observed a significant increase in EPHA4 mRNA expression when cells were cultured in spheres for seven days in comparison with 2D-cultivated cells (Fig. 1A). Furthermore, we analyzed *EPHA4* expression at various stages of differentiation of Human Embryonic Stem Cells (hESCs), ranging from embryonic stem cells to neurons. Assessing mRNA levels in two Embryonic Stem Cell lines (hESCs) BR1 and BR6, EPHA4 expression was highest in both lines in the Embryonic Body (EBs) stage (3D culture), while in monolayer EPHA4 expression peaked in neurons at 7 days of differentiation (Fig. 1B).

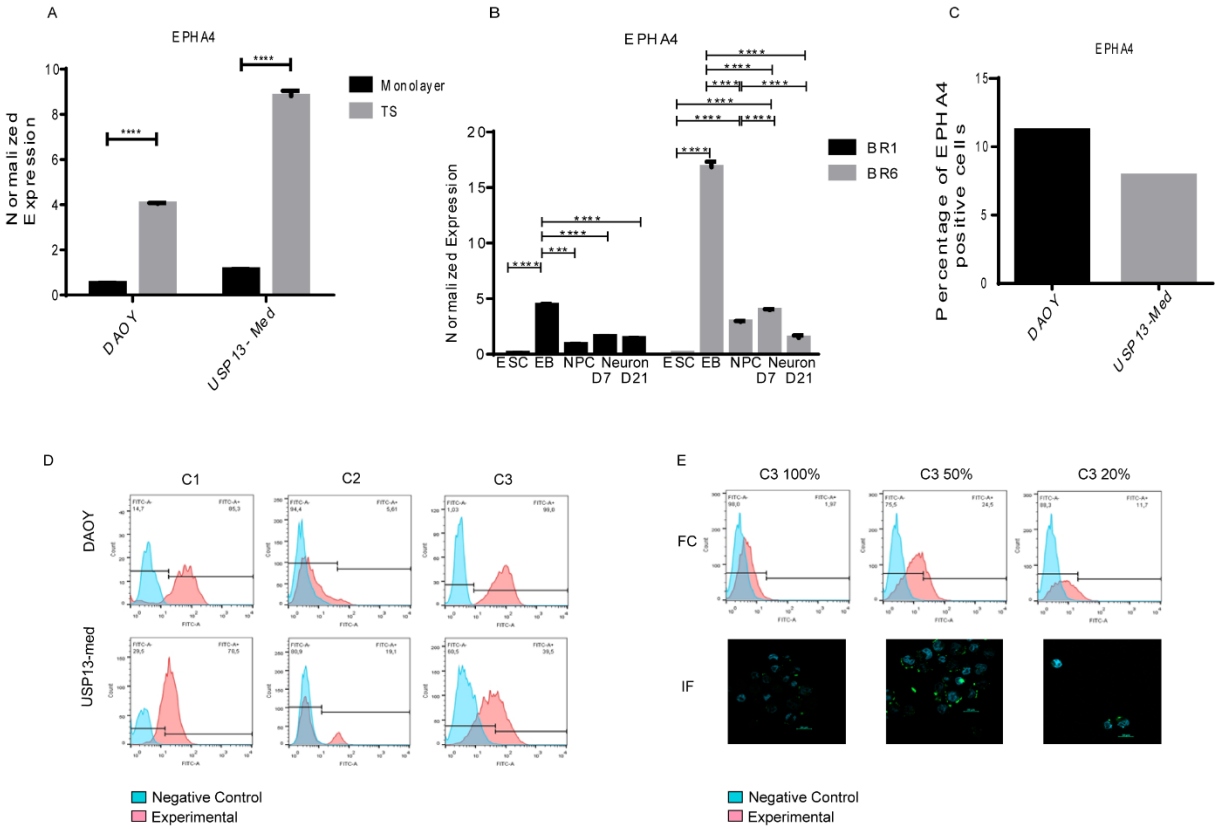

Figure 1: *EPHA4* gene expression is increased in 3D cultures and relates to culture confluence. **a.** mRNA levels of *EPHA4* in medulloblastoma cell lines DAOY and USP13-Med in 2D and 3D. **b**. mRNA levels of *EPHA4* in hESCs in different stages of neuronal differentiation. **c**. Percentage of EPHA4-positive cells in the mixed population the cells lines DAOY and USP13-Med. **d.** Representative flow cytometry analysis of each single cell clone sorted out of the EPHA4- positive cells in the mixed population the cells lines DAOY and USP13-Med. **e**. Representative flow cytometry analysis and immunofluorescence of the C3 clone of the DAOY cell line in different cultured confluences.

To explore the properties of the tumor cells that expressed *EPHA4*, we isolated EPHA4-positive cells from the mixed population and cultured each cell separately (Fig. 1C). After one month of cultivation, we checked *EPHA4* expression in each population obtained from the single cell clones (C1, C2 and C3) from both cell lines (Fig. 1D). We observed that the expression of each population greatly varies regardless of whether it was positive at sorting. Since the cells did not maintain their EPHA4-positive phenotype, and expressed higher *EPHA4* mRNA levels when cultured in 3D, we wondered whether EPHA4 expression could reflect a particular type of cell-cell contact. To test this, we cultured individual clones at different confluences and measured the EphA4 expression in each condition (Fig. 1E).We observed that cells display a higher expression of EphA4 when 50% confluent, compared to confluencies of 20% and 100% at which EPH4A is less expressed.

While these results suggest that *EPHA4* expression is dependent on cell-to-cell contact, it did not explain its relation to cell proliferation. Therefore, to understand whether EPHA4 expression would increase or decrease tumorigenicity, we next compared *EPHA4* gene expression in medulloblastoma samples and healthy tissues in several previously published datasets (Fig. 2A). Surprisingly, *EPHA4* gene expression was significantly decreased in transformed medulloblastoma cells compared to healthy tissue in each data set.

As EPHA4 levels appear to be decreased in medulloblastoma samples, we then investigated whether inhibiting the phosphorylation of EPHA4 would yield the same effect as EPHA4 downregulation, namely the stimulation of tumor sphere formation (Fig. 2B and C). For this, we used a peptide that inhibits EPHA4 phosphorylation specifically (KYL peptide)(I et al., 2012) and found that inhibition of EPHA4 phosphorylation indeed triggers proliferation of CSCs in tumor spheres (Fig. 2B and C). We conclude that downregulation of EPH4A protein or EPHA4 phosphorylation both promote the growth of medulloblastoma tumor spheres, suggesting a role for EPHA4 signaling in medulloblastoma CSC biology.

2.2- EPHA4 binds to VAPB in NPCs but not in Medulloblastoma cells

It has been previously published that VAPB interacts with EPHA4 (Tsuda et al., 2008) but its effect on the receptor activation is not well understood. In addition, VAPB has been described to be upregulated in breast cancer(Rao et al., 2012), which suggests that it is more available to interact with EPHA4. Therefore, we next investigated the interaction between EPHA4 and VAPB.

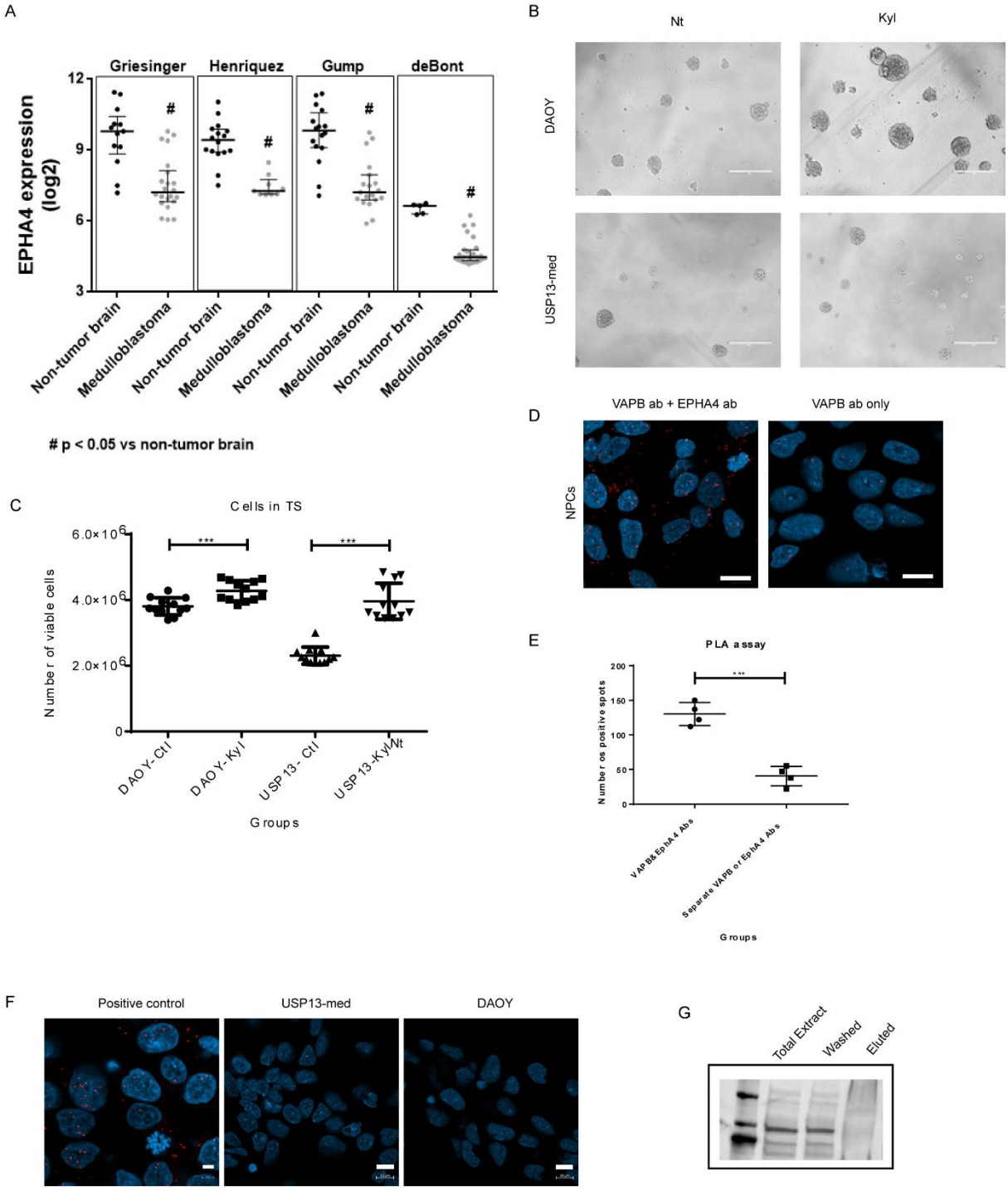

Figure 2: EPHA4 gene expression is decreased in medulloblastoma samples and when phosphorylation is inhibited it increases CSCs sphere formation. a. *EPHA4* gene expression in primary non-tumor brain and tumor samples. Microarray gene expression from non-tumor brain (NTB, n=50) and Medulloblastoma (MED, n=77) samples were obtained from 4 cohorts and viewed by the Gliovis portal(Bowman et al., 2017) : Griesinger (NTB n=13; MED n=22), Henriquez (NTB n=16; MED n=9), Gump (NTB n=16; MED n=19) and de Bont (NTB n=5; MED n=27). **b**. Representative phase contrast images of tumorspheres at 144 hours post cell plating with or without KYL peptide. Scale bar, 400 μm. **c.** Quantification of the number of viable cells after dissociation of tumorspheres at 144 h post cell plating with or without KYL peptide (*, $P < 0.05$; **, $P < 0.01$; and ***, $P < 0.001$, one-way ANOVA with Tukey multiple comparison test; n = 7 per group). **d.** Representative images of Proximity Ligation Assay for VAPB and EPHA4 in NPCs cell lines. Negative control using only one

of the antibodies. Scale bars, 10 µm. **e**. Quantification of the number of dots present in the Proximity Ligation Assay for VAPB and EPHA4 in NPCs cell lines (***, P < 0.001, Kruskal-Wallis test n = 8 fields per group).**f**. Representative images of Proximity Ligation Assay for VAPB and EPHA4 in NPCs(Scale bar 5 µm) (positive control), DAOY (Scale bar 10 µm) and USP13-med (Scale bar 10 µm) cell lines. **g**. Western blot using anti-HA tag antibody for the CO-IP total extract, washed and eluted fractions using anti EPHA4 antibody.

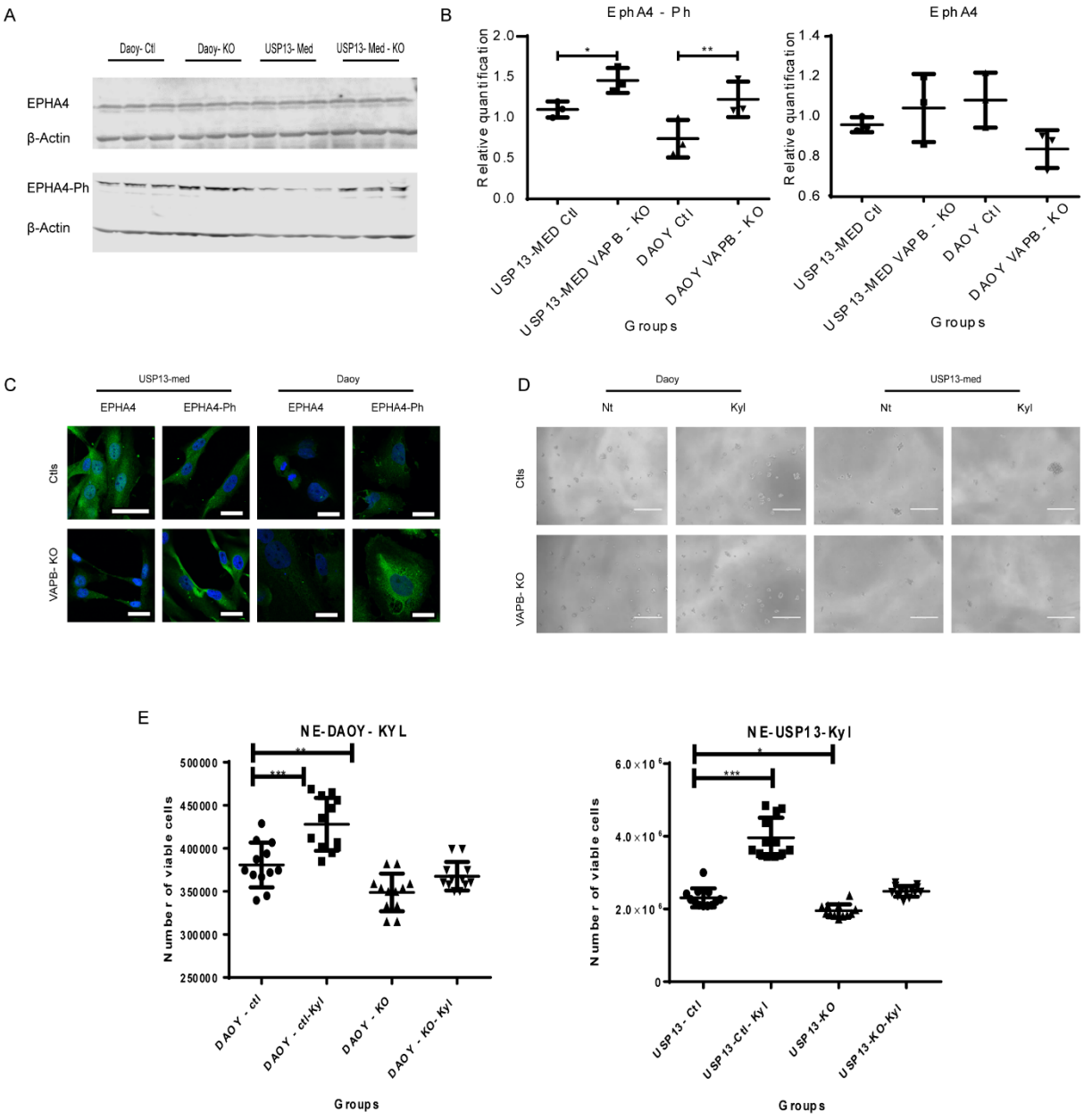

Figure 3: VAPB does not physically bind EPHA4 in medulloblastoma cells and inhibits the receptor phosphorylation. a. Western blot of DAOY and USP13 single cell clones of VAPB-KO and controls blotted using anti-total EPHA4 and anti-Tyr phosphorylated EPHA4. **b.** Quantification of the corresponding densitometry of total EPHA4 and tyr-phosphorylated EPHA4 protein bands. Data are expressed as mean ± SEM (*P < 0.05, **P < 0.01, t test analysis, n = 3 per sample). **c.** Representative images of immunofluorescence staining of total EPHA4 and tyr-phosphorylated EPHA4 in DAOY and USP13 single cell clones of VAPB-KO and controls. Scale bar 20µm, **d**. Representative phase contrast images of tumorspheres at 96h post-cell plating of DAOY and USP13 single cell clones of VAPB-KO and controls treated with vehicle or the EPHA4 phosphorylation inhibitor Kyl peptide (25

µM) Scale bars 400 µm. **e**. Quantification of the number of viable cells after dissociation of tumorspheres at 96 h post-cell plating of DAOY and USP13 single cell clones of VAPB-KO and controls treated with vehicle or the EPHA4 phosphorylation inhibitor Kyl peptide (25 µM) (*, $P < 0.05$; **, $P < 0.01$; and ***, $P < 0.001$, two-way ANOVA with Tukey multiple comparison test; n = 12 per group).

To understand how EPHA4 and VAPB interact, we first checked whether VAPB and EPHA4 directly interact in normal CNS cells. To this end, we performed a proximity ligation (PLA) assay, which revealed an interaction between VAPB and EPHA4 in non-transformed NPCs (Fig. 2 D and E). To test whether this interaction also exists in medulloblastoma cell lines , we generated medulloblastoma cell lines expressing HA-tagged VAPB and performed co-immunoprecipitation and PLA assays using monoclonal antibody against the HA tag and another monoclonal antibody against EPHA4. However, in this experiment we failed to detect a direct interaction between both proteins in the tumor cells (Fig. 2 F and G). As we could not find evidence for a direct interaction between VAPB and EPHA4 in medulloblastoma cells, we then investigated whether the absence of VAPB would affect the expression or phosphorylation of EPHA4.

2.3- Medulloblastoma cell proliferation is restored by inhibition of EphA4 phosphorylation in VAPB-KO cells

For this, we generated VAPB-knockout (KO) cells using CRISPR-Cas9. While inactivation of VAPB did not change the total amount of EPHA4 (Fig. 3A and 4B), we did observe that EPHA4 phosphorylation was significantly increased in VAPB-KO clones compared to control cells (Fig. 3A - 4C). To test the functional relevance of this observation, we used a KYL peptide to inhibit EphA4 phosphorylation(I et al., 2012) and determined the effect on proliferation of VAPB-KO cells. Intriguingly, while untreated VAPB-KO clones had a decreased capability of forming spheres compared to control cells (Fig. 3D and E), this was rescued by the KYL peptide treatment. KYL peptide treatment increased the number of viable cells in the VAPB-KO spheresand recovered VAPB-KO cells proliferation rates, although proliferation rates of in VAPB-WT cells also increased (Fig. 3D and E). We conclude that even though VAPB does not directly bind EPHA4 in the medulloblastoma cell lines, it somehow interferes with the phosphorylation of the receptor, possibly acting as an antagonist. Therefore, in VAPB-KO clones there is a higher phosphorylation of EPHA4, which decreases cell proliferation rates, which are then recovered when the phosphorylation is inhibited.

3- DISCUSSION

Here, we investigated the relevance of EPHA4 expression in normal and CNS cancer cells. Briefly, we show that EPHA4 is more expressed in 3D-based culture in CNS-induced cells from hESCs and in medulloblastoma cell lines (DAOY and USP13) in comparison with 2D cultured cells. However, in monolayer cultures, EPHA4 expression was more correlated with cell density. In addition, we show that the inhibition the phosphorylation of the EPHA4 by an antagonist peptide increases the ability of CSCs sphere formation. Complementarily, we also demonstrate that the non-classical modulation of the Ephrin pathway by the VAPB protein regulates medulloblastoma stem cell self-renewal. Taken together, our results demonstrate that VAPB interacts with EPHA4 through direct binding in CNS non-transformed cells, but indirectly through modulation of its phosphorylation in the medulloblastoma cell lines. Low expression levels of VAPB are associated with decreased proliferation of medulloblastoma cells and associated with increased levels of phosphorylated EPHA4. Indeed, inhibition of EPHA4 phosphorylation in VAPB-KO cells could rescue their proliferation rate, achieving rates comparable to untreated VAPB-expressing control cells. However, it is important to note that proliferation of VAPB-WT cells was also stimulated by inhibition of EPHA4.

Previous work has shown that EPHA4 expression is associated with increased proliferation and migration of glioma cells (Fukai et al., 2008). However, it was also shown that its expression inhibits tumor progression(Y et al., 2016; KT et al., 2018). We found that *EPHA4* expression is downregulated in medulloblastoma samples, possibly implying that cancer cells with decreased EPHA4 mRNA levels had a proliferation advantage over the cells with higher expression. Moreover, expression of EPHA4 in the medulloblastoma cells studied actually decreases the proliferation of CSCs, while inhibition of EPHA4 phosphorylation increased the ability to generate CSCs.

Possibly, soluble signaling molecules alter the downstream effects of EPHA4. VAPB is a protein whose cleaved domain MSP binds to EPHA4 and can compete with ephrins. Importantly, expression of VAPB has been associated with increased proliferation of breast cancer cells (Tsuda et al., 2008). However, to our knowledge, the interaction between VAPB and EPHA4 has never been studied in cancer. We show for the first time that VAPB and EPHA4 do not physically interact in the medulloblastoma lines we studied, in contrast to what was observed in non-transformed neuro-progenitor cells. Even though this needs further investigation, our work suggests that the MSP domain of VAPB is not cleaved in this type of cells and, therefore, does not interact with the EPHA4 receptor in the membrane. An alternative explanation is that EphA4 levels are decreased in medulloblastoma cells compared to neuro-progenitors, and therefore we failed to detect an interaction.

Even though we did not find evidence for a direct protein-protein interaction between EPHA4 and VAPB, we did find that loss of VAPB protein significantly increased phosphorylation of the EPHA4 receptor, suggesting that VAPB acts on cellular pathways that inhibit phosphorylation of the receptor. This would increase cell proliferation, in line with our observations using the inhibitory peptide (KYL). However, how exactly VAPB acts on receptor phosphorylation still needs further work. One possible explanation might come from VAPB's role in maintaining homeostasis of the ER (Peretti et al., 2008). Endocytosed

molecules are transported from the plasma membrane to endosomes, where they are sorted for transport to other compartments(Moustaqim-barrette et al., 2014). ER and endosomes form dynamic membrane contact sites (Eden, 2016), which can be mediated by VAP and lipid-binding proteins(JR et al., 2013). This interaction can induce protein phosphorylation and degradation. One example is the interaction between the ER-localized protein tyrosine phosphatase PTP1B, which dephosphorylates the endosome-associated epidermal growth factor receptor (EGFR), which leads to its degradation (ER et al., 2010). This could also be the case with VAPB and EPHA4, but awaits functional testing.

Despite the low incidence, malignant tumors of the CNS have a high lethality and often leave severe sequelae, including cognitive and motor deficits, which significantly affect patients' quality of life. Therefore, understanding the relationship between VAPB, a ubiquitously expressed protein and the highly CNS expressed EPHA4 that is responsible for maintaining the undifferentiated status of neural stem cells, and associated with more aggressive features of tumor cells, is extremely important as it may reveal new targets for therapies to inhibit tumor development.

In conclusion, our results show that downregulated expression of EPHA4 promotes tumor progression and that activation of EPHA4 is likely to reduce proliferation in medulloblastoma cells. Our results suggest that that VAPB somehow inhibits EPHA4 phosphorylation and as such stimulates cell proliferation. Therefore, downregulation of VAPB may be an interesting strategy to increase EPHA4 phosphorylation and control proliferation of medulloblastoma cells.

4- METHODS

Cell lines and cultures

Two embryonal CNS tumor cell lines: DAOY (medulloblastoma, ATCC HTB-186) and USP13-MED (medulloblastoma, in-house established; ref. 23), one control human-induced pluripotent stem cell (hiPSC, C2535, in-house reprogrammed) and its derived NPCs were analyzed. Generation and characterization of hiPSCs and NPCs was done as in Oliveira et al. 2020(Oliveira et al., 2020) . DAOY was grown according to ATCC recommendations, and cell authentication was performed by high-resolution karyotype analysis. USP13-MED was isolated and characterized as previously reported(PB et al., 2016). After thawing, all cell lines were cultured under standard conditions (5% CO_2 (g) at 37°C) up to 4 weeks (passages 1–4) and tested for Mycoplasma contamination by PCR (Cat. MP002; Sigma-Aldrich), before use in the described experiments.

Gene expression analysis

Total RNA was extracted from tumors and hESC using the RNeasy Mini Kit (Qiagen, Hilden, Germany), according to the manufacturer's instructions. RNA concentration was determined by absorbance at 260 nm with NANO DROP (Qiagen). A total of 1 μg of RNA was reverse transcribed with the SuperScript III Reverse Transcriptase Kit (Invitrogen) according to the manufacturer's instructions. Quantitative PCR was performed in a 7500 Real-Time PCR System Thermal Cycler (Applied Biosystems, Carlsbad, CA). Expression analysis of *EPHA4* was performed with Platinum SYBR Green qPCR SuperMix-UDG (Life Technologies), using GAPDH as endogenous control. Reaction specificity was assessed by dissociation curve analysis. Primer sequences: GAPDH for: 5′-GCATCCTGGGCTACACTG-3′, GAPDH rev: 5′-CCACCACCCTGTTGCTGCTGTA-3′. RT-PCR quantification was based on linear regression analysis from standard curves with amplification efficiency ranging from 90% to 100%. Reactions were performed in triplicate.

Cell sorting

For fluorescence-activated cell sorting (FACS), cells were stained with anti EPHA4 primary antibody and secondary antibody anti rabbit-(FITC)-conjugated. All antibodies were stained at 0.1 mg/10^6 cells. Stained cells were then examined using BD FACS Aria Cell Sorting System with BD FACS Diva Software (BD Biosciences). Gated cells were sorted based on EPHA4 positivity.

Immunofluorescence

Cells were washed twice, fixed (3.7% formaldehyde RT for 20 minutes) and permeabilized for 30 minutes with 0.1% Triton X-100 and 5% bovine serum albumin in 1× PBS, prior to overnight incubation with the primary antibody (Supplementary Table S1) at 4°C. Cells were then washed 3 times in 1× PBS, incubated with the secondary antibody for 45min (Supplementary Table S1), and washed again 2 times in 1× PBS. Cell nuclei were stained with 1 μg/mL DAPI for 2 minutes and mounted on glass slides and cover slipped with VectaShield. All images were taken in confocal microscope (Zeiss LSM 800).

Statistical analysis

All experiments were performed in triplicate or more replicates as stated in the figures, and three independent experiments were carried out. Data were analyzed by one-way and two-way ANOVA followed by Bonferroni post hoc test. The t test with two-tailed unpaired test was used for pairwise comparison. Clinical and pathologic parameters were analyzed by the Fisher exact test. Graphpad Prism software was used to perform all statistical analysis (version 6.0 GraphPad Software Inc.). Quantification of data is represented as mean ± SEM, and P value threshold was as follows: *, 0.05; **, 0.01; ***, 0.001; and ****, 0.0001.

3D tumor spheroid assay

For tumorsphere formation, cells were seeded onto a 96-well ultra-low attachment plate in DMEM/F12 supplemented with B-27, N-2, 20 ng·mL^{-1} EGF, and 20 ng·mL^{-1} bFGF

(Invitrogen, Carlsbad, CA, EUA), at an initial density of 1500 cells·mL^{-1}. After 7 or 4 days of incubation at 37 °C with 5% CO_2 humidified atmosphere (as stated in each figure), spheres were dissociated for 20 min on Tryple at 37oC, centrifuged and counted with Trypan Blue to assess cell viability.

Plasmids

For CRISPR knockout of VAPB gene, three different guide RNAs were designed aiming the exon 2 of the VAPB gene according to the guide resource tool of the Zhang lab(Ran et al., 2013) and cloned into the lentiCRISPR plasmid as described in Shalem et. al 2014(O et al., 2014). The guide RNA that generated more out of frame sequences was chosen and applied to the cell lines used in this study.
To construct a doxycycline-inducible expression system for VAPB overexpression, full-length cDNA encoding VAPB was inserted between BamHI and EcoRI sites of the retroviral plasmid pRetroX-Tight-BlastR (Puromycin exchanged by Blasticidin.
For transient expression, pEGFPC1-hVAP-B was a gift from Catherine Tomasetto (Addgene plasmid # 104448)

Western Blot

Cells were harvested by trypsinization and lysed in elution buffer (150 mM NaCl, 0.1% NP-40, 5 mM EDTA, 50 mM HEPES pH7.5) containing complete protease inhibitor (Roche) for 15 minutes at 4oC. Then the samples were centrifuged at 300g, at 4°C for 10 min to remove insoluble residues. 20 µg of each sample was loaded on 10% polyacrylamide gels. Proteins were transferred to polyvinylidene difluoride (PVDF) membranes. After blocking in Odyssey blocking buffer (Li-cor Biosciences) at 4°C for 60 min, the membrane was incubated overnight at 4°C with the primary antibody (supplemental materials). Following incubation, the membrane was washed with 1X PBS containing 0,1% Tween 20 (Sigma) three times and incubated in secondary antibody for 1 hour at room temperature. The blots were detected by the Odyssey imaging system (Li-cor Biosciences). The protein bands were quantified with Image studio lite software (Li-cor Biosciences).

Duolink PLA

The Duolink PLA assay[56] was performed using Duolink in situ PLUS and MINUS probes and Duolink in situ detection reagents FarRed according to manufacturer's instructions (Sigma-Aldrich). At the end of the procedure the slides were mounted with a coverslip using Duolink® In Situ Mounting Medium which contains 4,6-Diamidino-2-phenylindole, dihydrochloride (DAPI) for nuclear staining. Imaging was performed by fluorescence or confocal microscopy as above.

GFP-TRAP affinity purification

Cells were washed once with PBS and lysed in 500 µL/well lysis buffer containing 20 mM Tris pH 8.0, 10% glycerol, 135 mM NaCl, 0.5% NP-40, and protease inhibitors (Complete, EDTA-free, Roche) for 15 min on ice. After scraping the cells off, lysates were centrifuged at 16,100 g for 5 min at 4°C to remove cell debris. The input was incubated with a mix of 2 µL GFP-TRAP_A beads (ChromoTek) and 8 µL empty Sepharose 4B beads (Sigma), equilibrated in wash buffer, for 1 hr at 4°C. After washing the beads 3× with wash buffer, beads were taken up in Laemmli loading buffer, boiled for 10 min at 95°C, and loaded on a SDS-PAGE. Proteins were detected by western blotting.

5- ACKNOWLEDGEMENTS

This work was supported by the Fundação de Amparo à Pesquisa do Estado de São Paulo (FAPESP), Conselho Nacional de Desenvolvimento Científico e Tecnológico (CNPq) and an Abel Tasman fellowship to AA awarded by the University of Groningen.

6- CONFLICT OF INTEREST DISCLOSURE

No financial interest/relationships with financial interest relating to the topic of this article have been declared.

REFERENCES

1. Barquilla, A. & Pasquale, E. B. Eph Receptors and Ephrins : Therapeutic Opportunities. *Annu. Rev. Pharmacol. Toxicol.* **55**, 465–87 (2015).
2. Pasquale, E. B. Eph-ephrin bidirectional signaling in physiology and disease. *Cell* **133**, 38–52 (2008).
3. Sheffler-Collins, S. I. & Dalva, M. B. EphBs: an integral link between synaptic function and synaptopathies. *Trends Neurosci.* **35**, 293–304 (2012).
4. Khodosevich, K., Watanabe, Y. & Monyer, H. EphA4 preserves postnatal and adult neural stem cells in an undifferentiated state in vivo. *J. Cell Sci.* 1268–1279 (2011). doi:10.1242/jcs.076059
5. Eberhart, J. *et al.* Expression of EphA4, ephrin-A2 and ephrin-A5 during axon outgrowth to the hindlimb indicates potential roles in pathfinding. *Dev. Neurosci.* **22**, 237–250 (2000).

6. Genander, M. *et al.* Dissociation of EphB2 Signaling Pathways Mediating Progenitor Cell Proliferation and Tumor Suppression. 679–692 (2009). doi:10.1016/j.cell.2009.08.048

7. Lisabeth, E. M., Falivelli, G. & Pasquale, E. B. Eph receptor signaling and ephrins. *Cold Spring Harb. Perspect. Biol.* **5**, 1–20 (2013).

8. Pitulescu, M. E. & Adams, R. H. Eph/ephrin molecules--a hub for signaling and endocytosis. *Genes Dev.* **24**, 2480–92 (2010).

9. Batlle, E. *et al.* EphB receptor activity suppresses colorectal cancer progression. **435**, 1–5 (2005).

10. Batlle, E. & Wilkinson, D. G. Molecular mechanisms of cell segregation and boundary formation in development and tumorigenesis. *Cold Spring Harb. Perspect. Biol.* **4**, a008227 (2012).

11. Pasquale, E. B. Eph receptors and ephrins in cancer: bidirectional signalling and beyond. *Nat. Rev. Cancer* **10**, 165–80 (2010).

12. Pasquale, E. B. Eph receptor signalling casts a wide net on cell behaviour. *Nat. Rev. Mol. Cell Biol.* **6**, 462–75 (2005).

13. Beauchamp, A. *et al.* EphrinA1 is released in three forms from cancer cells by matrix metalloproteases. *Mol. Cell. Biol.* **32**, 3253–64 (2012).

14. Falivelli, G. *et al.* Attenuation of eph receptor kinase activation in cancer cells by coexpressed ephrin ligands. *PLoS One* **8**, e81445 (2013).

15. Wykosky, J. & Debinski, W. The EphA2 receptor and ephrinA1 ligand in solid tumors: function and therapeutic targeting. *Mol. Cancer Res.* **6**, 1795–806 (2008).

16. Tsuda, H. *et al.* The Amyotrophic Lateral Sclerosis 8 Protein VAPB Is Cleaved, Secreted, and Acts as a Ligand for Eph Receptors. *Cell* **133**, 963–977 (2008).

17. Mao, D. *et al.* VAMP associated proteins are required for autophagic and lysosomal degradation by promoting a PtdIns4P-mediated endosomal pathway. *Autophagy* 1–20 (2019). doi:10.1080/15548627.2019.1580103

18. Rao, M. *et al.* VAMP-Associated Protein B (VAPB) Promotes Breast Tumor Growth by Modulation of Akt Activity. *PLoS One* **7**, e46281 (2012).

19. MacDonald, T. J., Aguilera, D. & Castellino, R. C. The rationale for targeted therapies in medulloblastoma. *Neuro. Oncol.* **16**, 9–20 (2014).

20. Dolecek, T. A., Propp, J. M., Stroup, N. E. & Kruchko, C. CBTRUS statistical report: primary brain and central nervous system tumors diagnosed in the United States in 2005-2009. *Neuro. Oncol.* **14 Suppl 5**, v1-49 (2012).

21. Rodini, C. O. *et al.* Aberrant signaling pathways in medulloblastomas: a stem cell connection. *Arq. Neuropsiquiatr.* **68**, 947–52 (2010).

22. Navin, N. E. Tumor evolution in response to chemotherapy: phenotype versus genotype. *Cell Rep.* **6**, 417–9 (2014).

23. Paguirigan, A. L. *et al.* Single-cell genotyping demonstrates complex clonal diversity in acute myeloid leukemia. *Sci. Transl. Med.* **7**, 281re2 (2015).

24. Manoranjan, B. *et al.* Medulloblastoma stem cells: modeling tumor heterogeneity. *Cancer Lett.* **338**, 23–31 (2013).

25. Singh, S. K. *et al.* Identification of a cancer stem cell in human brain tumors. *Cancer Res.* **63**, 5821–8 (2003).

26. Magee, J. A., Piskounova, E. & Morrison, S. J. Cancer stem cells: impact, heterogeneity, and uncertainty. *Cancer Cell* **21**, 283–96 (2012).

27. I, L. *et al.* Distinctive binding of three antagonistic peptides to the ephrin-binding pocket of the EphA4 receptor. *Biochem. J.* **445**, 47–56 (2012).

28. Bowman, R. L., Wang, Q., Carro, A., Verhaak, R. G. W. & Squatrito, M. GlioVis data portal for visualization and analysis of brain tumor expression datasets. *Neuro. Oncol.* **19**, 139–141 (2017).

29. Fukai, J. *et al.* EphA4 promotes cell proliferation and migration through a novel EphA4-FGFR1 signaling pathway in the human glioma U251 cell line. *Mol. Cancer Ther.* **7**, 2768–78 (2008).

30. KT, H. *et al.* miR-519d Promotes Melanoma Progression by Downregulating EphA4. *Cancer Res.* **78**, 216–229 (2018).

31. Y, S., J, Q., M, L. & H, X. Lower and reduced expression of EphA4 is associated with advanced TNM stage, lymph node metastasis, and poor survival in breast carcinoma. *Pathol. Int.* **66**, 506–510 (2016).

32. Peretti, D., Dahan, N., Shimoni, E., Hirschberg, K. & Lev, S. Coordinated lipid transfer between the endoplasmic reticulum and the Golgi complex requires the VAP proteins and is essential for Golgi-mediated transport. *Mol. Biol. Cell* **19**, 3871–84 (2008).

33. Moustaqim-barrette, A. *et al.* The amyotrophic lateral sclerosis 8 protein, VAP, is required for ER protein quality control. *Hum. Mol. Genet.* **23**, 1975–89 (2014).

34. Eden, E. R. The formation and function of ER-endosome membrane contact sites. *Biochim. Biophys. Acta - Mol. Cell Biol. Lipids* **1861**, 874–879 (2016).

35. JR, F., JR, D., M, W., AA, R. & GK, V. Endoplasmic reticulum-endosome contact increases as endosomes traffic and mature. *Mol. Biol. Cell* **24**, 1030–1040 (2013).

36. ER, E., IJ, W., A, T. & CE, F. Membrane contacts between endosomes and ER provide sites for PTP1B-epidermal growth factor receptor interaction. *Nat. Cell Biol.* **12**, 267–272 (2010).

37. Oliveira, D. *et al.* Different gene expression profiles in iPSC-derived motor neurons from ALS8 patients with variable clinical courses suggest mitigating pathways for neurodegeneration. *Hum. Mol. Genet.* **29**, 1465–1475 (2020).

38. PB, S. *et al.* Establishment of a novel human medulloblastoma cell line characterized by highly aggressive stem-like cells. *Cytotechnology* **68**, 1545–1560 (2016).

39. Ran, F. A. *et al.* Genome engineering using the CRISPR-Cas9 system. *Nat. Protoc.* **8**, 2281–2308 (2013).

40. O, S. *et al.* Genome-scale CRISPR-Cas9 knockout screening in human cells. *Science* **343**, 84–87 (2014).

GENERAL CONCLUSIONS AND FUTURE PERSPECTIVES

ALS and protein synthesis

As thoroughly mentioned in this work, Amyotrophic Lateral Sclerosis is a neurodegenerative disease for which there is currently no effective treatment. Therefore, it is of great importance to further investigate the mechanisms leading to motor neuron death to find new potential therapeutic targets. In this thesis, we deepen our understanding on 3 proteins involved in the pathogenesis of ALS, mainly by analyzing their effects when they are mutated, absent or their activity is inhibited.

In Chapters 1, 2 and 3, we describe and study how protein translation is one of the first and most important pathways affected by ALS-related mutations. Indeed, all mechanisms that are disrupted in ALS cells ultimately lead to downregulation of protein synthesis rates. In every ALS model analyzed until now, protein synthesis rates are decreased compared to controls(Cestra et al., 2017; Chen et al., 2018; López-Erauskin et al., 2018). Therefore, decreased protein synthesis might represent a hallmark of ALS pathogenesis.

ALS6, with mutations on the fused in sarcoma gene, is the type of ALS with the earliest mean age of onset of disease and thus represents an interesting type of ALS to be studied(Vance et al., 2009). We found that transcription levels, RNA quantity and localization are similar in ALS6 and control iPSC-derived motor neurons. We also show that the ALS6 cells exhibit reduced global translation when compared to control cells. The decreased protein synthesis appears to be a consequence of mutant FUS localized to the cytoplasm of ALS motor neurons as we find it to interact with proteins of the translational machinery and furthermore find that FUS protein levels are not altered in these cells.

Interestingly, we found that FUS is also mislocalized into the cytoplasm of iPSC-derived motor neurons generated from other types of familial ALS. Since *FUS* is not mutated in these cells, the reason for its localization in the cytoplasm requires further work. Regardless of the cause, we show an inverse correlation between FUS levels in the cytoplasm and the translation rates in each sample. Wild-type FUS thus appears to interfere with protein synthesis as much as mutant FUS, and both have this activity when mislocalized in the cytoplasm.

Reduced translation has been reported in the ALS literature before(Kamelgarn et al., 2018; N et al., 2019), but it is not fully understood whether this is a protective or deleterious property for the cells. In this thesis, we show that the cells with decreased translation rates are more susceptible to oxidative stress, which accumulate in human cells with age. Therefore, this

result suggests that the observed decreased translation rates are in fact detrimental for the motor neuros in ALS patients.

The exact cellular mechanism causing motor neuron degeneration in ALS patients is still unclear. However, one of the few common features found in different types of ALS are elevated inflammatory markers (Hu et al.). Since inflammation can be modulated with drugs, this is an interesting feature that should be further investigated and has potential therapeutic applicability(Béland et al., 2020).

Viral infections are considered risk factors for the development of ALS pathogenesis. And interferon-gamma (IFN-y) is a multifunctional cytokine, for which one of its roles is to help in the antiviral response. Moreover, this innate immune modulator is one of the cytokines that is differentially expressed in ALS patients and, interestingly, components of the innate immune system have been described as modulators of FUS expression(Lu et al., 2016; Lee et al., 2017; S et al., 2019). We therefore investigated the role of IFNy signaling in ALS6 MNs. We demonstrate a protective role of IFNy treatment for ALS6 cells in the presence of oxidative stress. Our results show that IFNy upregulates translation-associated genes specifically in ALS6 MNs and that cytoplasmic localization of FUS is reduced in ALS6 MNs after IFN-y treatment. Further studies are needed to better understand the mechanism by which IFN-y regulates FUS localization.

However, our work was performed in newly differentiated neurons and there is some debate about the different roles that the immune system might play during the development of the disease. In general, the initial response of the immune system to aggregated proteins or similar stressors is thought to be neuroprotective, but when the damage becomes unsustainable, the response transitions to increased neuroinflammation and neurotoxicity. Therefore, our study suggests that IFN-y could be used to treat ALS patients. However, to understand at what stages of disease progression patients would benefit needs further work.

In conclusion, in this thesis we highlight the importance of protein synthesis on ALS pathogenesis, show that it is decreased in ALS6 newly-differentiated motor neurons and suggest a possible treatment, by increasing translation with IFN-y.

Shared roles of molecular pathways between ALS and cancer

There is increasing evidence that common signaling transduction routes underlie development of ALS and cancer, although the type of deregulation might differ between both pathologies(Harris et al., 2014; Jaberi et al., 2020). In this thesis, we studied the functions of proteins with known activities in the ALS context in a neuroprogenitor-derived tumor, medulloblastoma.

We chose medulloblastoma for our study as the tumor has a similar cellular origin as ALS, and as it causes high morbidity and mortality in children, with a significant proportion of patients failing to respond to available treatments and/or developing motor and cognitive

disorders(MacDonald et al., 2014). We find that vesicle-associated membrane protein B (VAPB)(Nishimura et al., 2004) - which has lower mRNA levels in the cerebrospinal fluid of sporadic ALS cases(Deidda et al., 2014) - correlates with lower overall patient survival when expressed at higher levels in medulloblastoma. We also demonstrate a novel role for VAPB in cellular proliferation in medulloblastoma, as *VAPB* knockout causes the arrest of cells in G1/0. In addition, we found that transcript levels of many WNT-related proteins, including *CTNNB1*, were decreased in medulloblastomas that display low VAPB protein expression. Therefore, our results reveal a novel pro-oncogenic function of VAPB in medulloblastoma cells that involves modulation of the WNT pathway, a known regulator of cancer and neural development(Mulligan and Cheyette, 2012).

We also investigated the interaction between VAPB protein and ephrin receptor type A4 (EPHA4). EPHA4 is highly expressed in the CNS and has been shown to be a key factor in several nervous system diseases, including ALS and cancer(Fukai et al., 2008; A et al., 2012; Y et al., 2016; L et al., 2019). For example, lower expression of EPHA4 has been found to correlate with an increase in survival in ALS patients(A et al., 2012). In this work, we show that downregulation of EPHA4 appears to be beneficial for cell survival in medulloblastoma, as well as in ALS, as reported in literature(Y et al., 2016). Furthermore, we found that VAPB binds to EPHA4 in non-transformed neuronal tissues, but not in medulloblastoma cells. However, removal of VAPB in medulloblastoma increased EPHA4 phosphorylation, whereas inhibition of EPHA4 phosphorylation increased the cycling of VAPB-KO cells and increased their proliferation rate. The mechanism by which VAPB regulates EPHA4 phosphorylation requires further investigation. This is particularly important as the molecular mechanism underpinning how downregulation of VAPB increases EPHA4 phosphorylation and helps control proliferation of medulloblastomas may help to unravel the pathway.

These results highlight the interplay between different signaling pathways in cancer and ALS. We show that VAPB can regulate EPHA4 phosphorylation and WNT pathway gene expression. Moreover, there is evidence in the literature for crosstalk between the ephrin and Wnt signaling pathways (Peng et al., 2018). Together this work shows that both of these proteins, already known for their isolated and neurodegenerative functions, have the ability to interact and play an important role in cancer development.

Final conclusions and further perspectives

Amyotrophic Lateral Sclerosis is a devastating disease. Therefore, since it was first discovered in 1869, despite many heroic efforts, scientists are still struggling to find ALS treatment targets. One main conclusion from this thesis is that restoring protein translation might be a potential way to delay ALS onset and symptoms as besides FUS regulating translation rates in ALS6 MNs, all other proteins studied above were found to regulate protein synthesis.

For instance, cells harboring VAPB mutations have been reported to exhibit protein synthesis defects(Oliveira et al., 2020) and VAPB mutant inclusions were found within ribosome-rich areas particularly in motor neuronal dendrites(Kuijpers et al.). Furthermore, Wnt signaling is a known regulator of ribosomal biogenesis(Madan et al., 2018) and a global decrease in protein synthesis coupled with a halt in the cell cycle was observed when Wnt related proteins were inhibited in medulloblastoma cells(D and PP, 2003). Further, Ephrin-A stimulation was reported to inhibit mTOR, negatively, thus regulating local protein synthesis within the axon compartment of neurons(Sikkema et al., 2012).

Indeed, translation is a fundamental cellular process that governs cell fate(Kim, 2019). Importantly, the translation machinery also includes dozens of potentially druggable protein targets, therefore, pharma has significantly invested in the development of translation regulators. One way to target translation is by modulating the "integrated stress response" (ISR)(Bond et al., 2020). The ISR is induced by external factors (including essential nutrient deprivation and viral infection), as well as intrinsic factors (such as ER stress)(Baird and Wek, 2012). Central to the ISR is the regulation of translation initiation via phosphorylation of the eukaryotic initiation factor 2 α-subunit (eIF2α) to preserve protein homeostasis. Recently, one compound targeting the ISR showed promising results in the treatment of a rat model of Alzheimer's disease(Hosoi et al., 2016). This underscores the potential that these components to treat neurodegerative diseases.

Translation is one of the common pathways deregulated in both cancer and neurodegenerative diseases(Bader and Vogt, 2004; Serio and Patani, 2018). While downregulated in motor neurons of ALS patients, translation is generally upregulated in cancer cells to maintain the enhanced metabolism and proliferative state of these cells(Rozpedek et al., 2016; Kang et al., 2021). As such, cancer cells could well be susceptible to translation inhibitors.

Here, we add evidence to the hypothesis that neurodegeneration and tumorigenesis are the result of the same deregulated pathways, albeit in different directions. Therefore, it is of the utmost importance to apply the knowledge for cancer research on neurodegenerative diseases. This will not only lead to a better understanding of these devastating disease, but also could lead to new intervention strategies to improve the life of ALS patients in the future.

REFERENCES

1. Chen, K. *et al.* Neurodegenerative Disease Proteinopathies Are Connected to Distinct Histone Post-translational Modification Landscapes. *ACS Chem. Neurosci.* **9**, 938–948 (2018).
2. López-Erauskin, J. *et al.* ALS/FTD-Linked Mutation in FUS Suppresses Intra-axonal Protein Synthesis and Drives Disease Without Nuclear Loss-of-Function of FUS. *Neuron* **100**, 816-830.e7 (2018).
3. Cestra, G., Rossi, S., Di Salvio, M. & Cozzolino, M. Control of mRNA Translation in ALS Proteinopathy. *Front. Mol. Neurosci.* **0**, 85 (2017).

4. Vance, C. *et al.* Mutations in FUS, an RNA processing protein, cause familial amyotrophic lateral sclerosis type 6. *Science (80-.).* **323**, 1208–1211 (2009).

5. N, N. *et al.* TDP-43 enhances translation of specific mRNAs linked to neurodegenerative disease. *Nucleic Acids Res.* **47**, 341–361 (2019).

6. Kamelgarn, M. *et al.* ALS mutations of FUS suppress protein translation and disrupt the regulation of nonsense-mediated decay. *Proc. Natl. Acad. Sci. U. S. A.* **115**, E11904–E11913 (2018).

7. Hu, Y. *et al.* Increased peripheral blood inflammatory cytokine levels in amyotrophic lateral sclerosis: a meta-analysis study OPEN. doi:10.1038/s41598-017-09097-1

8. Béland, L.-C. *et al.* Immunity in amyotrophic lateral sclerosis: blurred lines between excessive inflammation and inefficient immune responses. *Brain Commun.* **2**, (2020).

9. Lee, S. H., Kwon, J. ye, Kim, S.-Y., Jung, K. & Cho, M.-L. Interferon-gamma regulates inflammatory cell death by targeting necroptosis in experimental autoimmune arthritis. *Sci. Reports 2017 71* **7**, 1–9 (2017).

10. S, S. *et al.* Interferon-γ Receptor 1 and GluR1 upregulated in motor neurons of symptomatic hSOD1G93A mice. *Eur. J. Neurosci.* **49**, 62–78 (2019).

11. Lu, C.-H. *et al.* Systemic inflammatory response and neuromuscular involvement in amyotrophic lateral sclerosis. *Neurol. - Neuroimmunol. Neuroinflammation* **3**, e244 (2016).

12. Jaberi, E., Tresse, E., Grønbæk, K., Weischenfeldt, J. & Issazadeh-Navikas, S. Identification of unique and shared mitochondrial DNA mutations in neurodegeneration and cancer by single-cell mitochondrial DNA structural variation sequencing (MitoSV-seq). *EBioMedicine* **57**, (2020).

13. Harris, R. A., Tindale, L. & Cumming, R. C. Age-dependent metabolic dysregulation in cancer and Alzheimer's disease. *Biogerontology* **15**, 559–577 (2014).

14. MacDonald, T. J., Aguilera, D. & Castellino, R. C. The rationale for targeted therapies in medulloblastoma. *Neuro. Oncol.* **16**, 9–20 (2014).

15. Nishimura, A. L. *et al.* A mutation in the vesicle-trafficking protein VAPB causes late-onset spinal muscular atrophy and amyotrophic lateral sclerosis. *Am. J. Hum. Genet.* **75**, 822–831 (2004).

16. Deidda, I. *et al.* Expression of vesicle-associated membrane-protein-associated protein B cleavage products in peripheral blood leukocytes and cerebrospinal fluid of patients with sporadic amyotrophic lateral sclerosis. *Eur. J. Neurol.* **21**, 478–85 (2014).

17. Mulligan, K. A. & Cheyette, B. N. R. Wnt Signaling in Vertebrate Neural Development and Function. *J. Neuroimmune Pharmacol.* **7**, 774 (2012).

18. A, V. H. *et al.* EPHA4 is a disease modifier of amyotrophic lateral sclerosis in animal models and in humans. *Nat. Med.* **18**, 1418–1422 (2012).

19. L, R. *et al.* Reducing EphA4 before disease onset does not affect survival in a mouse model of Amyotrophic Lateral Sclerosis. *Sci. Rep.* **9**, (2019).

20. Fukai, J. *et al.* EphA4 promotes cell proliferation and migration through a novel EphA4-FGFR1 signaling pathway in the human glioma U251 cell line. *Mol. Cancer Ther.* **7**, 2768–

78 (2008).

21. Y, S., J, Q., M, L. & H, X. Lower and reduced expression of EphA4 is associated with advanced TNM stage, lymph node metastasis, and poor survival in breast carcinoma. *Pathol. Int.* **66**, 506–510 (2016).

22. Peng, Q. *et al.* EPH receptor A2 governs a feedback loop that activates Wnt/β-catenin signaling in gastric cancer. *Cell Death Dis. 2018 912* **9**, 1–16 (2018).

23. Oliveira, D. *et al.* Different gene expression profiles in iPSC-derived motor neurons from ALS8 patients with variable clinical courses suggest mitigating pathways for neurodegeneration. *Hum. Mol. Genet.* **29**, 1465–1475 (2020).

24. Kuijpers, M. *et al.* Amyotrophic lateral sclerosis (ALS)-associated VAPB-P56S inclusions represent an ER quality control compartment. *Acta Neuropathol. Commun.* 24 doi:10.1186/2051-5960-1-24

25. Madan, B. *et al.* Oncogenic Wnt/STOP signaling regulates ribosome biogenesis in vivo. *bioRxiv* 326819 (2018). doi:10.1101/326819

26. D, R. & PP, P. Does the ribosome translate cancer? *Nat. Rev. Cancer* **3**, 179–192 (2003).

27. Sikkema, A. H. *et al.* EphB2 activity plays a pivotal role in pediatric medulloblastoma cell adhesion and invasion. *Neuro. Oncol.* **14**, 1125–35 (2012).

28. Kim, H. J. Cell fate control by translation: MRNA translation initiation as a therapeutic target for cancer development and stem cell fate control. *Biomolecules* **9**, (2019).

29. Bond, S., Lopez-Lloreda, C., Gannon, P. J., Akay-Espinoza, C. & Jordan-Sciutto, K. L. The integrated stress response and phosphorylated eukaryotic initiation factor 2α in neurodegeneration. *Journal of Neuropathology and Experimental Neurology* (2020). doi:10.1093/jnen/nlz129

30. Baird, T. D. & Wek, R. C. Eukaryotic initiation factor 2 phosphorylation and translational control in metabolism. *Adv. Nutr.* **3**, 307–21 (2012).

31. Hosoi, T., Kakimoto, M., Tanaka, K., Nomura, J. & Ozawa, K. Unique pharmacological property of ISRIB in inhibition of Aβ-induced neuronal cell death. *J. Pharmacol. Sci.* **131**, 292–295 (2016).

32. Serio, A. & Patani, R. Concise Review: The Cellular Conspiracy of Amyotrophic Lateral Sclerosis. *Stem Cells* **36**, 293–303 (2018).

33. Bader, A. G. & Vogt, P. K. An essential role for protein synthesis in oncogenic cellular transformation. *Oncogene* **23**, 3145–3150 (2004).

34. Rozpedek, W. *et al.* The Role of the PERK/eIF2α/ATF4/CHOP Signaling Pathway in Tumor Progression During Endoplasmic Reticulum Stress. *Curr. Mol. Med.* **16**, 533–44 (2016).

35. Kang, J. *et al.* Ribosomal proteins and human diseases: molecular mechanisms and targeted therapy. *Signal Transduct. Target. Ther.* **6**, (2021).

List of Publications

Kaid, C., Jordan, D., Bueno, H. M. de S., Araujo, B. H. S., Assoni, A., & Keith Okamoto, O. (2019). miR-367 as a therapeutic target in stem-like cells from embryonal central nervous system tumors. *Molecular Oncology*. https://doi.org/10.1002/1878-0261.12562

Goulart, E., De Caires-Junior, L. C., Telles-Silva, K. A., Araujo, B. H. S., Kobayashi, G. S., Musso, C. M., … Zatz, M. (2019). Adult and iPS-derived non-parenchymal cells regulate liver organoid development through differential modulation of Wnt and TGF-β. *Stem Cell Research and Therapy*, *10*(1). https://doi.org/10.1186/s13287-019-1367-x

Goulart, E., de Caires-Junior, L. C., Telles-Silva, K. A., Araujo, B. H. S., Rocco, S. A., Sforca, M., … Zatz, M. (2019). 3D bioprinting of liver spheroids derived from human induced pluripotent stem cells sustain liver function and viability *in vitro*. *Biofabrication*. https://doi.org/10.1088/1758-5090/ab4a30

Kaid, C., Goulart, E., Caires-Júnior, L. C., Araujo, B. H. S., Soares-Schanoski, A., Bueno, H. M. S., … Okamoto, O. K. (2018). Zika virus selectively kills aggressive human embryonal CNS tumor cells in vitro and in vivo. *Cancer Research*, *78*(12), 3363–3374. https://doi.org/10.1158/0008-5472.CAN-17-3201

Rodini, C. O., da Silva, P. B. G., Assoni, A. F., Carvalho, V. M., & Okamoto, O. K. (2018). Mesenchymal stem cells enhance tumorigenic properties of human glioblastoma through independent cell-cell communication mechanisms. *Oncotarget*, *9*(37), 24766–24777. https://doi.org/10.18632/oncotarget.25346

Assoni, A., Coatti, G., Valadares, M. C., Beccari, M., Gomes, J., Pelatti, M., … Zatz, M. (2017). Different Donors Mesenchymal Stromal Cells Secretomes Reveal Heterogeneous Profile of Relevance for Therapeutic Use. *Stem Cells and Development*, *26*(3), 206–214. https://doi.org/10.1089/scd.2016.0218

Coatti, G. C., Frangini, M., Valadares, M. C., Gomes, J. P., Lima, N. O., Cavaçana, N., … Zatz, M. (2017). Pericytes Extend Survival of ALS SOD1 Mice and Induce the Expression of Antioxidant Enzymes in the Murine Model and in IPSCs Derived Neuronal Cells from an ALS Patient. *Stem Cell Reviews and Reports*, *13*(5), 686–698. https://doi.org/10.1007/s12015-017-9752-2

Gomes, J. P. A., Assoni, A. F., Pelatti, M., Coatti, G., Okamoto, O. K., & Zatz, M. (2017). Deepening a Simple Question: Can MSCs Be Used to Treat Cancer? *Anticancer Research*, *37*(9), 4747–4758. https://doi.org/10.21873/anticanres.11881

Valadares, M. C., Gomes, J. P., Castello, G., Assoni, A., Pellati, M., Bueno, C., … Zatz, M. (2014). Human Adipose Tissue Derived Pericytes Increase Life Span in Utrn (tm1Ked) Dmd (mdx) /J Mice. *Stem Cell Reviews and Reports*, *10*, 830:840. https://doi.org/10.1007/s12015-014-9537-9

Vieira, N. M., Valadares, M., Zucconi, E., Secco, M., Bueno Junior, C. R., Brandalise, V., … Zatz, M. (2012). Human Adipose-Derived Mesenchymal Stromal Cells Injected Systemically Into GRMD Dogs Without Immunosuppression Are Able to Reach the Host Muscle and Express Human Dystrophin. *Cell Transplantation*, *21*(7), 1407–1417.

Acknowledgements

I would like to thank everyone who has been involved in this project in any way. Whether it be in academic discussion, bench work, or in life.

Anyone who knew me before this PhD knows that I have changed, hopefully into a better version of myself. This long journey has been a challenging experience for which I am very grateful, especially for finding the most extraordinary people I could have. I am honored to have shared all the amazing and not so amazing experiences with all of you.

I do not usually let anyone go without telling them how important they are to me, and I truly believe that each of you know how much you mean to me. Anyway, I want to emphasize that without you, this work and my entire PhD experience would not be as valuable to me as it is, or maybe even be finished at all. So here goes:

I would like to thank Keith, my PhD supervisor, who trusted me immediately when I started as his PhD student, and who has always been so understanding and supportive, and always there when I (and I know his other students) needed him most.

I am also grateful to Mayana, who got to know me in my teen years and continues to support me in many ways to this day, from letting me study valuable patient cells to the new job opportunities you offer me. I want you to know that you have always been an example of dedication to science and to the patients we hope to one day help. Thank you.

I also want to thank Floris. You did not know me and yet you invited me to your lab. I am glad we had a long road and in the end we were able to understand our ways. I admire you so much for your enthusiasm and brilliant ideas. It was a great opportunity to see how you work during the time I spent in your lab. Thank you so much for your patience and guidance, I really needed that.

I would like to thank Sophia for trying to help me when she saw that I was unwell. It meant a lot to me to know that someone was looking out for me, thank you so much.

I am also grateful to my lab mates, both in Brazil and in Groningen. Bia, Pati Benites, Pati Semedo, Kaidita, Thithi, Danyllo, Ernesto, Luiz, Gerson and Kayque without you I would not have even started, it was super fun and I love the experience of working with you every day. Thank you for all the conversations, the "bear hugs" and the many times you saved my PhD by helping me with documents and other things. I would like to thank all of you at Fleury who always make me feel welcome, even when I disappear sometimes, it is a pleasure to work with you. Thank you Klaske, Laura and Chrystie, I had no idea how everything worked at ERIBA, thank you for being so friendly and helpful. Lin, Catalina, Sahil, Arun, Othman and Siqi, thank you for sharing with me the struggles of being a foreigner and for always being easy to be with and for sharing all the laughs. Petra and Andrea, I am sooo grateful for the hugs and

understanding you gave me just by looking at me. I will always have fond memories of you and I feel lucky to have met you.

Besides the lab, I had the opportunity to make the best friends anyone could have. Thank you, Arthur, my brother. That sentence says it all. Thank you Bjorn and Danielle for taking me in so quickly and accepting me into your external programs. Danielle, my parents still talk about you and how nice and kind you were to me and them. I am proud to have known you. To my Groningen family, Carmem, Tabitha, Marcel, Rapha, Hector, Obedin, Humbertinho, Leo, Carmen and Plankita: you know you guys mean the world to me, without you I would not have survived this PhD. I love you and you will forever have a special place in my heart, hopefully one day we will not be as far apart as we are now.

I am also thankful that I can keep my old friends. Babi and Gabi, thank you so much for listening to all my podcasts, you have been a ray of sunshine in my rainy days (hehehe). Our friendship has grown so much even though we were far apart, and now I know I can count on you wherever we are. Please know that you can count on me too. Nani, once again I have returned to where I know I have a home, and living with you has shown me that our friendship will last forever. Fifs, I admire you and love you, our trip together was so unique, I will never forget how you crossed the ocean to meet me. There are also friends I meet up with once a year, but every time I do, I am glad to have you in my life and it's like we just saw each other yesterday. Thank you for that Mamao, Cauêzetz, Rapidoca xuba, Anna (bebe), Dia, Laís and Aninha florzinhas and Daniê.

I also want to thank Teks who read all this work and helped me a lot and Elisa who I just met and who has already helped me so much.

If you'll excuse me, I'd like to thank my parents in Portuguese:

Agradeço muito aos meus pais, que acreditam em mim e no meu potencial. Agradeço simplesmente por tudo, sou muito feliz e orgulhosa por ser filha de vocês. Meus amigos e companheiros. Amo vocês!

Back to English. Thank you to everyone I have worked with. Each of you has helped me grow as a person and academically. I will never forget you and hope that you all succeed and that we meet again sometime in our lives.

Finally, I would like to acknowledge the financial support of this work by FAPESP, CNPQ, Grupo Fleury, the University of Groningen and UMCG.